NTNU – Trondheim
Norwegian University of
Science and Technology

Engineering geological assessment and structural comparison of the Vollan and Ivasnasen rock slopes at Sunndal, Norway

Gudrun Majala Dreiås

Geology
Submission date: November 2012
Supervisor: Krishna Kanta Panthi, IGB
Co-supervisor: Thierry Oppikofer, NGU

Norwegian University of Science and Technology
Department of Geology and Mineral Resources Engineering

Abstract

This master thesis has interest in analyzing the two unstable rock slopes Ivasnasen and Vollan. These rock slopes are located in a U-shaped valley in Sunndal municipally (Møre & Romsdal, western Norway). The analyses are based on a combined approach using detailed geomorphic, structural and geological field mapping. This along with interpretation of high-resolution digital elevation models (DEM) and orthophotos, LIDAR-scans from one of the sites (Ivasnasen 2010 and 2011), numerical analysis, kinematic analysis, XRD analysis and laboratory testing.

The two sites, Ivasnasen and Vollan are both unstable. Ivasnasen is classified with a historical rockslide and an unstable rock slope, this because a remaining unstable part is detected in the elongation of the back scarp for the historical rockslide. For Vollan an earlier event is still active. It is important to analyze both sides of the valley to get a best knowledge of the possible consequences and the history.

The software Ante-Rockslide Topography (ART) is used to reconstruct and construct the topography for Ivasnasen. Detailed volume estimation is used further in the software Slope Local Base Level (SLBL) and a manual ART reconstruction in the PolyWork (software). The calculated volume estimates for the historical rockslide at Ivasnasen range from 5.2Mm^3 -1.2Mm^3 and from 0.6-2.1Mm^3 for the unstable rock slope. The software Phase^2 has been used for the numerical modeling. The reconstructed and constructed topography for Ivasnasen have been used for a detailed study of the parameters and trigger factors that affected the slope stability in Phase^2.

The back scarp at Vollan contains quartzite and the back scarp at Ivasnasen contains augen gneiss. The main failure mechanism is toppling at Vollan and planar sliding at Ivasnasen. The study of Vollan and Ivasnasen provides useful findings for the understanding of potential present rock slope instabilities.

It has been concluded that it have been two different events at Ivasnasen, based on analyses that discovered two different back scarps. Due to the numerical modeling in Phase^2 the main triggers at Ivasnasen is the groundwater table and most likely a progressive accumulation of rock weakening, where it also include rich biotite layers. A growing tension was build up in the cracks and the slope failed.

For Vollan the analysis concludes that it is a really “slow movement” process acting. Due to the analyses that have been done until now shows that it cannot be characterized as significant movements. For this site it is important to do further investigations over a longer period to have a more determined conclusion.

The analyses that have been done in this thesis can be used as good inputs to further investigations.

Sammendrag

Analysene som er gjort av de to ustabile fjellsidene Ivasnasen og Vollan ligger i en U-formet dal i Sunndal kommune (Møre og Romsdal). Analysene er basert på detaljert geomorfologisk, struktur og geologisk feltarbeid. Dette sammen med tolkning av høy oppløselige digitale terrengmodeller (DEM) og flyfoto, LIDAR skann fra ett av områdene (Ivasnasen 2010 og 2011), numerisk analyse, kinematisk analyse, XRD analyse og laboratorietesting.

Begge sidene, Ivasnasen og Vollan er ustabile. Ivasnasen er klassifisert med en historisk hendelse og en ustabil del. Dette på bakgrunn av at den gjenstående ustabile delen av Ivasnasen er i forlengelse av bakskrenten på det tidligere historiske skredet. En tidligere hendelse på Vollan er fremdeles aktiv og det er viktig å analysere eventuelle framtidige konsekvenser.

Den tidligere topografien ved Ivasnasen er rekonstruert ved hjelp av programvaren ART (Ante-Rockslide Topography). Volumberegning er gjort ved hjelp av programvaren SLBL (Slope Local Base Level) hvor deretter en manuell rekonstruksjon av topografien ved hjelp av PolyWork (også programvare) er blitt gjort. Volumberegningene for Ivasnasen viser et volum fra 5.2Mm^3 -1.2Mm^3 for det historiske skredet, og det ustabile fjellpartiet har et estimert volum på 0.6-2.1Mm^3. Programvaren Phase^2 har blitt brukt for de numeriske modelleringene. Den rekonstruerte og konstruerte topografien for Ivasnasen har blitt brukt for detaljerte analyser av parameterne og utløsningsmekanismene som påvirker skråningsstabiliteten.

Bakskrenten av Vollan består av kvartsitt, mens den består av øyegneis på Ivasnasen. Hoved utglidningsmekanismene er "toppling" på Vollan, mens det er planar utglidning på Ivasnasen. Resultatene fra studiene gjort på Vollan og Ivasnasen gir gode indikasjoner for å forstå eventuelle framtidige utglidninger.

Det har blitt konkludert med to tidligere utglidninger for det historiske skredet ved Ivasnasen på bakgrunn av de to synlige bakskrenter. Ved numerisk modellering i Phase^2 har hoved utløsningsmekanismene vist seg og mest sannsynlig å være progressiv forvitring av bergarten, hvor det også er rike biotitt lag. En økende trykkspenning ble mest sannsynlig bygd opp i sprekkene og utglidning var dermed et resultat av dette.

På Vollan har det blitt konkludert med at det er en pågående veldig sakte bevegende prosess som skjer. Analysene som har blitt gjort viser at det ikke kan bli karakterisert som signifikant bevegelse. Det er derfor viktig med videre undersøkelser over en lengre tidsperiode for å få en mer fastslått konklusjon. Analysene som har blitt gjort, kan brukes som godt informasjonsgrunnlag til videre undersøkelser.

Preface and acknowledgements

This master's thesis is part of my master's degree in engineering geology. It is written in collaboration with The Geological Survey of Norway (NGU) and Norwegian University of Science and Technology (NTNU). The fieldwork started already summer 2011, continued through the autumn and started again when it was free of snow in 2012. The analysis and writings has been done from January 2012 to the end of November 2012. This thesis is equivalent to 60 credits (ECTS), and accomplishes the master's degree in engineering geology at the Department of Geology and Mineral Resources Engineering at NTNU.

The thesis was signed after my exchange year in Switzerland (2010) that got me in contact with Thierry Oppikofer (co-supervisor) at the NGU. The topic for this thesis was suggested by Oppikofer after a summerjob at the NGU, summer 2011. My supervisor Krishna Panthi at NTNU, was contacted and also helped with the formulations.

I want to thank my co-supervisor, Thierry Oppikofer, for all the help and learning he has given me during this thesis, I have learned a lot from him! He has given advices and he really knows everything about unstable rock slopes! This thesis would not have been the same without him and his knowledge, encouragement and helpfulness.

To my supervisor at the university, Krishna Panthi, thank you for your expert advice during the writings of my thesis.

All the softwares that have been used trough this thesis has been available through the university and NGU, all thanks for that.

A special thanks to my husband and my family that always believes in me. For giving me motivation and inspires me. Without you there would not have been any me. Especially thanks to my husband, Victor, who always shows such an interest in geology when we are hiking, and for joining me as an assistant for my fieldwork.

To my fellows at my study and desk –thank you so much for all the good tea-times, study group and for being my friends! To Nina Helen Lønmo and Yngvild Solberg Kvalvik for being such great friends to join me on my fieldworks, even when it was a bit risky. To Nina Ulfstein for reading through my thesis, giving valuable feedback and for giving good motivation!

Trondheim, 30th November 2012

Gudrun Majala Dreiås

Table of content

1.0 Introduction

During the last several glaciations of Norway, the topography has been formed and contains unique large and steep valleys. These valleys give Norway a different landscape compare with other countries, and tourists are visiting Norway just to get a view of this unique landscape. It is true that the view is amazing, but there are also hazards threatening because of the potential of rock slope failures. Since the last glaciation period in Norway (~12000 years BP), the Norwegian fjords have had numerous large rock avalanches that caused catastrophic tsunamis in the narrow fjord. The failures in Loen (1905 and 1936) and Tafjord (1934) (villages in the western part of Norway) are examples of rock avalanches with disastrous consequences (Braathen et al., 2004, Oppikofer et al., 2012). Historical data shows that Møre & Romsdal and Sogn & Fjordane (counties western part of Norway) are those counties in Norway that is most exposed to rock avalanches and injuries that can cause death in Norway (Henderson and Saintot, 2007).

The topography of Norway is the main reason for the numbers of huge rock avalanches with serious injuries in the history, and is still threatening. The database of Geological Survey of Norway (NGU) contains a huge amount of historical events from long time ago to present date. NGU has also registered unstable rock slopes many places in different sites of Norway, where the counties of Møre & Romsdal, Sogn & Fjordane and Troms has the highest amount of unstable rock slopes.

A report from NGU in 2010 describes that 11 historical rock avalanches has taken place in Sunndal, and 5 new potential rock avalanches has been identified (Dalsegg et al., 2010). Sunndal is a valley that reach approximately 35 kilometer WNW-ESE, have steep valleysides with a U-formed shape that is formed by the ice erosion (Dalsegg et al., 2010, Saintot et al., 2008). It is Ivasnasen and Vollan close to the village Gjøra, which will be researched to get a better understanding of in this thesis.

The main reason with the thesis is to consider the potential for a huge rockslide to happen in elongation of the historical rockslide at Ivasnasen. This through use of numerical analysis, kinematical analysis and LiDAR (Light Detection And Ranging laser) data. New methods (the Slope Local Base Level (SLBL) and Ante-Rockslide-Topography (ART)) have been used at Ivasnasen to get a detailed volume estimation of the site. At Vollan it was important to do detailed fieldwork to get a good impression of the site. Structural measurements was done with geological mapping, these information were thereafter used in kinematical analysis of the unstable rock slopes. The structural measurements from Vollan and Ivasnasen were also used to draw a geological profile of the entire area.

LiDAR scans of Ivasnasen were done in 2010 and 2011, it were used a terrestrial scanner (ground borne) and an airborne scanner. The results from the scans are representative to the structural field measurements for the sliding surface.

It has been some problems in the field to get good measurements of the joint sets, since the terrain at Vollan and Ivasnasen are steep and inaccessible. The inaccessible terrain is also the main reason why the scan has been taken at Ivasnasen, to make it easier to get a better understanding of the joint sets. It is more difficult to get good scans at Vollan since the area is so big and inaccessible. Any LiDAR scans at Vollan have therefore not been performed.

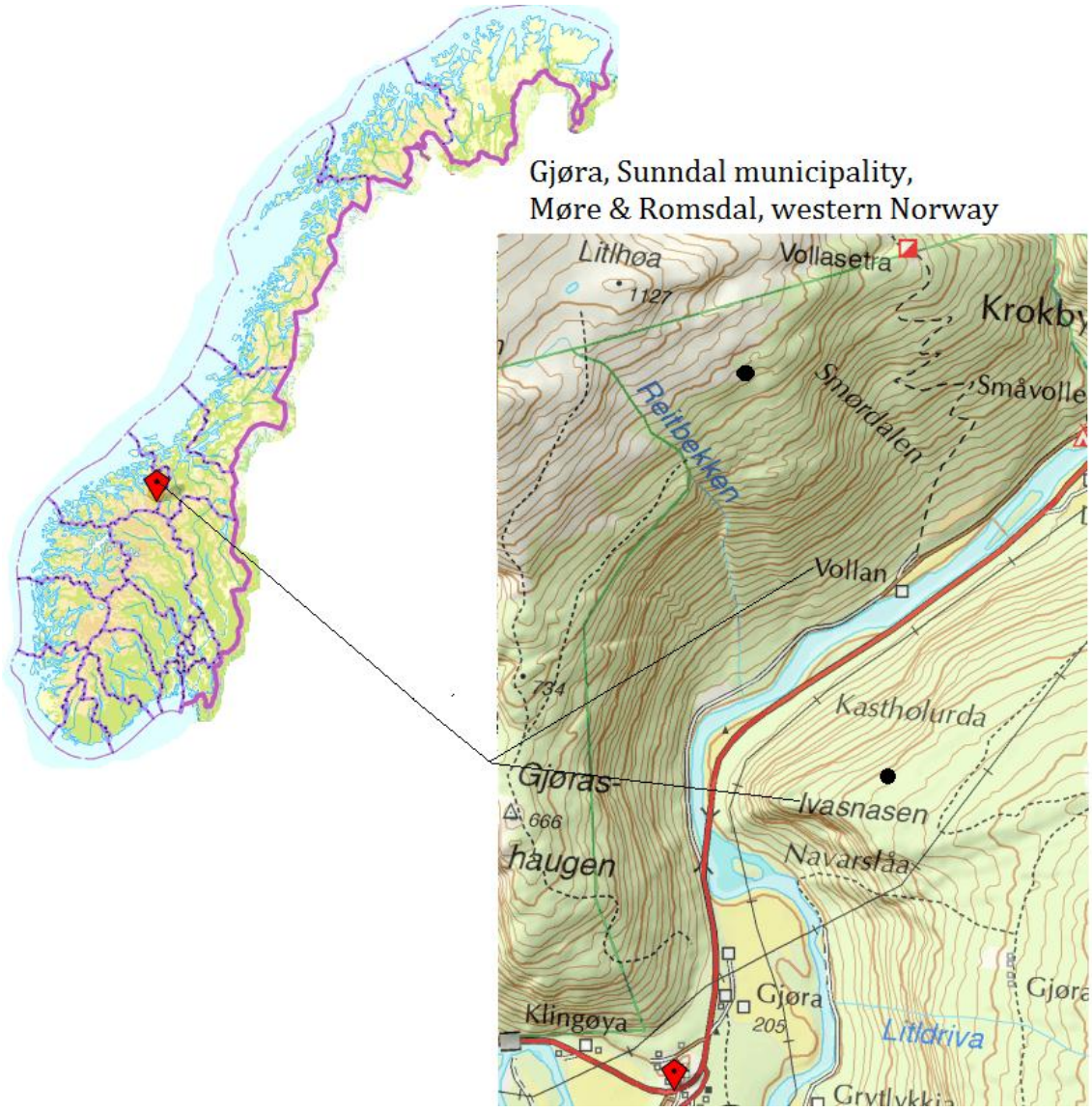

Figure 1 Overview of the study area, the map are found from www.norgeskart.no, overview of Norway and a zoom in to Ivasnasen and Vollan (areas are marked with black dots, scale 1:500m).

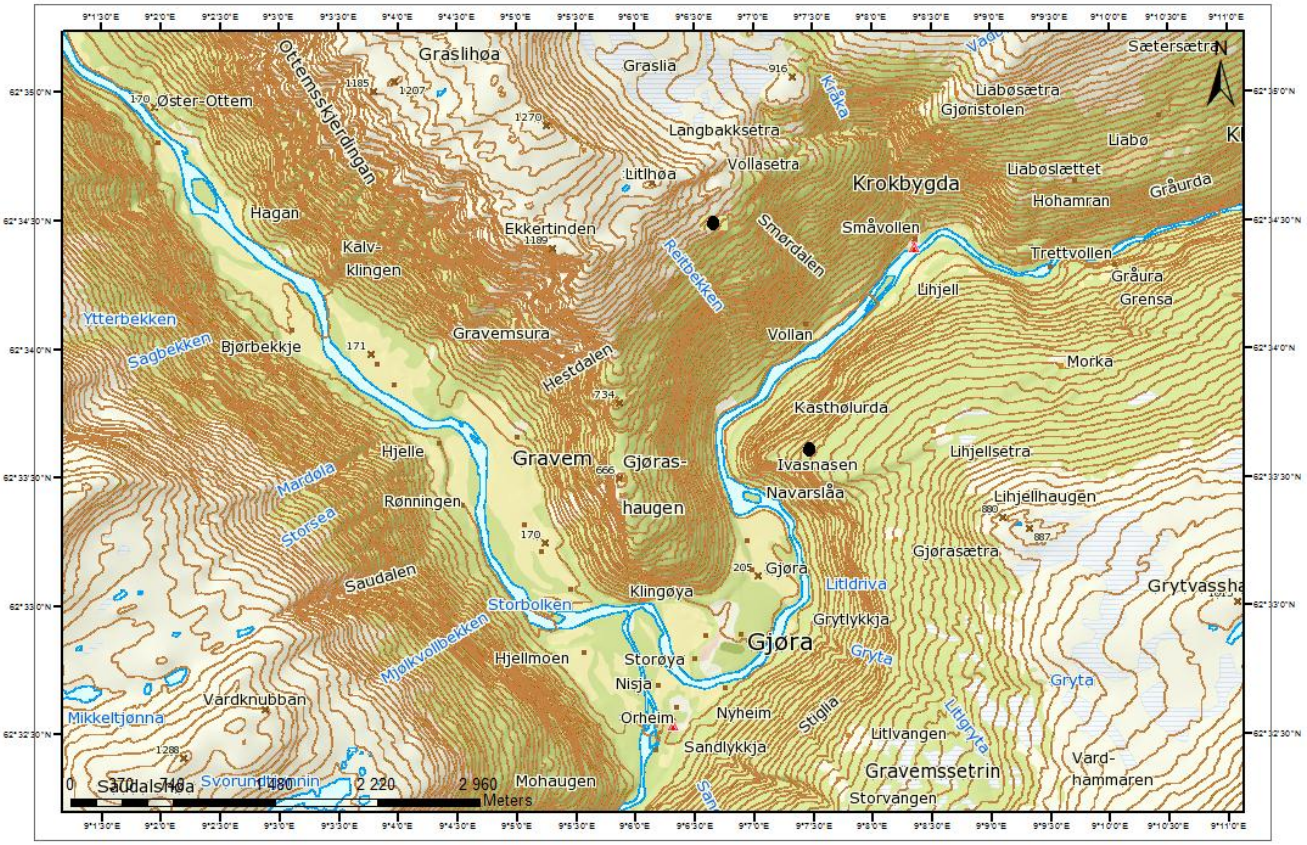

Figure 2 Ivasnasen and Vollan on a topographic map made from ArcGIS, shows part of the valley Sunndal and the river Driva running through.

1.1 Background

Ivasnasen was discovered during a helicopter survey in August 2007. Vollan was observed on aerial photos during the winter of 2007 (Saintot et al., 2008). Based on the article from Saintot et al., (2008) it was decided that the potential unstable rock slopes in Sunndal needed more analysis to get a better knowledge about the area. This thesis has done the investigation of the unstable rock slopes close to the village Gjøra. An investigation of a potential large-scale failure by using numerical modeling, kinematic analysis and LiDAR (Light Detection and Ranging laser) scans of the slope has been done.

A national webpage called "www.skrednett.no" is in collaboration between governmental units in Norway (Norges vassdrags- og energidirektorat (NVE), Norges geologiske undersøkelser (NGU), Statens vegvesen, Jernbaneverket og Forsvarets militærgeografiske tjeneste) established to register all forms of landslide occurrences. NVE has the main responsibility for the webpage. At skrednett.no it is possible to zoom in on a map to see if there have been any registered landslides in the past. Figure 3 shows Ivasnasen and Vollan (marked with a red rectangle) after zooming in at

skrednett.no and shows the information that is available. There are no big occurrences registered at Vollan and Ivasnasen.

At Vollan it has been a snow avalanche registered the 15th of April in 1714 (marked as a blue dot in the red triangle, figure 3). In this accident there were two people killed. It is also information about "Stor Ofsen" in 1789, where Vollan were almost totally destructed. There is written that the houses were destroyed but this was most likely because of inundation. "Stor Ofsen" is the name of the inundation that happened in Norway from the 21.-23.th of July in 1789, the reason for the inundation was late snow melting, heavy precipitation and rapid exchange in temperature (also in the mountains). A lot of people lost their lives during these days in July 1789 and a lot of farms were destroyed (Roald, 2008, Dørum, 1989). Close to Ivasnasen there has been registered a block fall (black dot) dated the 14th of April in 2005, this does not give any further information to set the year for the historical rockslide event but shows sign of activity. The deposits from the historical rockslide and the steep angle of gradient give the deposits an easy way down to the main road. It is therefore not strange that some block fall do occur.

Closer to the village Gjøra there is an occurrence marked with a yellow dot (landslide) and is dated to the 22th of July in 1789. This is the most interesting information of the area, and might be related to the historical occurrence at Ivasnasen. From skrednett.no it is written: "*During Ofsen 22/23th of July in 1789 was the farm Gjøra, on the northern side of Driva (river) exposed for big damages. West of the farm the water pressed out huge rock masses. The rock masses slide out abeam the river to the northern side where the avalanche went above the cultivated land and destroyed their houses. Also a water barrage came, resulted in total destruction of the cultivated land and meadow*" (Skrednett, 2012). The description is "the farm Gjøra, on the northern side of Driva, and that the water pressed out huge rock masses that were transported with the river". Since there are not any dates for the historical rockslide at Ivasnasen, it is likely to think that it happened during "Stor Ofsen".

The process of dating the historical rockslide at Ivasnasen has been started, but the results are not finished when this thesis is delivered. When the year is set, further analyses will be possible to do.

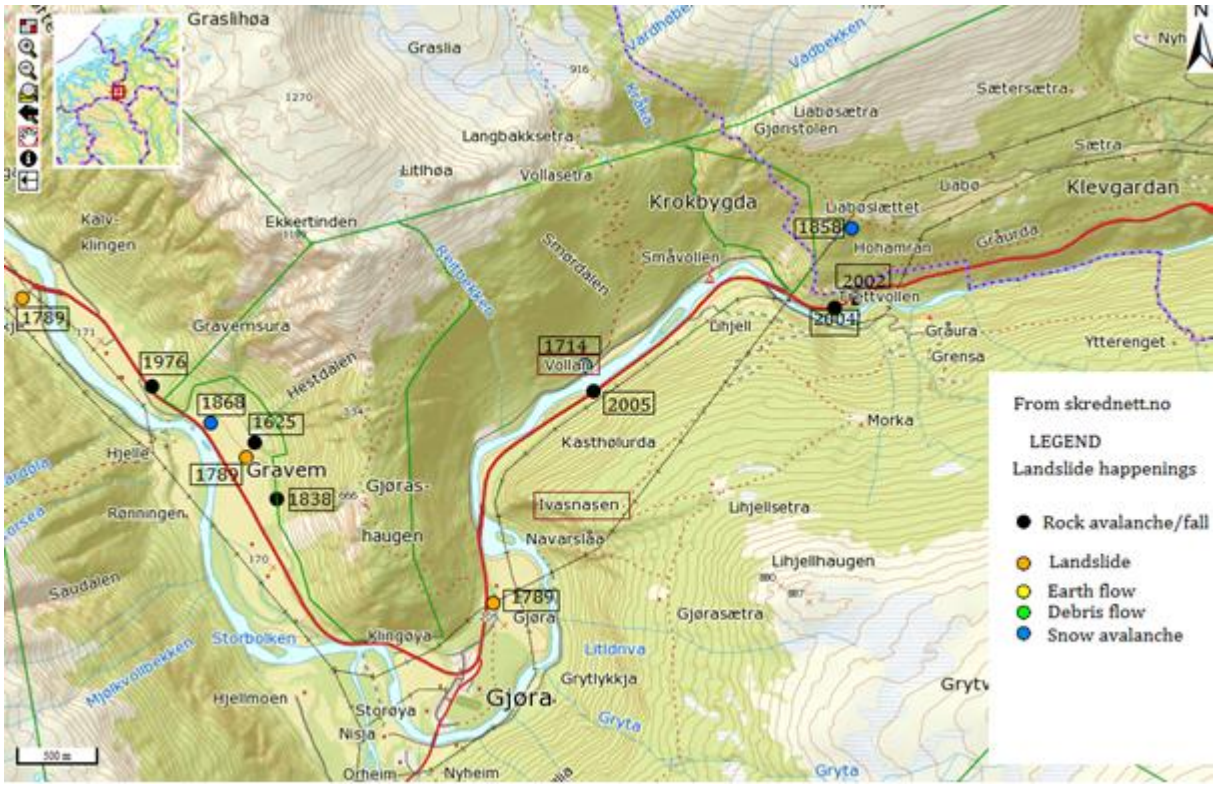

Figure 3 Modified map from skrednett.no, shows the happenings at Vollan and Ivasnasen (marked by a red triangle) and the historical happenings around Gjøra.

1.2 Aims of the thesis

This master's thesis shall focus on identifying geological, structural and engineering geological differences between the two unstable rock slopes at Vollan and Ivasnasen. The thesis shall include:

- Detailed geological mapping of both rock slopes and their surroundings, which shall also include sampling and XRD analyses, structural measurements of discontinuity sets etc.
- Geomorphological mapping of main features related to slope deformation including landslide extent, limits of sub-blocks with different deformation styles and amount.
- Quantify the present total displacements at Ivasnasen, e.g. opening of the back-scarp, and of present displacements using terrestrial laser scanning and available extensometer and differential GPS data.
- Kinematic assessment of the rock slope failure.
- Analysis of rock mass properties based on field mapping and laboratory testing
- Numerical analyses of unstable rock slopes and of the past rock slide that occurred at Ivasnasen

1.3 Available data

- Articles from Saintot et al 2008 and 2011
- GPS report from Eiken, T., 2011
- Digital Terrain Model (DEM), Statens kartverk
- LiDAR scan, 2010 and 2011, from Oppikofer, T., NGU

2.0 Theory on rock slope failures

2.1 Rock slope principles

The terms rock avalanche and rockslide are both subtitles of a landslide. There are two characteristics that can describe and classify any landslide, these are the material and the type of movement (Cruden and Varnes, 1996). The description of an avalanche is "*An avalanche is rapid gravitational movements of wet or dry rock debris, snow or their mixture, occurring on steep slopes. These mass movements are also called "catastrophic", because rapid often means faster than an escaping human can run and the speed of large avalanches can be as high as 50-80ms^{-1}*" (Voight, 1978, Blikra and Nemec, 1998). The content of the material in the landslide describes the type of the process (example rock, soil, earth). Landslides are often classified by the type of movement (examples slide, topple, flow). Occasionally the single event is more complex, where a combination of different types of movement and materials are involved. Their analysis often requires detailed interpretation of both landforms and geological sections, or cores. "*Landslides occur when gravitational and other types of shear stresses within a slope exceed the shear strength (resistance to shearing) of the materials that form the slope*" (Meng, 2012). Continuously processes can build up the shear stress, including the gradient of the slope, natural erosion or excavation, loading of the slope, water infiltration and a rise in the ground water table. Natural stresses, such as earthquakes and heavy precipitation, can be triggers for a landslide. The shear strength is dependent of the frictional strength and the cohesive strength, where the frictional strength, which is resistant to moving and the cohesive strength, is the bonding between the particles (Meng, 2012).

The types of materials (table 1) are from Varnes's classification (1978) and are divided in rock, debris and earth. The movement to a landslide is divided into five different types of movement: falls, topples, slides, spreads and flows (Cruden and Varnes, 1996).

Table 1 Varnes's material and movement classification, from Cruden & Varnes (1996).

	Type of material		
		Engineering soils	
Type of movement	Bedrock	Predominantly coarse	Predominantly fine
Fall	Rock fall	Debris fall	Earth fall
Topple	Rock topple	Debris topple	Earth topple
Slide	Rock slide	Debris slide	Earth slide
Spread	Rock spread	Debris spread	Earth spread
Flow	Rock flow	Debris flow	Earth flow

The displacement of materials in a rockslide is along one or different discrete shearing surfaces. The sliding can occur along a broadly planar surface (translational slide, figure 4 B) and extend downward and outward, or as a rotational slide (figure 4 A) along a concave-upward shear surfaces. A translational slide typically takes place along structural features, such as a bedding plane or interface between resistant bedrock and weaker overlying material. "*A translational slide is sometimes called a mud slide when it occurs along gently sloping, discrete shear planes in fine-grained rocks (such as fissured clays) and the displaced mass is fluidized by an increase in pore water pressure*" (Meng, 2012). The axis of a rotational slide is roughly parallel to the contours of the slope in a rotational slide (Meng, 2012).

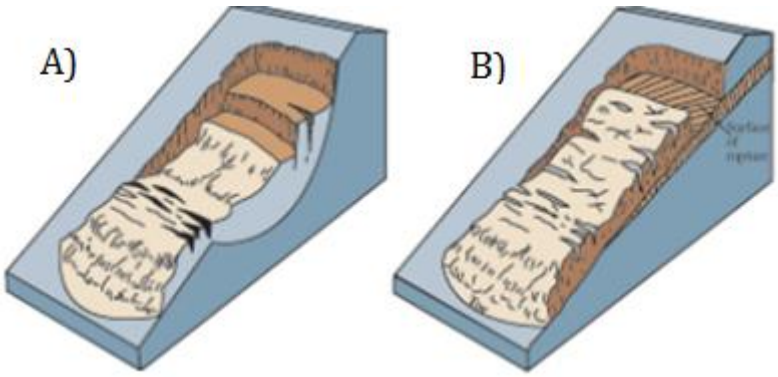

Figure 4 Illustrates A) Rotational slide and B) translational slide (USGS, 2006).

Avalanche is described as a sudden, rapid movement of disaggregated ice, snow, earth or rock down a slope (Kearey, 2001). An avalanche has a huge volume (up to millions of tons) of avalanching rock or debris. It is triggered by earthquake shock or torrential rain in mountainous relief with steep gradient. The avalanche can reach a velocity of more than 50meters per second and leave a long trail of destruction (Meng, 2012).

For all the bedrock that exists there are joints and gouges, and a chemical disintegration will occur when the water infiltrates in these. The variations in temperature and frost weathering can case a slope failure and open cracks if circumstances like angle, fall and terrain are correct. Due to the deposits it is possible to calculate if the occurrence has been a rock fall, rockslide or a rock avalanche (Sørbel, 2011).

Table 2 shows the definition of each terminology that is used for figure 5. The terminology is picked from Cruden & Varnes (1996) and Wyllie & Mah (2004). Figure 5 shows the idealized path of the terms that is used for a landslide and is found from an article in USGS (2006). These terms can be used in all categories of landslides; even if it is rocks, debris, earth or snow. As described earlier, it is the content of the material in the landslide that describes the type of the process and landslides are often classified by type of movement (Meng, 2012).

Table 2 Definitions of landslide features, from Cruden & Varnes (1996) and Wyllie & Mah (2004).

Name	Definition
Crown	Practically undisplaced material adjacent to highest parts of main scarp.
Main scarp	Steep surface on undisturbed ground at upper edge of landslide caused by movement of displaced material away from undisturbed ground; it is visible part of surface of rupture.
Head	Upper parts of landslide along contact between displaced material and main scarp.
Minor scarp	Steep surface on displaced material of landslide produced by differential movements within displaced material.
Main body	Part of displaced material of landslide that overlies surface of rupture between main scarp and toe of surface rupture.
Foot	Portion of landslide that has moved beyond toe of surface of rupture and overlies original surface.
Toe	Lower, usually curved margin of displaced material of a landslide, most distant from main scarp.
Surface of rupture	Surface that forms (or that has formed) lower boundary of displaced material below original ground surface.
Toe surface of rupture	Intersection (usually buried) between lower part of surface of rupture of a landslide and original ground surface.
Surface of separation	Part of original ground surface, now overlain by foot of landslide.

An avalanche path has three well known terms, figure 5 (right). The releasing area is located at the top of the path where the topography is steeper than 30 degrees. The releasing area can be related to the crown and the main scarp on figure 5 (left). The avalanche channel is where the avalanche will pass without leaving much material behind, the slope angle is here around 30-10 degrees. The avalanche channel can be related to the main body at figure 5 (left). In the bottom of the path is the discharged area, where all the materials that have been transported by the avalanche will be deported, and is the toe of the figure.

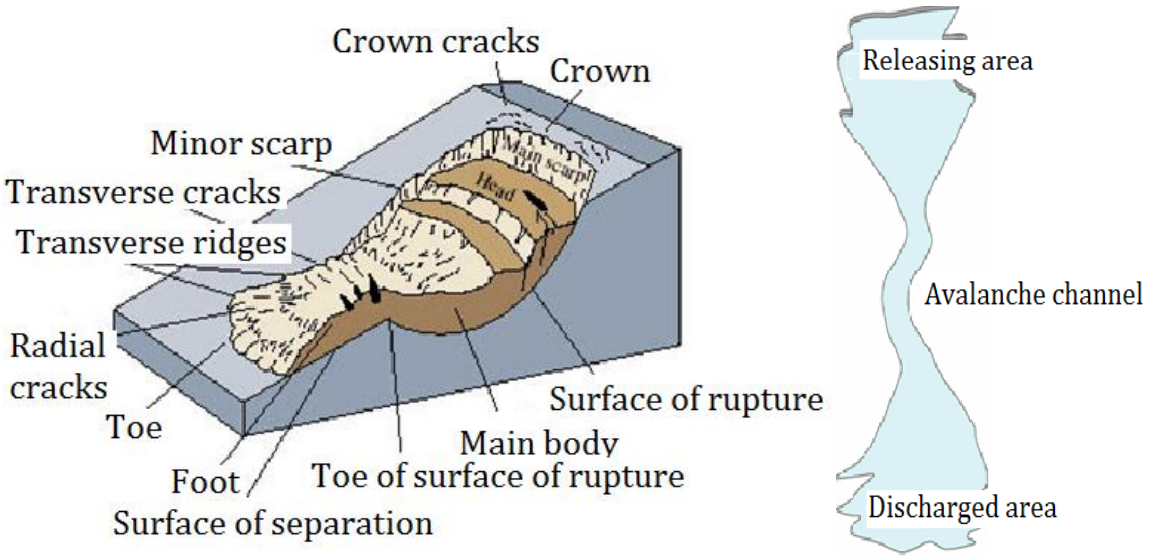

Figure 5 Left: Terminology for the avalanche processes modified from USGS 82006. Right: avalanche path, modified from NGI (NGI, 2012).

There are many potential causes for an avalanche, and different trigger mechanisms are classified by terms: geological, morphological, physical and human activity. All these terms that is listed are important trigger factors for an avalanche. If more than one condition takes place, it can cause a terrible accident, and in worst case –life can be threatened and infrastructure can be destroyed. Many small efforts may be done in order to secure an area of such hazardous events. One example is to remove the water influence to reduce the water pressure, no blasting is another, and no removing of masses in these areas and so on. It is easier to take care of those triggers that are human made, since the geological conditions is naturally placed, it is what it is. But it is important having knowledge about all the aspects of the triggers to better know what to do and a detailed knowledge of what the triggers can be for each site.

The listed terms have been found in Wyllie & Mah (2004) and Cruden & Varnes (1996):

Geological:

- Weak and sensitive material
- Weathered material
- Jointed and cleaved material
- Negative discontinuities and foliation
- Contrasts in permeability or stiffness
- Shear strength
- Faults and shear zone
- Structures in the bedrock

Morphological:

- Tectonic or volcanic uplift = tilting
- Glacial rebound
- Fluvial, wave or glacial erosion of the slope toe and lateral margins
- Slope topography –exceptional stable above 30-35 degrees

Physical:

- Water and groundwater pressure
- In-situ stress conditions
- Freeze- and thaw weathering
- Seismic activity –caused by earthquake
- Removed vegetation (caused by fire, exsiccate)
- Rapid snow melting and intense precipitation
- Gravitation –force of gravity
- Wind
- Vegetation –can keeps the ground steady, but also cause root action
- Erosion in the zone; rivers and waves can erode the toe of a slope
- Shrink and swell weathering

Human activity:

- Excavation and groundwork of the slope or toe
- Loading of slope or its crest (supply of masses) or mass movement
- Deforesting
- Imitated watering
- Mining
- Artificial vibrations (blasting etc.)
- Water leakage
- Damming
- Drawdown (of reservoirs)

Figure 6 is illustrating the triggering mechanism for slope failures that is listed, in a good and understandable way and is found in Jaboyedoff et al. (2005).

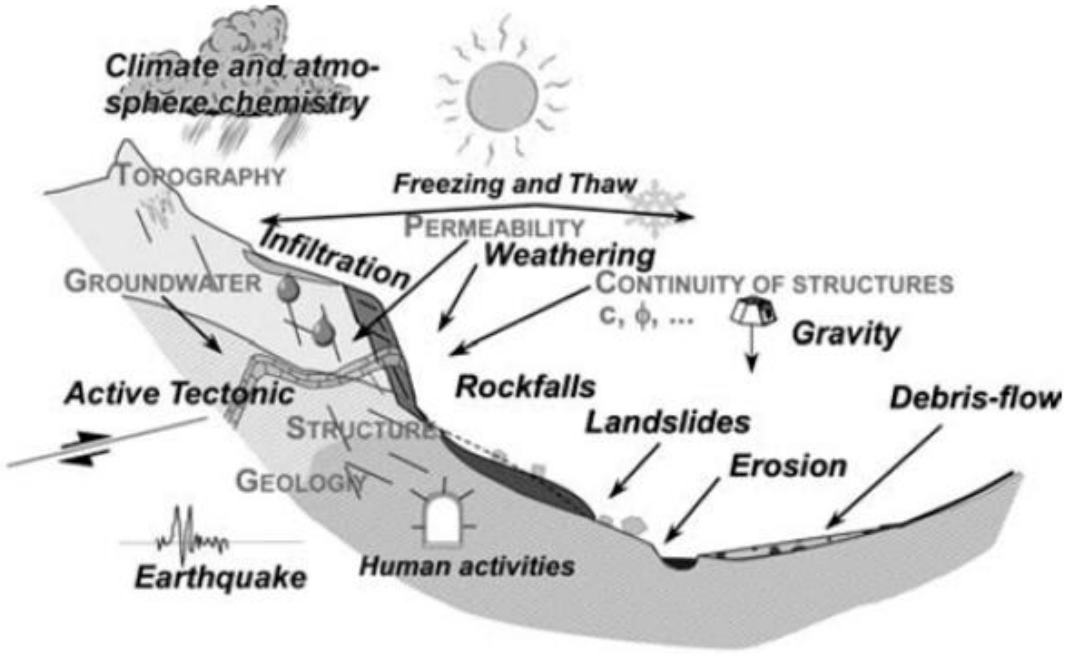

Figure 6 Illustration of the trigger mechanism for slope failure. The roman font represents the internal parameters and the italic font represents the external factors (Jaboyedoff et al., 2005).

2.2 Different slope failure mechanism

The different category of slope failure depends on the total volume of the deposits and the sizes of the blocks. In-situ there is not easy to tell what kind of failure it is, most of the time the failure can be a combination of different kind of mechanism. A rock slope failure is where part of the mountainside slides out. A weathering process can result in part of the mountain side slides out. The volume for rock avalanches are greater than 100 000 m^3, a rock slide has a volume greater than 1000 m^3 and a rockfall has a volume less than 100 m^3 (Nilsen and Broch, 2009, NGI).

2.2.1 Rockfall

Rockfall (figure 7) can be a single block that has slipped out to a few cubic meters of masses in total (not more than 100 m^3). The single blocks are not bigger than it can be moved manually. These processes is often caused by freeze- and thaw weathering. The freeze- and thaw weathering is a mechanical disintegration where water penetrates in joints and a frost weathering can occur. The weathering is caused because of the increase in volume, when water goes from liquid to ice it expands with 9%. The

weathering is effective when the temperature is around- 5 ^{0}C, and all liquid water is frozen. Frequently block fall is a detail stability problem, this because it might be an early warning of an upcoming major event. Rockslide has bigger volume (around 20 000 – 100 000 m^3) and the sizes of the blocks are also bigger (Cruden and Varnes, 1996, Nilsen and Broch, 2009).

A rockfall starts from a steep slope along the surface, and contains either soil or rock with no or little shear displacement. The terminology falling, bouncing or rolling describes how the material descends. The movement of a rockfall is very rapid to extremely rapid. The forward motion of the material below is often sufficient for free fall in the slopes and exceed 76 degrees, angle below this will dominate of rolling (Cruden and Varnes, 1996, Kearey, 2001).

Figure 7 Illustrates rockfall (USGS, 2006).

2.2.2 Toppling failure

A toppling failure is also described as topples (figure 8). These failures are distinguished by the forward rotation of a rock or rock masses, with a plate-shaped or flakes shape, about a point or axis below the center of gravity of the displaced mass or low in the mass. The assumption for this failure to take place is a marked, steeply standing joint set with an almost parallel dip to the slope. The action of gravity and forces exert by adjacent masses in cracks, and the joint sets must fall out from the slope (USGS, 2006, Couture, 2011, Cruden and Varnes, 1996, Nilsen and Broch, 2009). A toppling often starts with a rotation of a fixed block. This rotation arise when this block is removed by the tallest columns of blocks topple because their center of gravity lies outside the base. The tension crack is often wider at the top than at the base (Wyllie and Mah, 2004).

Toppling can also be rotation of other materials than rock masses. It can also contain debris, or earth, outward from a steep slope face. This type of movement can subsequently cause the mass to fall or slide (Meng, 2012). This failure of movement range from extremely rapid to extremely slow, sometimes accelerating throughout the movement (Cruden and Varnes, 1996).

There are also different types of toppling; flexural toppling, block toppling, chevron topples, block-flexure toppling, secondary toppling modes and a complex rock topple – rockslide (Wyllie and Mah, 2004). Goodman and Bray (1976) described flexural toppling as: "*A flexural toppling occurs in rocks with one preferred discontinuity system, where the continuous columns break in flexure as they bend forward because of a sliding, undermining or erosion of the toe. And that this failure occurs most in thinly bedded shale and slates, phyllites and schists, which orthogonal jointing is not well developed".* Block toppling is individual columns that are divided by widely-spaced joints, and occurs in strong rock, individual columns are formed by a set of discontinuities dipping steeply into the face. A second set of widely spaced orthogonal joints will then define the column height. The short columns forms the toe are pushed forward by the loads from overturning columns behind. The toe will slide and further toppling may develop further up (Wyllie and Mah, 2004, Cruden and Varnes, 1996). Chevron topples are block topples where the dips and the toppled beds are constant. The change of dip is concentrated at the surface of rupture (Cruden et al., 1993). Block-flexure toppling is pseudo-continuous flexure of long columns through accumulated motions along numerous cross joints, and results from accumulated displacements on the cross-joints. Here the failure takes place because of a large number of small movements, and there are fewer tension crack, edge-to-face contacts and voids than in the other toppling mechanism (Goodman and Bray, 1976, Wyllie and Mah, 2004). Secondary toppling modes are initiated by some undercutting of the toe of the slope. These can be natural agencies or human made activities. Sliding or physical failure of the block are the primary failure in all cases. The toppling will occur in the upper part of the slope as a result of this primary failure (Wyllie and Mah, 2004). A complex block topples – rock slide is several distinct movements, and may be identified as a movement with modification of water flows (Giraud et al., 1990).

It is always important to analyze the dimension of each block in a toppling analysis. In some cases there may be circumstances where there are external forces acting on the stability of the slope, like water forces acting on the sides and bases for the blocks, earthquake acting on each block and point loads produced by example bridge priers (Wyllie and Mah, 2004).

Figure 8 Illustrates toppling failure (USGS, 2006).

2.2.3 Plane failure

A failure through a planar slide is the most common slope failure mechanism in strong and not weathered rock masses. If the overlying material moves as a single, little-deformed mass, it is called a planar slide or a block slide, (figure 9). This type of failure happens along a weakness zone. The failure can goes through a single plane or through a surface of fracture that exists of different parallel, originally disconnected weakness zone. The failure happens in rock containing persistent joints dipping out of the slope face, and striking parallel to the face (Meng, 2012, Wyllie and Mah, 2004, Nilsen and Broch, 2009).

There are different conditions that must be complied with if a planar failure can occur. These are picked from Nilsen & Broch (2009) and Wyllie & Mah (2004):

1. The plane on which sliding occurs must strike parallel or nearly parallel to the slope face (the angle of intersection of the horizontal plane must be less than about 20^0).
2. The angle of the surface of fracture must be less than the slope; the surface of fracture must be outgoing in or above the foot of the slope. This means that the dip must be less than the dip of the slope face, $\psi_p < \psi_f$ (see chapter 2.3).
3. The frictional resistance or the shear strength along the sliding plane must conquer the driving forces. So that the dip of the sliding plane must be greater than the angle of friction of this plane, $\psi_p > \phi$.
4. The upper end of the sliding surface either intersects the upper slope, or terminates in a tension crack.
5. It must be joints or plane of weakness that is oriented so the rock masses are not too highly restrained at the sides.
6. Release surfaces that provide negligible resistance to sliding must be present in the rock mass to define the lateral boundaries of the slide. Alternatively, failure can occur on a sliding plane passing through the convex “nose” of a slope.

It is often a relief plane behind the rock masses, called a tension crack, when a planar failing happen. This tension crack has also an influence that the failure can occur (Nilsen and Broch, 2009, Wyllie and Mah, 2004). There is also often water entering the sliding surface and fill the vertical tension cracks and cause an atmospheric pressure where the sliding surface daylights in the slope face. Then the normal stress, σ, will act at the surface and a failure rock mass can occur. There are only the water present in the tension cracks along with the sliding surface that influences the stability of the slope, this is not the whole truth since this is the same as saying that the rock mass are impermeable, something that it is not true. This is because water pressure may develop only in the tension cracks in rare conditions example; heavy rainstorm after a long dry period or freezing where the frost penetrates only a few meters behind the slope face.

The presence of water reduces the stability of a sliding surface with 10% (Wyllie and Mah, 2004).

Seismic activities also reduce the stability and these five slope parameters have been developed by Keefer (1992) to give facts about the greatest influence on stability during earthquakes (Wyllie and Mah, 2004, Keefer, 1992):

1. Slope angle –rock falls and slides rarely occur on slopes with angles less than about 25^0.
2. Weathering – highly weathered rock comprising core stones in a fine soil matrix, and residual soil are more likely to fail than fresh rock.
3. Induration – poorly indurated rock in which the particles are weakly bonded is more likely to fail than stronger, well-indurated rock.
4. Discontinuity characteristics –rock containing closely spaced, open discontinuities are more susceptible to failure than massive rock in which the discontinuities are closed and healed.
5. Water – slopes in which the water table is high, or where there has been recent rainfall, are susceptible to failure.

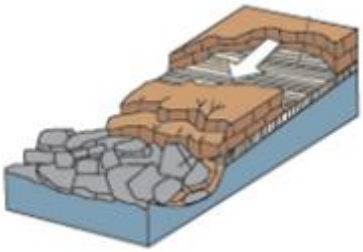

Figure 9 Illustrates a block slide, or planar sliding (USGS, 2006).

2.2.4 Creep

Creep (figure 10) is described as a "slow, steady, downward movement" of slope-forming soil or rock. The process is a continuous movement which proceeds at an average rate of less than a foot per decade, a deformation that continues under constant stress (Cruden and Varnes, 1996). It is a largely continuous process of deformation occurring below the elastic limit in response to prolonged stress, all deformation that is not wholly elastic. Movement is caused by shear stress sufficient to produce permanent deformation, but too small to produce shear failure. There are three types of creep, where one is seasonal and the movement is within the depth of soil are depended of the seasonal changes in soil moisture and soil temperature. The second one is continuous creeps, where shear stress continuously exceeds the strength of the material. The last, the third one is the progressive creep, where slopes are reaching the point of failure as

other types of mass movements. Generally creep is indicated by curved tree trunks, bent fences or retaining walls, tilted poles or fences and small soil ripples or ridges (USGS, 2006, Kearey, 2001).

This is an extremely slow rate of movement and "creep" is not a recommended term to use today. It is better to use the terminology 'very slow or extremely slow movement' (Couture, 2011). According to Cruden & Varnes (1996) the term very slow and extremely slow are defined as <1,6m/year (very slow) and <60mm/year (extremely slow), while the rapid or extreme rapid downslope movement are defined as >5m/sec.

The extremely slow rate of a landslide movement is also characterized as "deep-seated gravitational slope deformations" (DGSD). They may represent the initial stage of slope movements which might lead to accelerated deformations and finally large-scale rock avalanches (Oyagi et al., 1994).

According to (Dramis and Sorriso-Valvo, 1994) the DGSD can be described as a group of mass movement phenomena characterized by the following conditions:

- The deforming mass may or may not be bounded by a continuous yielding surface; however, the continuity of such surface is not indispensable to explain the surficial deformations.
- The volume of masses involved is the order of several hundred thousands of cubic meters or more, the thickness is several tens of meters or more.
- Scale factors, as discussed by (Goguel, 1978), may influence the mechanical properties of rock and, consequently, the deformation mechanism.
- The total displacement is small in comparison to the magnitude of the mass.

Figure 10 Illustrates the creep mechanism (USGS, 2006).

The mechanism for a deep-seated gravitational slope deformations can be divided into three groups, see figure 12. The strain may be represented by the equation (Jaeger and Cook, 1968):

$$\epsilon = \epsilon_e + \epsilon_1\ (t) + Vt + \epsilon_3\ (t) \qquad \textit{Equation 1}$$

ϵ_e is the instantaneous elastic strain, $\epsilon_1(t)$ is the transient movement, Vt is the steady-state movement, and $\epsilon_3(t)$ the accelerating movement.

Figure 11 might be described as follows, for each region of the graph (Jaeger and Cook, 1968):

I. The strain-time curve is concave downwards; the movement in this region is called primary or transient.
II. The strain-time curve has approximately constant slope, the movement in this region is secondary or a steady-state movement.
III. The strain-time curve is accelerating; the movement in this region is tertiary and leads rapidly to failure.

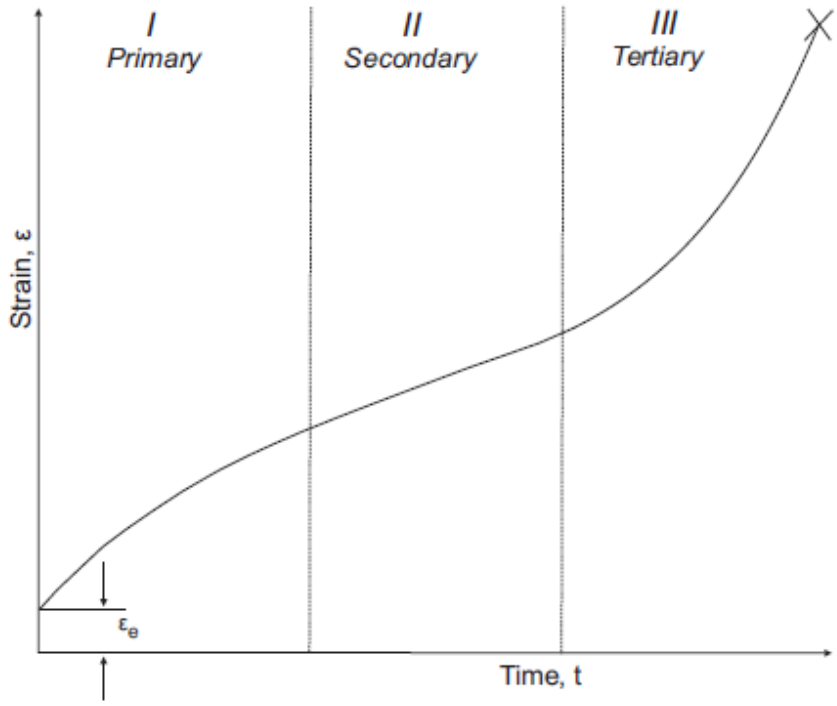

Figure 11 Idealized behavior for deep-seated gravitational slope deformations rock materials and cohesive soils movement, from (Grøneng, 2010).

2.2.5 Wedge

A wedge failure happens when the sliding occurs along the line of intersection between two planes of discontinuities that has a maintained contact on both planes (Wyllie and Mah, 2004). These two planes of discontinuities release a wedge formed rock mass that might slide with the two planes of discontinuities as sliding planes.

Some of the same conditions as for a plane failure must find place (Nilsen and Broch, 2009, Wyllie and Mah, 2004):

1. The slope angle to the line of intersection must be less than the slopes dip angle.
2. The driving forces must be greater than the friction along the sliding plane.
3. The line of intersection must dip in a direction out of the face for sliding to be feasible.

Comparing wedge failures with plane failure the wedge failure can occur over a much wider range of geological and geometric conditions. The plunge of the line of intersection is about $50\text{-}55^0$, and the friction angle of the joints around $35\text{-}40^0$. This means that the line of intersections dips steeper than the friction angle (Wyllie and Mah, 2004).

It is more complex to calculate the factor of safety on a wedge failure because it is necessary to have details about the geometry of the shear strength for the wedge and the water pressure, but each of the discontinuities sets must be above 30^0 (Wyllie and Mah, 2004).

2.2.6 Circular failure

The rock masses might slide after a double curved sliding plane. Such sliding might happen in strongly weathered and closely fractured rock masses with randomly oriented dip directions, with no systematical joint sets, but most common in uncompact material (Nilsen and Broch, 2009). A circular failure, as the name describes, is a slide surface that mostly takes form as a circle. It is, also here, the geological conditions that cause the shape of the failure. Like in a homogenous weak, weathered rock or a rock fill, the failure is likely to form as a shallow, large radius surface extending from a tension crack close behind the crest to the toe of the slope (Wyllie and Mah, 2004).

Conditions for a circular failure to take place, from Wyllie & Mah (2004):

1. Homogeneous material in the slope, with uniform shear strength properties along the slide surface.
2. The shear strength is characterized by cohesion and a friction angle.

3. Failure occurs on a circular slide surface, which passes through the toe of the slope.
4. A vertical tension crack occurs in the upper surface or in the face of the slope.
5. The factor of safety of the slope is a minimum for the slope geometry and ground water.
6. Ground water conditions vary between dry and fully saturated.

2.3 Stability analysis

The stability of rock slopes is influenced by the structural geology of the rock that naturally occurring, breaks in the rock such as discontinuities (bedding planes, joints and faults). It is also strongly influenced by the dip and the sliding surface, and also the depth of the water in the joints (Wyllie and Mah, 2004).

Slope stability can be expressed in one or more of the following terms (Wyllie and Mah, 2004);

- Factor of safety, FS –stability quantified by limit equilibrium of the slope, the slope is stable if FS > 1.
- Strain –to prevent safe operation for the slope, the failure defined by onset strains must be great enough, or the rate of movement exceeds the rate of mining in an open pit.
- Probability of failure – stability quantified by probability distribution of differences between resisting and displacing forces (probability distributions).
- LRFD (load and resistance factor design) – stability defined by the factored resistance being greater than or equal to the sum of the factored loads.

The factor of safety, FS, is the most common method for slope design. Wyllie & Mah (2004) express the factor of safety as:

$$FS = \frac{resisting\ forces\ (R^d)}{driving\ forces\ (F_d)} \qquad \textit{Equation 2}$$

Due to this equation the failure will theoretically occur when the driving forces (F_d) are larger than the resisting forces(R^d), when FS >1, as described. The driving forces can be for instance gravity and water pressure, and the resisting forces can be the roughness of

the rock, illustrated in figure 11 (Wyllie and Mah, 2004, Nilsen and Broch, 2009), please see figure 12, for the illustration of the factor of safety, FS.

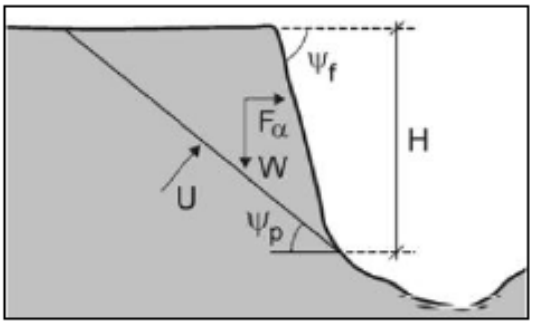

H = height of slope (m)
ψ_f = dip angle of slope (^{0})
ψ_p = dip of the sliding plane (^{0})
W = load of potential sliding rock mass (kN/m)
U = water pressure (kN/m)
α = seismic acceleration, part of g (m/s^2)
$F_\alpha = m\alpha$ = earthquake force (kN/m)
φ_{ca} = characteristic active friction angle (^{0})
$R_d = (W\cos \psi_p - F_\alpha \sin \psi_p - U)tg\varphi_{ca}$
$F_d = W\sin \psi_p + F_\alpha \cos \psi_p$

Figure 12 Illustration from Nilsen & Broch (2009) of limit equilibrium.

There is a wide experience of the factor of safety when it comes to all kind of slope stabilities. Table 3 shows a range of values of minimum total safety factors and for all types of geological conditions (Terzaghi and Peck, 1967, Society, 1992, Wyllie and Mah, 2004).

Table 3 Values of minimum total safety factor, from Wyllie & Mah (2004).

Failure type	Category	Safety factor
Shearing	Earthworks	1.3 – 1.5
	Earth retaining structures, excavations	1.5 – 2.0
	Foundations	2.0 – 3.0

2.4 Remote Sensing Technology

Remote sensing technologies include LiDAR (Light Detection and Ranging) scan, and is a strategic technology to use when analyzing slope stability. The LiDAR scanner scans the surface topography by a laser beam that sends out a point cloud of thousands of laser beam pulses per second. These laser beams measure the direction and time for sending and receiving and create a quadrate of 3-D surfaces. The scanner measures the 3-D point clouds of objects as far as 150 m along the line-of-sight. After the topography has been measured by the laser beam to an object, a 3-D digital model is being created based on the laser beams (Chan and Lau, 2007). In this thesis a terrestrial LiDAR (TLS) from 2010 and 2011 have been used to construct a high-resolution DEM (digital elevation model) and 3-D digital models. With different scans of the same area, it is possible to compare the scans for further analysis and detect if there has been any movement or not.

Terrestrial laser scanning is described as an active remote sensing technic based on the time-of-flight principle of a laser pulse that is sent out, back-scattered by the topography and recorded by the instrument. An effective resolution of 86% of the laser beam is found to be optimal, but a finer resolution is allowed by most TLS devices. For practical reasons it is useful to choose a large point spacing, where the laser will not use so much time (acquisition time), the file size will be smaller and the results will still be presentable (Oppikofer et al., 2008b, Oppikofer, 2009).

An Airborne LiDAR (ALS) dataset have also been available during the modeling for this master thesis. The Airborne LiDAR can survey a much larger area than the terrestrial LiDAR, this makes the airborne scanner more efficiently. The difference of these two methods are that the airborne LiDAR is doing the scans with help of an airplane/helicopter and use a multi-return LiDAR to measure multiple returns for each laser pulse. Each laser pulse can cover approximately one meter in diameter on ground. An advanced numerical algorithm (Interactive Closest Point) takes the last beams that comes from the ground surface and extract them and filter out error-returns (vegetation, building structures etc.). This technology is more and more common to use for remote sensing technology to produce fine-scale topographical maps and DEM (Chan and Lau, 2007).

By using the LiDAR scans we get overlapping point clouds, but it has been developed an algorithm that solves this, see figure 13. To get a better understanding about this, it can be described as the overlapping point clouds get in a common reference system, where the LiDAR uses the algorithm Interactive Closest Point (ICP) developed by Besl and McKay (1992), see equation 3, where it use a cost function ε (Besl and McKay, 1992). The cost function ε is formed by the sum of the squared distances between the points belonging to two objects A and B (Teza et al., 2007). The ICP algorithm is demonstrated in figure 13, the goal is to minimize the function to match object A and B, where A and B

can both be point clouds, surfaces or either A be the point cloud and B be the surface, (Oppikofer, 2009).

$$\varepsilon(Q) = \sum_{a \epsilon A} [Qa - N_B(Qa)]^2 \qquad \textit{Equation 3}$$

In the equation 3 where a∈A , N_B (a) ∈ B is its nearest neighbor and Q is the affine transformation given by a rot translation matrix (Oppikofer, 2009).

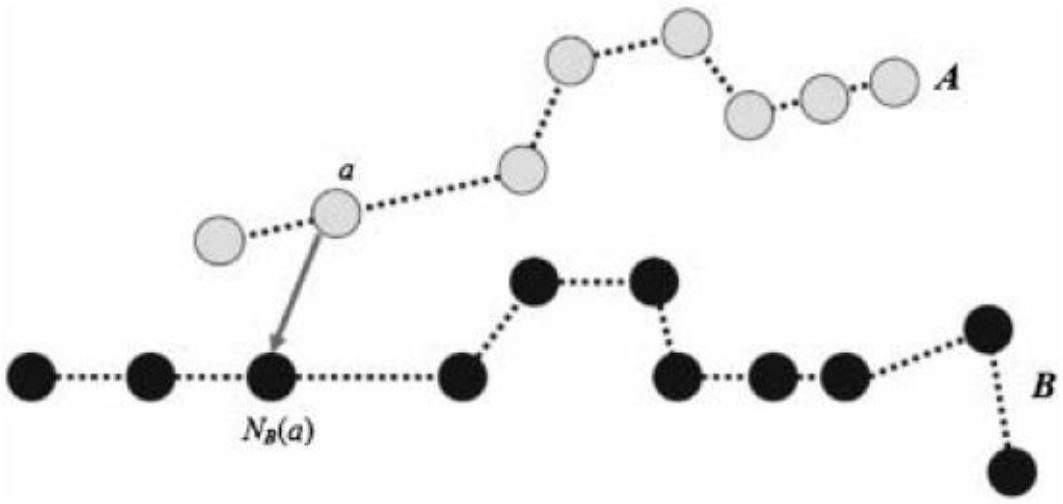

Figure 13 Principle for the ICP co-registration technique. For each point a in the dataset A, the nearest neightbour in the reference set B is found. The quadratic error is minimized by the ICP algorithm by using the affine transformations to achieve the best match (Teza et al., 2007, Oppikofer, 2009).

Figure 14 shows a flowchart over the terrestrial LiDAR. The data acquisition and analysis procedures are based on Conforti (2005). To get a complete 3D model of an area with different viewpoints and/or different view directions are acquired from TLS (Conforti, 2005). Oppikofer (2009) describes how to get the ideal scan sites for monitoring of slope movement should contain:

- Get a good view of the landslide area. Make sure to be located in front of the sliding area or around it.
- Scan stable areas, this is necessary for landslide displacement analyses to compare the sequential datasets.
- Avoid larger vegetation and other disturbing objects in the foreground of the laser.
- It should be relatively easy to access with the equipment.

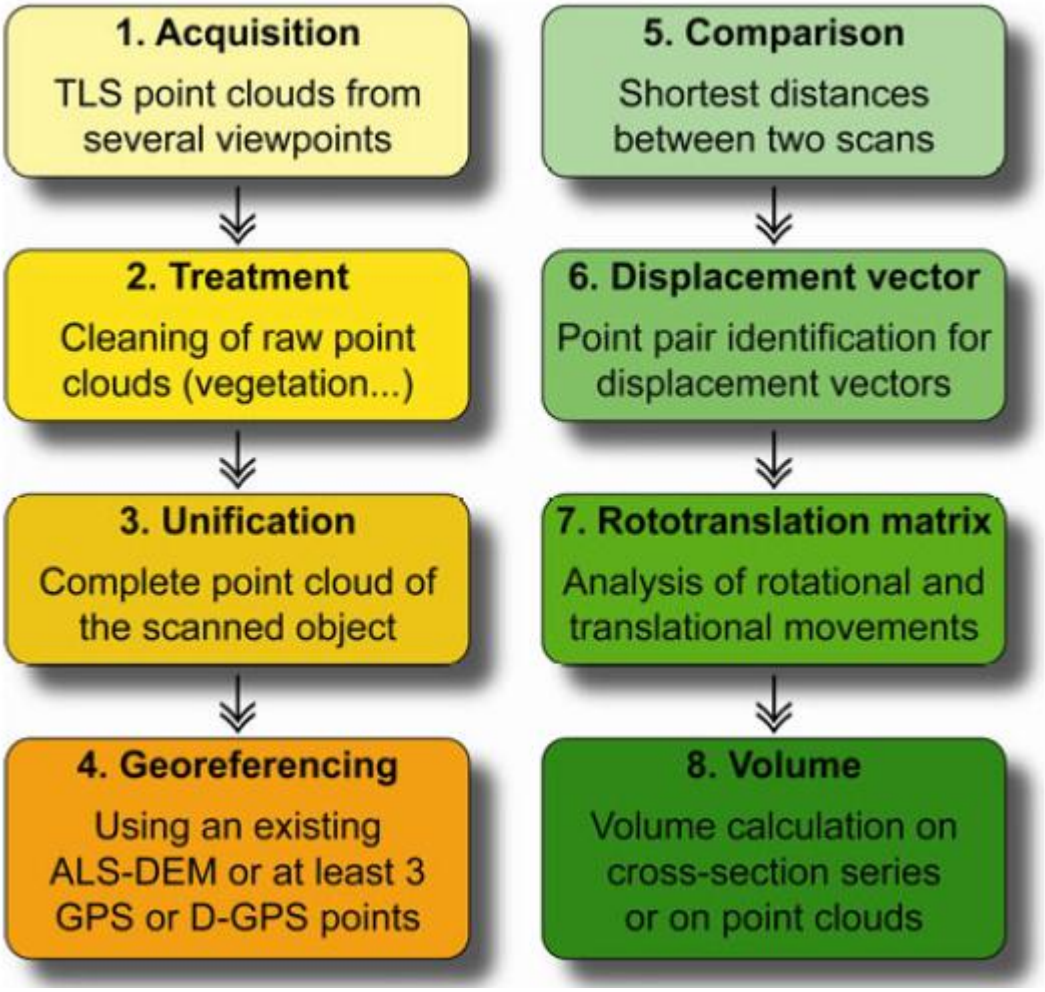

Figure 14 A flowchart of the TLS data acquisition and analysis. The yellow, left part, concerns single TLS scans. The green, right part, treats with sequential TLS point clouds, figure from (Oppikofer et al., 2008a).

Statistically, Norway will be affected by two to three big rock avalanches during a period of hundred years. Each of these accidences will cost twenty to two hundred innocent peoples life. It is not easy to tell where and when the catastrophe will be a reality, but science in the present and monitoring of the mountainside using radars and LiDAR from the ground and controls of the joints does the knowledge a bit easier. With the new technics of monitoring it is possible to give an early warning to the inhabitants when the movement is a reality (Sørbel, 2011).

3.0 Case description

The areas of interest for this master's thesis are located in Sunndal municipality, in Møre & Romsdal county, Norway. The areas that have been mapped are Vollan and Ivasnasen. These two sites are located on both sides of a river (Driva) close to the town Gjøra. The sites are located in a bedrock area, gneiss region, where the bedrock partly is affected by the Caledonian orogeny, please see figure 15.

The Western Gneiss-Region consists of granitic gneisses and migmatites formed about 1700-1500 Ma. The age of the bedrock that is dominating between Molde and the fjord of Trondheim is around 1686-1653Ma and contains of gabbroid gneiss, granitic gneiss, magmatic gneiss and granite. The geological structures in this region are a result of the Caledonian orogeny, in Silurian/Early Devonian times with the collision between Laurentia and Baltica. The Precambrian rocks along the western part of Baltica were forced down during the collision and underwent high-grade metamorphism (Nordgulen et al., 2007, Gee, 1975).

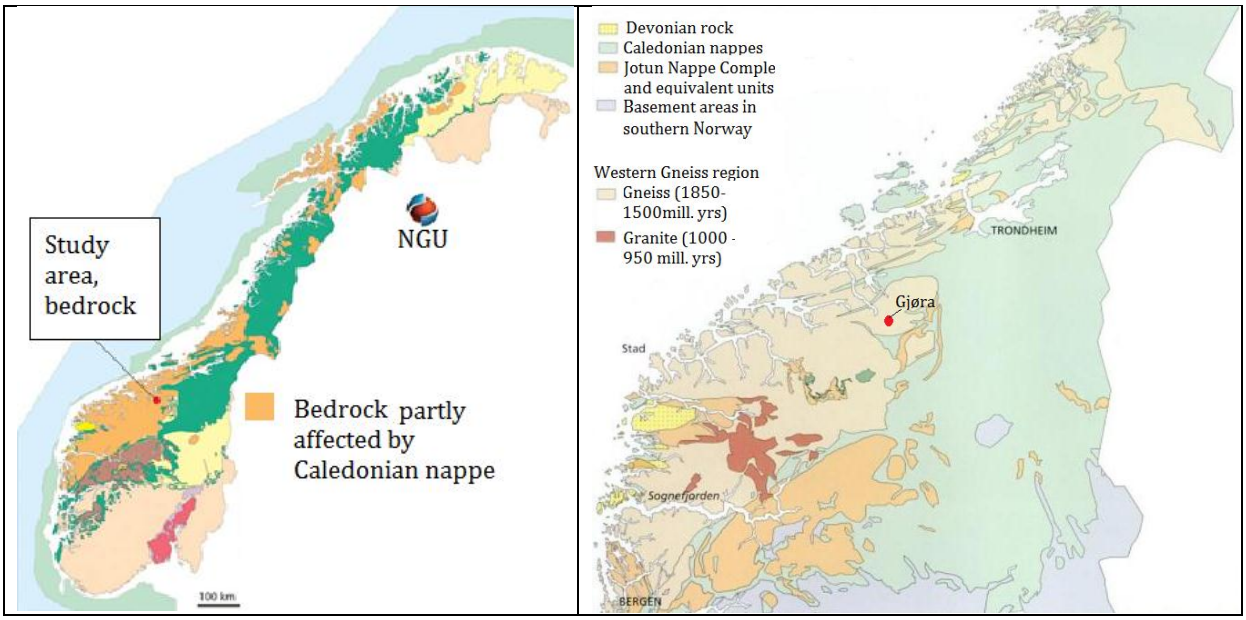

Figure 15 Left: Geological map from NGU's webpage (NGU, 2012) shows the study area where it is bedrock that dominates, in the Western Gneiss Region (WGR, scale 1:100km). Right: The major part of the WGR consist of granitic gneisses and migmatites (dated to be developed between 1700 and 1500 million years ago, scale unknown), map modified from (Ramberg et al., 2007).

3.1 Topography

The topography of Sunndal valley is really steep (figure 16) and has an average elevation of around 1200-1300 meter above sea level. The back scarp at Vollan is located around 1000 meter above sea level, and the back scarp at Ivasnasen is located at around 500 meter above sea level. The valley is a typical U-formed valley, with steadily increasing gradients from the fjord.

Figure 16 shows the area around Ivasnasen and Vollan as steep, with a potential slope angle of gradient of the entire site that might cause landslides. At Ivasnasen the processed map shows a slope angle of around 30-45 degrees, and Vollan has an angle of around 30-75 degrees. It must be taken in concern that the DEM that is used for the upper part of Vollan and the part behind the back scarp at Ivasnasen is a DEM of 10 meters. This DEM is not detailed enough to get a correct impression. The DEM that covers Ivasnasen (the unstable rock slope and the historical rockslide part), also including the lower part of Vollan have a DEM of 1meter. This part with a DEM of 1meter is therefore more precise and reliable, than the upper part of Vollan with a DEM of 10meter. The DEM of 10meter is more inaccurate, and it seems like the degrees of the slope angle gradient are too high, compare to the lower part. With the DEM of 1meter for the lower part at Vollan shows an angle of the slope gradient to be around 30-45 degrees. It is therefore reliable to assume that the upper part is the same.

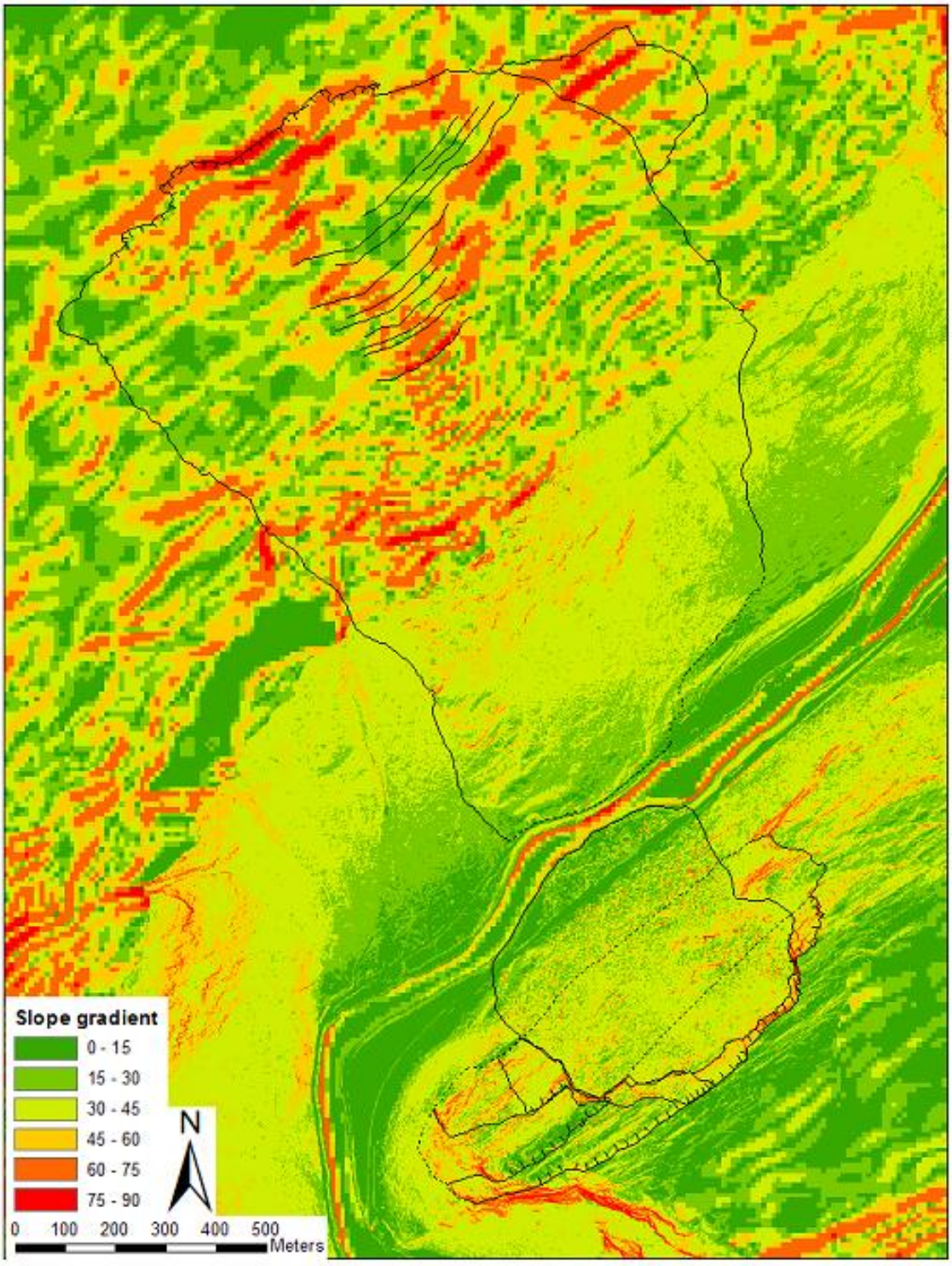

Figure 16 Slope angle of gradient of the area, where it shows that Ivasnasen has a slope gradient of around 30-45 degrees, and Vollan has a slope gradient of 30-75 degrees. It is important to be aware of that it is used a DEM of 1m in the area of Ivasnasen and half way up at Vollan (bottom of the valley). A DEM of 10m is used for the upper part of Vollan (the boarder is really clear where it is more detailed in 1m compare with the one of 10m). The colors of the contour lines have been changed to black to be more visible.

3.2 Geology

Ivasnasen was detected during a helicopter survey in August 2007 and Vollan was located on aerial photography mapping winter 2007 (Saintot et al., 2008). From Saintot et al., (2011), it has been prepared a more detailed geological map, figure 17. The geological map is more precise with a smaller scale and is more true to the fieldwork the author has done in the same area. The map has also contour lines (dashed lines) of the unstable area of Vollan and Ivasnasen, the historical rockslide at Ivasnasen is also marked. The geology goes from (top to bottom) diorite –granite gneiss, quartzite, calcareous phyllite and garnet mica schist, quartzite again to augen gneiss. The figure shows the sole detachment of allochtone and the GPS positions, that do the yearly measurements, are also marked and mapped in detail.

A huge synclinal covers the U-shaped valley of Gjøra and the area around Sunndal is part of three tectonic units. These units mostly contains gneiss, and is eroded down in two Precambrian gneiss units, referred to as the Western Gneiss-Region (figure 15), in the autochthone (created at the place) bedrock. Today the Precambrian gneiss units are detached by a steep tectonic contact and reach from the counties, Sogn & Fjordane (in the western part of Norway) to Nord Trøndelag (in the middle part of Norway). In the eastern part of the autochthonous unit it is lenses of mica schist that goes abeam the valley (Dalsegg et al., 2010). The middle allochtone is a tectonic complex and is dominated of strongly deformed Precambrian crystalline rocks and tick late- Proterozoic psammites (Roberts and Gee, 1985, Øiesvold, 2007). The parts from the middle allochtone are found in the northern part to north-west and contain Precambrian granitic to diorites gneisses. A partly horizontal shear zone contains thin layers of metasandstone and schist. This is the contact between the underlying autochthone unit and the upper allochthone unit. A thin layer of four different, stretched tectonic units is taking place in the eastern part of the area. This layer contains the autochthone unit, together with the middle and upper allochthone unit. The contacts between these are zones with huge faults (Dalsegg et al., 2010, Saintot et al., 2008).

Ivasnasen and Vollan lies in a zone of intense tectonic deformation where a major amount of thrusted units were emplaced during Caledonian times. The report from Saintot et al, 2008 describes that Ivasnasen shows an old slide with a maximum failed volume of $5Mm^3$, (Saintot et al., 2008). The bedrockmap, figure 17, shows that for the slope instability for Vollan is located in an allochthonous sheet of micashists, and that the foliation in the area is sub-vertical and parallel to the valley (Saintot et al., 2008).

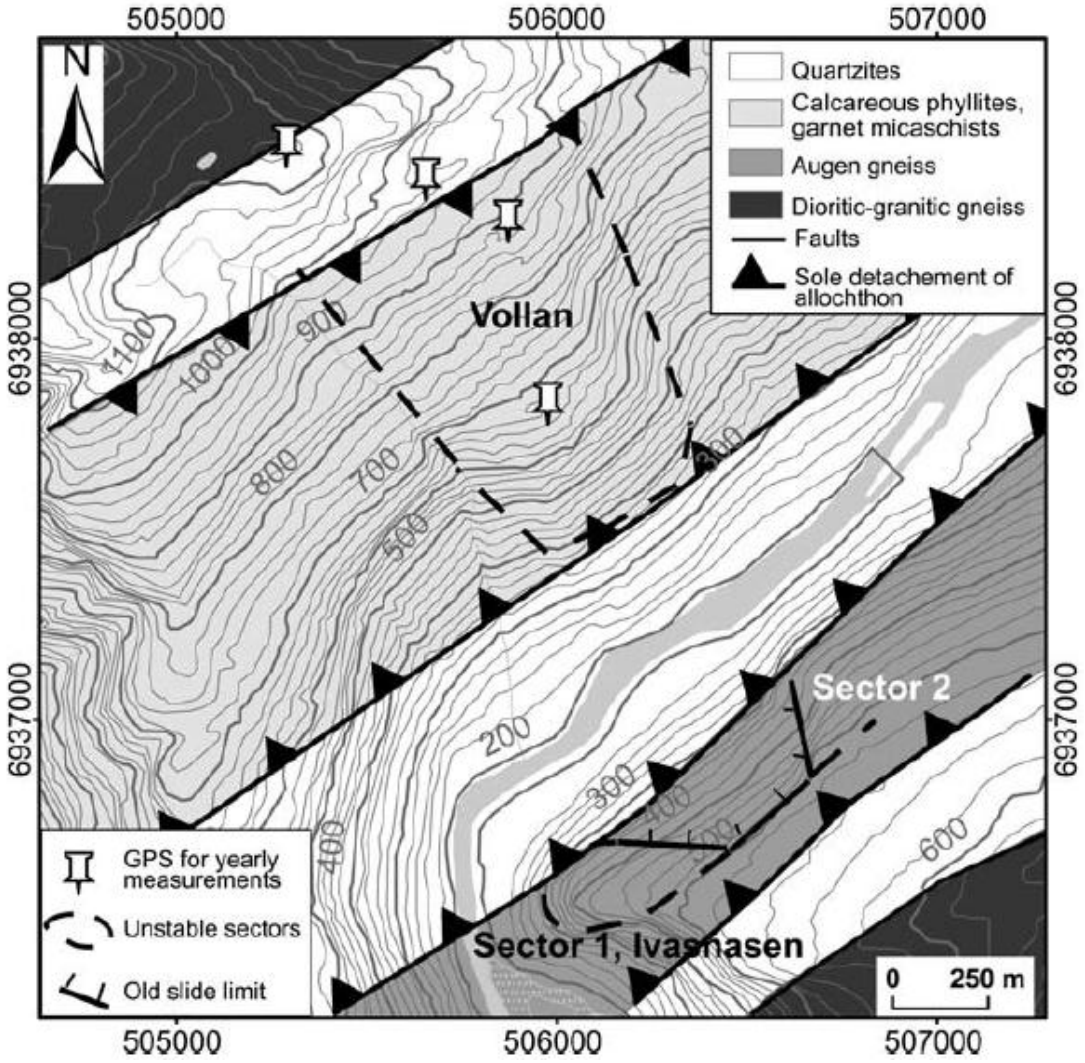

Figure 17 A more detailed geological map from the studiearea from the article of (Saintot et al., 2011).

Figure 18 are published in the article from Saintot et al. (2008), and shows the potential unstable rock slopes at Ivasnasen and Vollan south-east in the geological map. The map is in a big scale (1:250.000), so it is normal that the fieldwork and the map in figure 17, is more detailed. But the map is shown to give a better understanding of the surrounding area. The map also shows that the Sunndal valley has been and is exposed for slope failures.

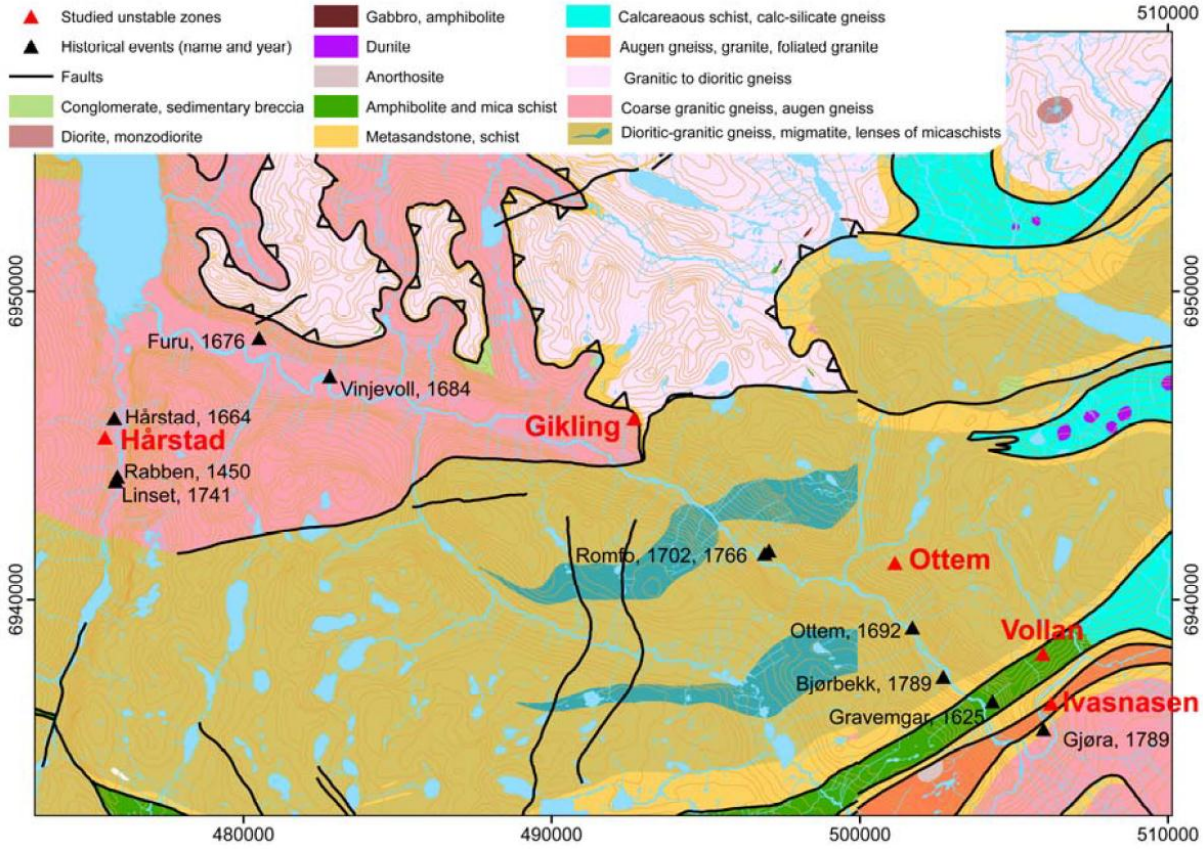

Figure 18 Geological bedrockmap of Sunndal valley. The historical rockslopes are marked with a black triangle and font, and the unstable rockslopes are marked with a red triangle and font (Dalsegg et al., 2010, Saintot et al., 2008, Tveten, 1998).

The augen gneiss that is found for the sliding surface at Ivasnasen is massive with a huge different in the size of "augens". The sliding surface at Vollan contains quartzite. Both of the instabilities appear along the NE-SW trending river (Driva) and are probably due to its tectonic setting.

The geological profile (figure 19) has been drawn based on field work and interpretation from the geological map "Røros & Sveg" made and published of NGU (Nilsen and Wolff, 1989). The geological map that is in a scale of 1:250'000, so it is not a detailed map. Since there does not exist any more detailed geological map or information of the area, the profile is a result of this.

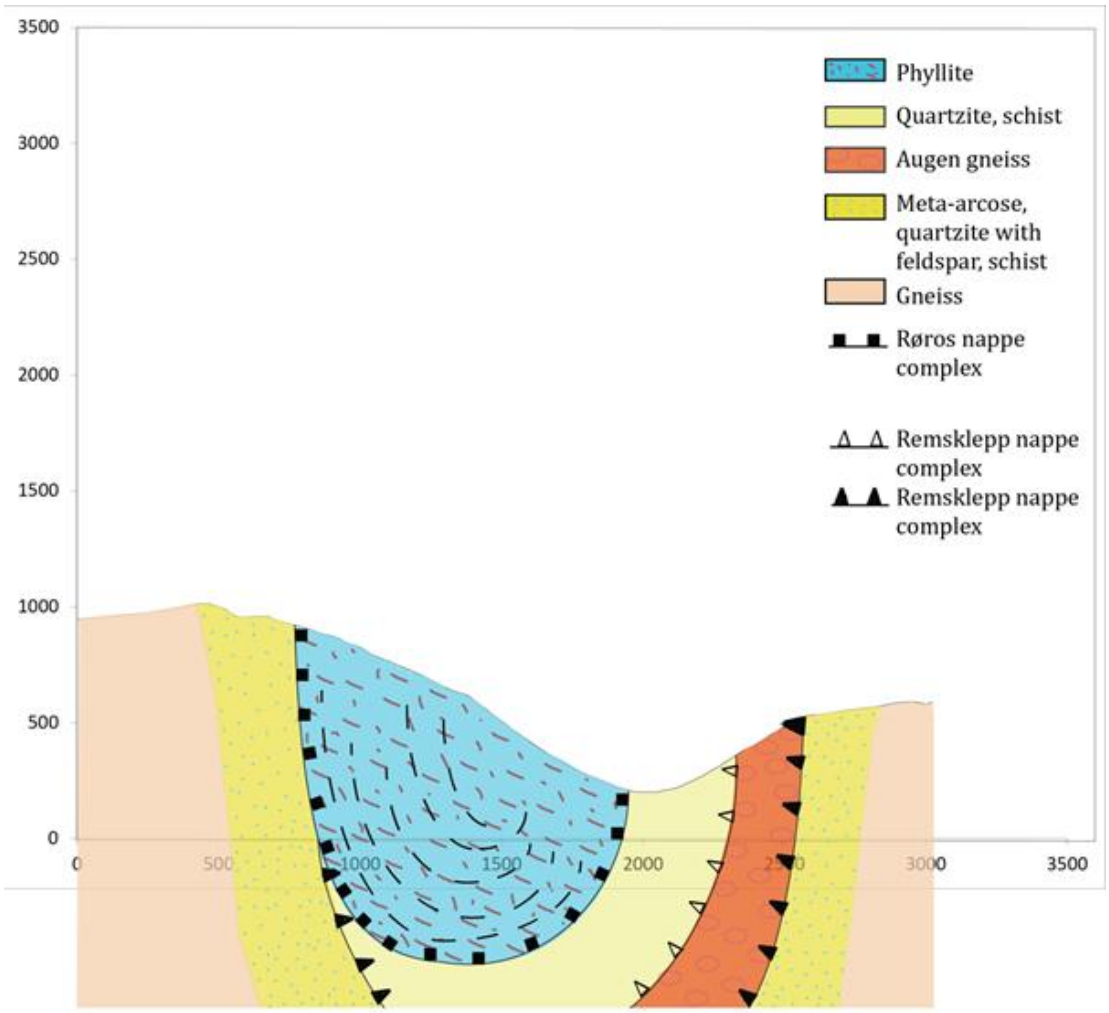

Figure 19 Geological profile from Vollan to Ivasnasen, based on fieldwork and available information from the NGU map "Røros & Sveg" (1989).

The geological profile, figure 19, shows different geological complexes where the Røros nappe complex belongs to the upper nappe complexes. It is just Trondheims nappe complex above. The Røros nappe complex is from early Ordovician and the rocks from Cambrian to Ordovician. The calcareous phyllite belongs to the allocthone units, with a calcareous spar and calcareous rich silica that generate amphibole and granite schist. The calcareous rich phyllite is drawn in the geological profile. These again contain peridotite, serpierite, gabbro and amphibolite. Remseklepp nappe complex is in the middle series of the nappes, where Remseklepp is in the bottom with Risberg- and Dalvolsjø nappe. These are intagliated in early Ordovician rocks from Proterozoic time, above with the augen gneiss. The quartzite that belongs to the Remseklepp nappe complex is a feldspar carrier quartzite with sill of metadiabas from the western part of the Sætre nappe.

The augen gneiss that is found in the study area belongs to the Risberg- and Dalvolsjø nappe. The age of the augen gneiss is set to be about 1600 million years based on

radiometric age detecting. The last, the bottom, nappe complex is Kvitvold, where the quartzite with feldspar and gneiss belongs to. This is early Ordovician with rocks that belongs to late- middle Proterozoic time (Nilsen and Wolff, 1989).

Figure 20 describes where the geological profile (figure 19) is picked from. It was important that the profile covers the unstable rock slope area at Vollan and the historical rockslide at Ivasnasen. This is to get a better understanding of the geology in the representative areas. The profile's contour line is drawn on a geological bedrock map in a scale of 1:250 000.

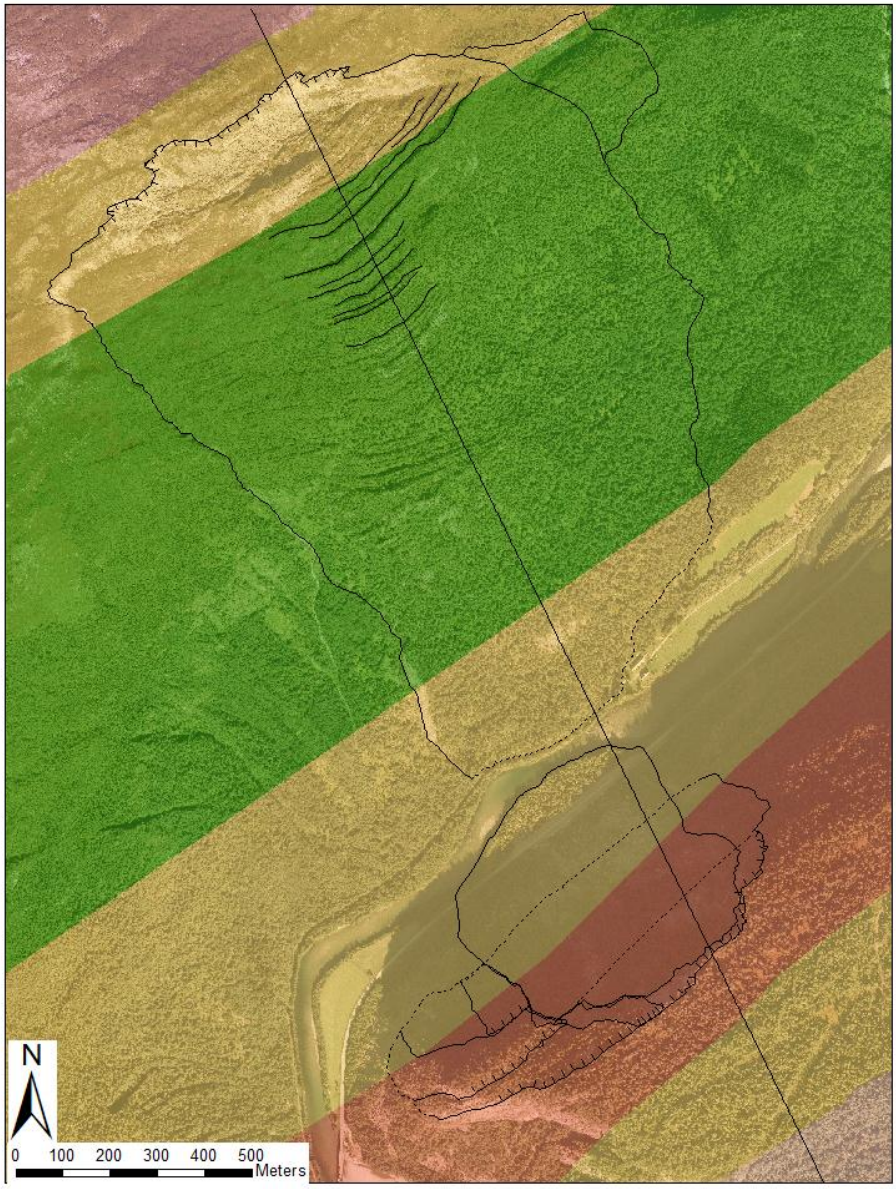

Figure 20 Describes where the information to the geological profile is picked out, see the long black straight line that goes through the unstable part of Vollan and the historical rockslide at Ivasnasen.

3.3 Hazards

The hazard and the problems for the sites at Vollan and Ivasnasen are related to the instability. The failure mechanisms are different, where there is a complex kinematical failure at Vollan, but toppling failure is the dominating mechanism here. For Ivasnasen the main failure mechanism is planar failure. For detailed kinematical analysis for both sides, please see chapter 6.

At Vollan it has already been a rock failure with a toppling mechanism, and it is still a bit active, based on fresh patina and blocks in the path. A huge past event of toppling failure in the quartzite seems to be the main reason for the creep, or the really slow movement, in the slope where it is phyllite that is dominating. It seems like the pressure and the load from the quartzite has activated a really slow movement process for the phyllite. The worst-case scenario at Vollan and the main hazard here is if the whole mountainside will slip out because of the phyllite layer that might be moving downward. And the related consequences this might have. There has been placed out four different GPS stations, in different positions of Vollan (please see figure 17 for the positions) that do a yearly measurement. Based on the monitoring from the GPS it should be possible to get knowledge if there are any displacements in the ground. If there are displacements the GPS monitoring may hopefully give an answer to how critical it is.

At Ivasnasen there is a scar of a historical rockslide, the age of this event is not set but the event might have happened during “Stor Ofsen”, the flood that made a lot of damage in Norway in 1789. This year, 1789, is not for sure and must be taken as a wild guess. The year will be set later with further analysis. The main hazard at Ivasnasen is that a remaining unstable part is left. LiDAR scans have been done in 2010 and 2011. Also some extensometer bolts have been placed in cracks to see if there are any movements. A rebuilding of the topography and calculated volume estimates for the historical event will give valuable information for further investigations for the unstable part. It is also important to get a good understanding about the unstable area to have knowledge about the volume that might slip out. Different analysis of the entire area may give valuable results to understand the past and the future. The results may also make it possible to predict the damaging consequences to a possible future event.

Further investigations in the next chapters will hopefully give some answers to some of the questions that are related to the hazards in the areas.

4.0 Description of used softwares

4.1 Coltop 3D

Two Terrestrial Laser Scanning (TLS) dataset was provided by NGU in 2010 and 2011. Original data are provided in yxz direction. In Coltop3D these data were converted and opened as a cloud of points in xyz.

Coltop 3D is a software developed at Institute of Geomatics and Risk Analysis (IGAR, Lausanne, Switzerland). *Coltop3D* is a full featured LiDAR data processing and analyzing software for geologists. It is designed for the interactive analysis of orientation of airborne and terrestrial LiDAR data and digital elevation models (DEM) at local and regional scale (Oppikofer et al., 2012, Terranum, 2011). The software is designed to measure the orientations of the discontinuities (different sets, angle, sliding plane, eg) on the digital elevation model (DEM) using a Hue-Intensity-Saturation coding in a stereographic projection. Each dip and dip direction are coded in one colour (Derron et al., 2005). The software provides several types of point cloud representations, according to the altitude (lower left), the slopes dip/dip direction (middle) and the sun's shading (lower right) (Terranum, 2011). The software Coltop 3D uses directly the point yxz, and this makes it possible to see the landscape in 3D. The usefulness of seeing the study area in 3D is huge, since it is rotatable and there might be joints that can hide behind the cliffs. After manually selecting the different discontinuities set by the different colour each orientation have the software gives out the measured dip direction and dip angle. Thereafter it is possible to open the files (shapefile) in ArcMap and see the orientations better with all the classifications that have been done, (Metzger and Jaboyedoff, 2008).

4.2 Dips

Dips (Rocscience) is a software designed for the interactive analysis of orientation based on geological data (Rocscience, 2012). After getting the information of each discontinuities sets from *Coltop 3D* it is then possible to use the data in *Dips*. All the data are plot as poles in a stereonet set by their orientation and color (please see figures 35-42, except fig 38, chapter 6.0 Kinematical analyses). All the plots are relevant, and are plots from the scans taken in 2010 and 2011 with the LiDAR. Some of them give some uncertainties because of the scanned area are big and the colors might look quite similar, but they all have a uncertainty less than ~20%, something that is really good and representative. The figures show the contours very clearly, and give an image of how the orientations are, and the structural measurements in field are similar.

Thereafter the software was used to classify all the structural measurements done by fieldwork.

The kinematics analysis is done to identify possible mechanism of slope failure. When using the software *Dips* the overall purpose is to define a set or sets of discontinuities, or a single feature such as a fault, which will control stability on a particular slope. The software makes it possible to test with different orientations of the topography and to see how each orientation will respond during a kinematical analysis (chapter 6).

4.3 Digital Elevation Model (DEM)

The earth's surface can be illustrated in three dimensions with a Digital Elevation Model (DEM). From a raster (grid of square cells with a constant and known cell size) or as a triangular irregular network (TIN) based on vectors the topography can be presented in 3D as a DEM (Oppikofer, 2009). Each specific cell in the DEM will have a value which represents the elevation of the area (Elgin, 2005). By using DEM, morphological structures (faults, open cracks and other discontinuities) related to landslides can be detected and investigated.

DEMs are today frequently produced from remote sensing data, for instance Interferometry Synthetic Aperture Radar (InSAR), Shuttle Radar Topography Mission (SRTM), and Light Detection Ranging (LiDAR). This include also Aerial Laser Scanning (ALS) and Terrestrial Laser Scanning (TLS) (Oppikofer, 2009).

The main uses of DEM regarding rockslides are listed below (Oppikofer, 2009, Sandøy, 2012):

- Slope angle and slope aspect.
- Shaded relief maps (or hill shade); visualize the terrain.
- Hydrological tools; perform hydrogeological analysis on the regional scale. Can be used to e.g. identify sinks and find flow networks.
- Coltopd3D: software that allows structural analysis to be performed on DEM. The principle is that this software gives each grid cell a color representing the main orientation (dip direction and dip) of discontinuities.
- Kinematic stability assessment by using Matterocking. This software is developed to compare geological structural data with the topographic DEM surface to determine potential failures (i.e. planar, wedge or toppling).
- Finding potential unstable volume with Slope Local Base Level (SLBL).
- Regional rock fall analysis by using critical slope angle, SLBL method (to identify erodible areas) and the present of discontinuities that can develop failure (planar, wedge or toppling failure).

- DEM differences are useful to quantify erosion and deposition processes, using multi-temporal DEM created by various techniques such as photogrammetry, digitized topographic maps and different remote sensing techniques (especially ALS and TLS).

The grid cell size that is used in a DEM is normally from 30 meter to 0,1 meter, and the choice of grid cell size is one of the major sources of uncertainty, since the accuracy of analysis is depending on type and spatial resolution of the raw data (Oppikofer, 2009). The raw data may also include buildings and vegetation, in which it is defined as a Digital Surface Model (DSM). A filtering of these features from the raw data gives a DEM that represents the "bare" earth surface (Elgin, 2005, Köthe, 2000).

4.4 PolyWorks

The TLS datasets are treated and analyzed by using *PolyWorks*. It is possible to manually remove the vegetation by using the software on the raw scans ('directly' from the LiDAR scanner). This is done by drawing a polygon in the LiDAR scans where the vegetation is to mark them and then remove them. PolyWorks give a 3D view of the area, this makes it easier to see where the area is covered by vegetation and where it is bedrock (Oppikofer, 2009).

After cleaning the vegetation from the files there is possible to put all the data's together from the different years the LiDAR scan was taken, and then compare them to see if there has been any block fall or other sign of movement.

4.5 IMinspect

This software is used to compare data to each other, and this is done by geographical referring. Since the coordinates to the LiDAR scan is known, we have a known point where we can refer from. First it is used a manual fit, where different fixed point (like the bridge, the river, road, back scarp of a landslide etc.) are set. After finding the matching points the different pictures are put together in one.

4.6 Volume estimations

By using the ante-and post-landslide DEMs the volume of a landslide can be estimated. The volume for the present slope instabilities can be found by using the modeled BFS (basal failure surface) and the present DEM, with using the difference between the reconstructed ART and the post-landslide DEM. For estimation of the denudation potential in the rock fall susceptibility assessment using SLBL (slope local base level) surface and then DEM (Oppikofer and Jaboyedoff, 2008a, Oppikofer, 2009).

4.7 Slope local base level, SLBL

The software *slope local base level (SLBL)* makes it possible to make an extrapolation, where the software makes it possible to make a surface above the past rock avalanche. The software makes it possible to define the basal failure surface (BSF) above which rock masses are prone to be eroded by mass wasting within a geologically short period (around 50'000 years) (Jaboyedoff et al., 2004c, Jaboyedoff et al., 2004d). The BSF is essential for the estimation of the volume and instability mechanism that is affected by the gravitational movement.

The SLBL was done in 3D and correspond to a line drawing from the top to the bottom of the past rockslide. A point located above the mean of its neighbors will then replace this mean value with some tolerance. This will be done by using the highest and the lowest values among the four neighbors in a squared grid DEM. To get a 3D view of the past rockslide there must be set some fixed points. If there is no fixed points set, the result will be a flat area. The contours and the curvatures of the rockslide are important, and must be done precisely in advance. After the sliding plane has been defined precisely, the volume can be calculated (Derron et al., 2005).

The SLBL is computed in an iterative procedure, which flattens and lowers the spurs and spikes on the topography (see figure 21) (Jaboyedoff et al., 2004d).

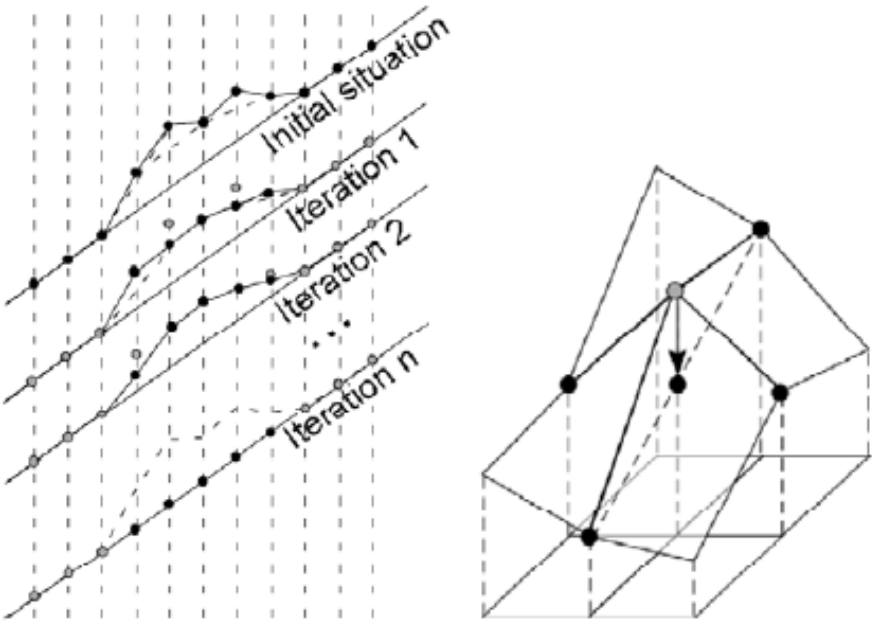

Figure 21 Illustration of the SLBL process, where a SLBL computation in 2D is on the left side, and is for a spur located on a slope. The points on the spur are lowered to form a straight line after n interaction steps. To the right is the SLBL computation in 3D where the central point is lowered to the mean value of the minimum and maximum altitudes of its four direct neighbors (Jaboyedoff et al., 2004d).

4.8 Ante-rockslide topography (ART)

From Oppikofer (2009) it is described that "*volume calculation of an ancient rockslide is important to characterize and necessary to reconstruct the ante-rockslide topography, and can be done by using aerial photographs* (Mora et al., 2003)*or topographic maps* (Evans et al., 2001) *acquired before the event"*. The event must be younger than around 75 years for the availability of ante-rockslide maps or photographs. This might cause some problems, especially when the date is unknown or the event is older than 75 years. The problems with the young age has been solved by other techniques that has focus on the surface reconstruction based on the present topography outside the scar and the ART within the rockslide area by following and completing the contour lines of the present-day topography (Brückl, 2001)or by interpolation methods (inverse distance weighting or kriging) (Gorum et al., 2008).

4.9 GPS

A Global Position System (GPS) is an inertial platform measuring system who gives the position in three dimensions with help of navigation satellites in combination with a set known GPS station, the positions to a GPS-receiver can be decided to an accuracy of m/mm. Different receivers can be placed directly in the preferred localities and the coordinates for the receivers is registered continuously. It is important that one receiver is placed on stable bedrock and is used as a reference for the other placed receivers, (Bjordal, 2011).

The measuring method that has been used at Vollan is a statistically relative phase measurement, where different point vectors in a network are measured. The network is build up so all the points is connected to at least three other different points. The interval for the measurement is set to be an epoch measurement that measures each fifth second, and the measuring time is at least 30 minutes each vector (Eiken, 2011).

4.10 Extensometer measurements

An extensometer is a distance meter installed between a crack to measure the distance in the movement of the crack or a bore hole. A known position of a bolt is set, and a periodically measurement (yearly, monthly etc.) of the distance can be done between two bolts (Bjordal, 2011).

When a set with different measurements of the distances have been collected it is possible to compare them to see if there has been any movement or not. The measurement is done by using a bit more advanced tape measurement where two bolts are placed; one on each side of the crack, and the deformation between the two bolts are measured.

4.11 XRD

The crystalline structures have atoms that are set in a regular manner on the points of a lattice (Bravais lattice). This crystalline lattice is a regular three-dimensional distribution of atoms in space, and are arranged as a series of parallel planes separated from each other by a distance (varies to the material). There are planes with numbers of different orientations and specific spacing for each crystal that can give an indication of which crystal it is. Structural analysis X-ray diffraction is a versatile, non-destructive analytical technique for identification and quantitative determination of the various

crystalline compounds, known as 'phases', present in solid materials and powders (Thornhill, 1999).

In x-ray diffraction (XRD), one of the characteristic wavelengths emitted by the tube anode material (mainly the K-Alpha line) is used to interact with solid samples in order to determine their crystalline phases. Identification is achieved by comparing the x-ray diffraction pattern - or “diffractogram” – obtained from an unknown sample with an internationally recognized database containing reference patterns for more than 50,000 phases. It is important when using the computerized system to check the results from such programs carefully, in order to ensure that correct interpretation of the diffractogram is made. That is e.g. when a sample does not contain identical constituents to any of the powder diffraction files then you may get an inappropriate interpretation as the software program may choose a near match from the powder diffraction files which is not actually present in the sample. In such cases it is always important to check minor peaks, not just the three strongest ones. Modern computer-controlled diffractometer systems use automatic routines to measure, record and interpret the unique diffractograms produced by individual constituents in even highly complex mixtures (Thornhill, 1999).

4.12 Phase^2

Phase^2 is described by Rocscience (2011) as a powerful 2D elasto-plastic finite element stress analysis program (FEM) for underground or surface excavations in rock or soil. The program can be used for a wide range of engineering purpose. Sample of engineering purpose; support design, finite element slope stability, groundwater seepage and probabilistic analysis are all examples for engineering purpose. The newest software version from Rocscience is version 8.01, (Rocscience, 2011), and a detailed description of the software are given in the tutorial from Rockscience (2011).

Figure 15 is modified from Grøneng (2010), and shows an overview of the constitutive models that is offered in Phase^2.

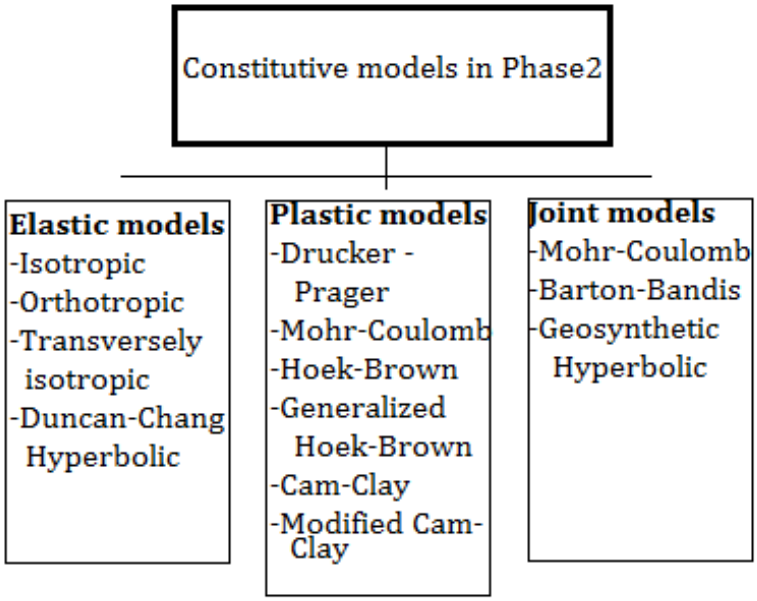

Figure 22 Constitutive models offered in Phase² modified from Grøneng (2010)

Phase² uses the Shear Strength Reduction (SSR) method to determine the factor of safety of a slope based on FEM. Either the Mohr-Coulomb or Hoek-Brown criterion can be used as strength parameters. The method reduces the shear strength of slope materials until it becomes unstable. When the finite element model does not converge to a solution, then failure is achieved. The critical factor at which failure occurs is taken to be the factor of safety, when the equilibrium cannot be maintained (Grøneng, 2010, Rocscience, 2011).

4.13 LiDAR

LiDAR is a laser scanner. Laser scanning is a widely used remote sensing technique for the acquisition of topographic information and creation of DEMs. The earth's surface is created by a contactless and reflectorless point cloud. The laser pulse that is sent out from the LiDAR is monochromatic and nearly parallel. The laser pulse is also sent out in a precisely known direction, back-scattered by the surface and the scanner record the return pulses. By using the time-of-flight principle, the distance between the instrument and the topography is calculates. To create the point cloud, the laser beam is sweeping in different directions, (Oppikofer, 2009). Please see chapter 2.3, Remote sensing technology, for further and more detailed information about LiDAR techniques.

5.0 Field investigation

The fieldworks were conducted by the author, Gudrun Majala Dreiås, in 2011 and 2012. Ivasnasen was discovered during a helicopter survey for NGU in August 2007. Vollan was observed on aerial photos during the winter of 2007 (Saintot et al., 2008). During the research of Saintot et al. (2008), it was concluded that the potential unstable rock slopes close to Gjøra in Sunndal county needed more analysis, to get a better knowledge about the area.

5.1 Vollan

Figure 23 Part of the study area at Volla. The entire slope cannot be seen, but the picture is shown to give an impression of the area. The slow movement process can partly be seen in the structures with snow covering. The back scarp is visible on the top of the mountain.

At Vollan there is plenty of incline slopes that can be detected from orthophotos. For the fieldwork it was important to detect these and map the lithology and the structures. An

open graben system is taking place at Vollan and can be seen in figure 24. To get a better impression of what has caused this it is relevant to see how far down the unstable slope goes, the lateral limits and where it stops. It is also important to see if there is any depressions or cracks on the other side of the river, SW-side of the main area that has been detected on orthophotos. A lot of structural measurements have been done at Vollan. Figure 24 also gives a good impression of how massive the quartzite at the back scarp is.

Figure 24 Overview of the main backscarp at Vollan, can also see a big amount of deposits in front of the back scarp. The open graben system is marked in the picture.

Figure 25 shows the contour lines that have been modeled and the structural measurements for the unstable rock slope at Vollan. Please see the legend for the back scarp, toe line etc. The reason that the symbols are different for the structural analysis are because of the orientations each of them have (added based on fieldwork). The unstable part of Vollan covers a huge part of the mountainside, as the orthophoto shows in the figure. The really slow movement process can be seen clearly from the figure (ridges downward to the valley). The figure does also visualize the U-shaped valley and that Ivasnasen is on the other side of the valley across from Vollan.

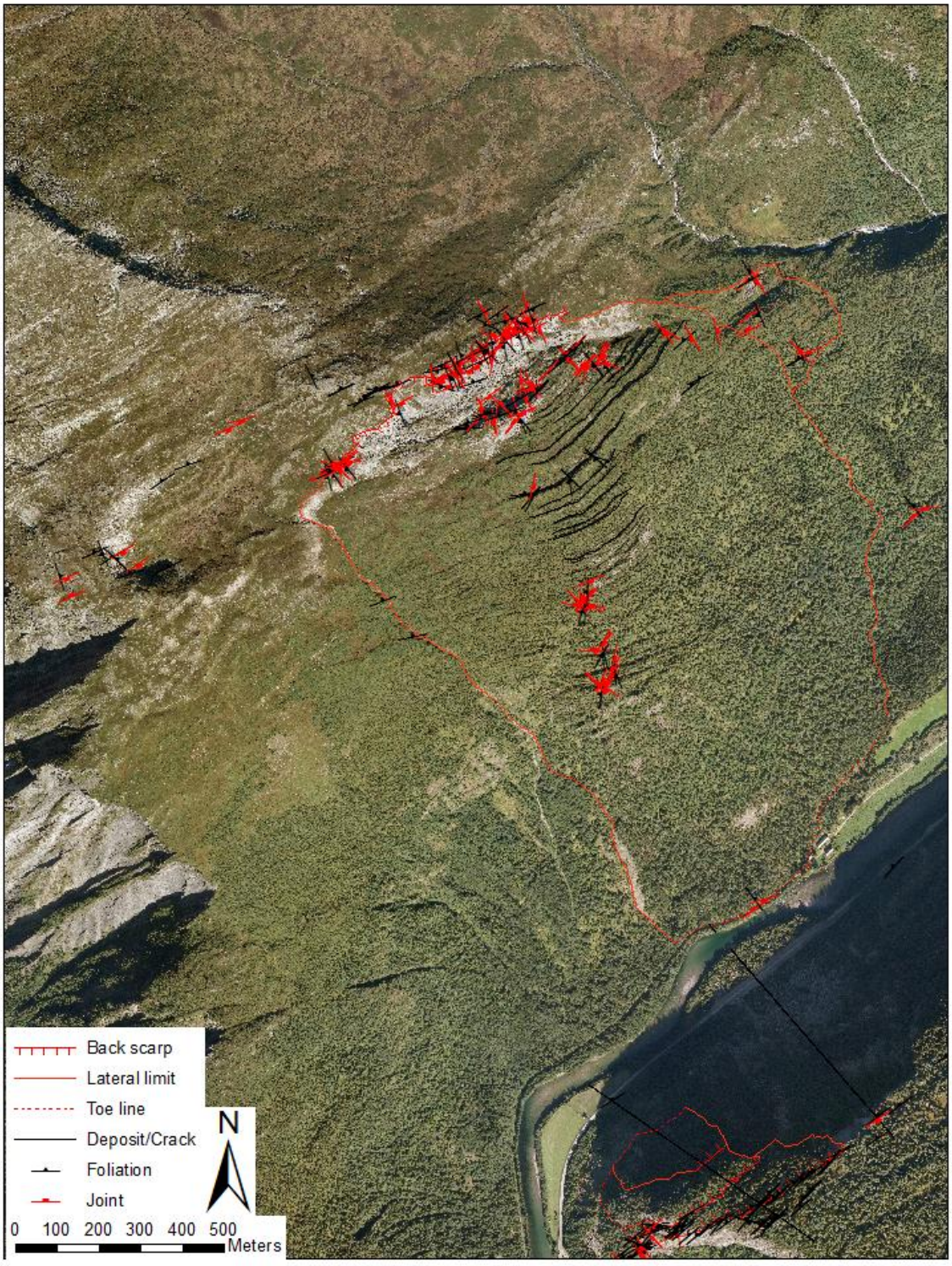

Figure 25 Contour lines for the unstable area at Vollan, the DEM that exsist for this area is just for 10 meters, so it is not reasonable to show the lineaments on that scale, the orthophoto is therefore used. The structural measurements is shown by different symbology for the foliation and the joint.

During fieldwork some open cracks were detected behind the back scarp (picture 3 in figure 26), but these cracks behind the back scarp do not seem to be that active. It might be results of the back scarp and that the ground has moved forward. Since the lithology is different here this might be the result of this, or it might be that the phyllite layer and the quartzite is in a contact zone, with different nappe complex. Those cracks behind are covered by vegetation, and has no other sign of activity that could be seen, like rocks in the open cracks or fresh patina. However there is fresh patina visible at the back scarp and this is sign of some activity at present. The back scarp is really fractured, as can be seen from figure 26 with loose blocks waiting to fall.

Figure 26 shows six different pictures taken from the area at Vollan.

- Picture 1 is taken just below the back scarp, in the middle of the deposits, where it shows the textures of the toppling failure in a small scale figure.
- Picture 2 and 6 is taken from the back scarp, the rocks are massive quartzite and the back scarp is really steep. It is also really fractured and fresh patina could be seen.
- Picture 3 is taken behind the back scarp, a horizontal long continuously crack, but it is filled with vegetation and does not seem to be too deep. Might be a result of the gravity when the massive back scarp failed.
- Picture 4 is taken above the back scarp, the texture of the rock is thinner, but it is still quartzite.
- Picture 5 shows partly the back scarp and the deposits below. Just part of the huge rock failure area.

Figure 26 Different pictures taken of Vollan during fieldwork. 1) shows a really good illustration of the toppling failure that is in the area, and this is a mini-scale figure of this. 2) & 6)are taken from the back scarp, it shows clearly that it is really steep,fracutred and contains massive quartzite. 3) shows a huge horizontal crack behind the back scarp. 4)is taken behind the back scarp, and they layers are quite thin here, but still quartzite. 5)partly overview of the area, back scarp to the right. Photo taken by the author and Yngvild S. Kvalvik.

During the fieldwork it was important to investigate the changes in the geology on both sides of the small river running through the southern side of Vollan. From the observation in field concludes the geology to be the same on both side of the small river, but the deformation is larger in the unstable area of Vollan. From the other side of the river (SW-side), the cliff had a bigger rock surface area that made it easier to detect the limits of the lithology.

The ortophotos shows a clear direction of the structures, and this could also be seen in the field. The structures of the deformation have all the same direction (NE), and all of this is observed on permanent ground. These observations make a good argument to say which direction the deformations are dipping.

At Vollan, we can observe a clear toppling movement that has taken place for the back scarp. On the western part of the back scarp it is a more vertical structure than it is on the eastern side. On the eastern side the back scarp is straight and is dipping a little toward us when we are standing below the scarp. It has been some rotation, extension and some slope failure. The biggest rotation gave also the biggest deformation. The degree of fracturing is also different. Where the back scarp is less fractured, the deposits on both the sides of the back scarp have a grade of medium fractured. The deposits in the middle (below the back scarp) are most fractured. One cause might be that a large block has been rotated in the middle, which has caused the heavy fracturing.

Behind the back scarp (1109 meters above sea level) the lithology was clearly different. Here it was observed dioritic and granitic gneiss. And the foliation is still parallel (something that is common in Norway).

Figure 27 show a picture of the slow movement process that is taking place at Vollan. The picture is taken by Thierry Oppikofer during a helicopter survey for NGU, August 2011. The slow movement process might be linked to a thrust fault. A lot of displacement has been picked up by the phyllite layer. The picture shows this as a possibility since it looks like all the layers have been displaced.

Figure 27 The really slow movement process of the ground is really easy to see in the field and by orthophoto, this picture is taken by T. Oppikofer, NGU with helicopter in August 2011.

5.1.1 GPS measurements

There were three different GPS stations established at Vollan in 2008. One fixed point was established at the same time at the highest point in the area name "Litlhøa" (1127m.a.s.l). The three different stations (figure 28) were placed at different potentially unstable blocks in the valley side. The fixed station (figure 28, marked VOL-FP) was set with an absolute precise method, and the other GPS stations are measured relatively to the fixed point through vector measurements (Eiken, 2011).

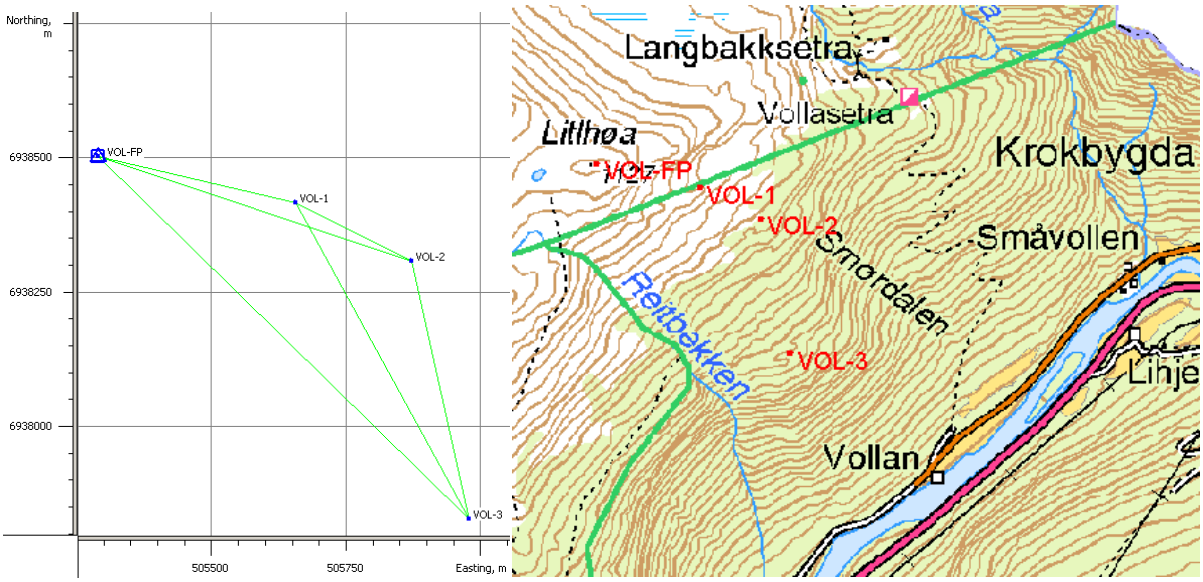

Figure 28 Placed vectors and map over the GPS positions, from Eiken (2011).

The GPS measurements took place in 2009 and 2011, and the results (table 4) shows some sign of movement for Vol-1 and Vol-3. The total movement for Vol-1 is 5mm and 8mm for Vol-3, but they are not reliable since they are pointed in different direction than it did for the 2009 measurements. The total movement is therefore not significant since NGU do cooperate with an error of measurement of approximately 3mm in the horizontal position and three times higher for the vertical position. The tendency for these years is that the movements are moving north in 2008-2009 and the next year in the opposite direction. VOL-3 has a black arrow outside the red ellipsoid that shows error of measurement (figure 29). Due to this it can be told that this is significant, but it has too low correct error of measurement. Since it also goes in different directions, it does not make it reliable that it has been any movement here. A comment to the report that was made after the GPS measurements is that: "*Normally there have been some problems due to the meteorological conditions in the area, where it is extremely high moist conditions, but most of the measurements can still be characterized as good*" (Eiken, 2011). It seems like the meteorological conditions are variable in the area, and that this could affect the measurements. Still the movements are not significant since they are too small and the errors of measurements have not been considered enough.

Figure 29 Ellipsoids, where the black arrow shows some tendency to movement for VOL-3, figure from Eiken (2011).

Table 4 shows that it has been some movements over a period of 3 years, but this is not enough to be classified as significant. Since the tendency is so different from each year, it is not trustworthy. It is not enough yearly measurements to get a good picture of the movements. These movements take time and need to be followed up for a long, long time in the future if any significant movement shall be discovered.

Table 4 Distinction between the GPS measurements done at Vollan, table modified from Eiken, 2011.

Point	Year	dN (m)	dE (m)	Distinction (m)	Direction (g gon)	dH (m)
Vol-1	2008-09	0.0033	-0.0032	0.005	350.98	-0.006
Vol-1	2009-11	-0.0013	0.0041	0.004	119.55	-0.001
Vol-2	2008-09	0.0001	-0.0016	0.002	303.97	0.000
Vol-2	2009-11	-0.0016	0.0047	0.005	120.89	0.000
Vol-3	2008-09	0.0002	-0.0081	0.008	301.57	-0.002
Vol-3	2009-11	-0.0054	0.0103	0.012	130.74	-0.012

5.2 Ivasnasen

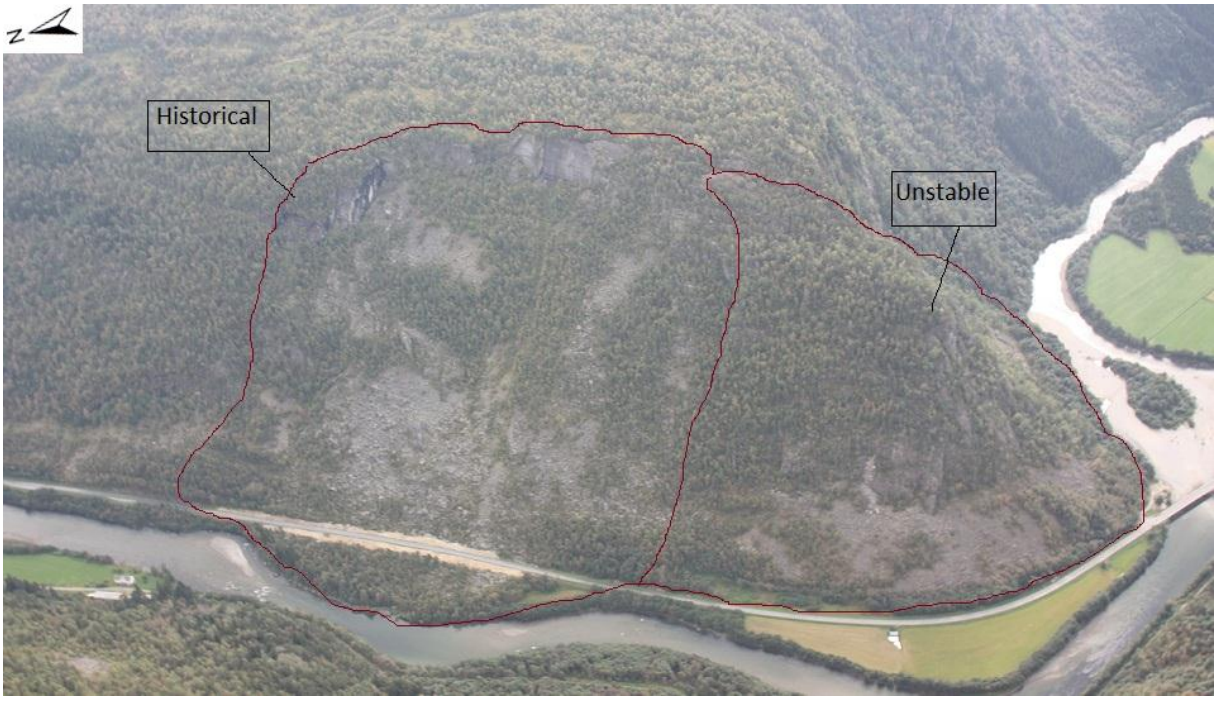

Figure 30 Illustration of Ivasnasen. Left: the historical rockslide. Right: the unstable rock slope. Picture taken by T. Oppikofer, NGU with helicopter, August 2011.

Figure 30 is an overview picture of the whole area at Ivasnasen, both the historical rockslide to the left and the unstable rock slope to the right hand side. The picture is taken by NGU during a helicopter survey in August 2011. LiDAR scans have been done by a terrestrial LiDAR in 2010 and 2011 and with an airborne LiDAR in 2011. The scans have been done to detect if there are some movements in the elongation of the back scarp to the historical rockslide.

Based on fieldworks it has been detected some huge cracks in the elongation of the back scarp, but these are covered by vegetation and is not open. They are therefore not extremely active. Ivasnasen is located in a steep area, so it was not easy to enter all the different places, but most of them have been discovered and a good understanding of the geological structures is a result of all the structural measurements that have been done.

Southwest of Ivasnasen it has been detected large structures dipping towards the valley. The main focus here would be to find out if this is part of the sliding surface that has gone.

A result of the old rockslide at Ivasnasen is deposits of large blocks. The source area is clearly visible, where it is a large sliding surface on the top of the hill and the structures goes along the lateral limit. Larger deformations are also visible behind the back scarp.

Figure 31 and 32 shows all the structural measurements that have been done at the historical rockslide (figure 31) and for the unstable part (figure 32) at Ivasnasen. Please have a look at the legend to find out which symbols that represent the foliation and the joints. Unfortunately the area is big so the symbols are hard to see. The figures also show the back scarp, lateral limits, deposits and the toe line. The contour lines are drawn with a DEM of 1meter, with help of the software ArcScene that makes it possible to draw in 3D. Since the DEM of 1meter is so detailed, the deposits for the historical rockslide are visible because of this. It is also possible to detect the cracks and other contours based on the detailed DEM.

For the historical rockslide that has taken place at Ivasnasen it might look like there have been two different scenarios. The first scenario seems taken place where the bottom toe line is drawn. The second scenario could have taken place where the upper toe line is drawn. See figure 31, as dashed toe lines in the middle of the scar. The possibility of two events has been taken in concern for the analysis and this is the reason that two different toe lines have been drawn in the figure.

For the unstable part of Ivasnasen there has been drawn in three different possible back scarps (figure 32). The reason for this is that it looks like there might be some deformation that is visible. Since there also have been drawn two different toe lines in figure 31 for the historical rockslide, it is reasonable to think of the unstable part as several different scenarios as well. Especially since the deformations are in the elongation of the old back scar. Further analysis have therefore been done for a scenario 1,2 and 3 all for the different back scarps at the unstable part.

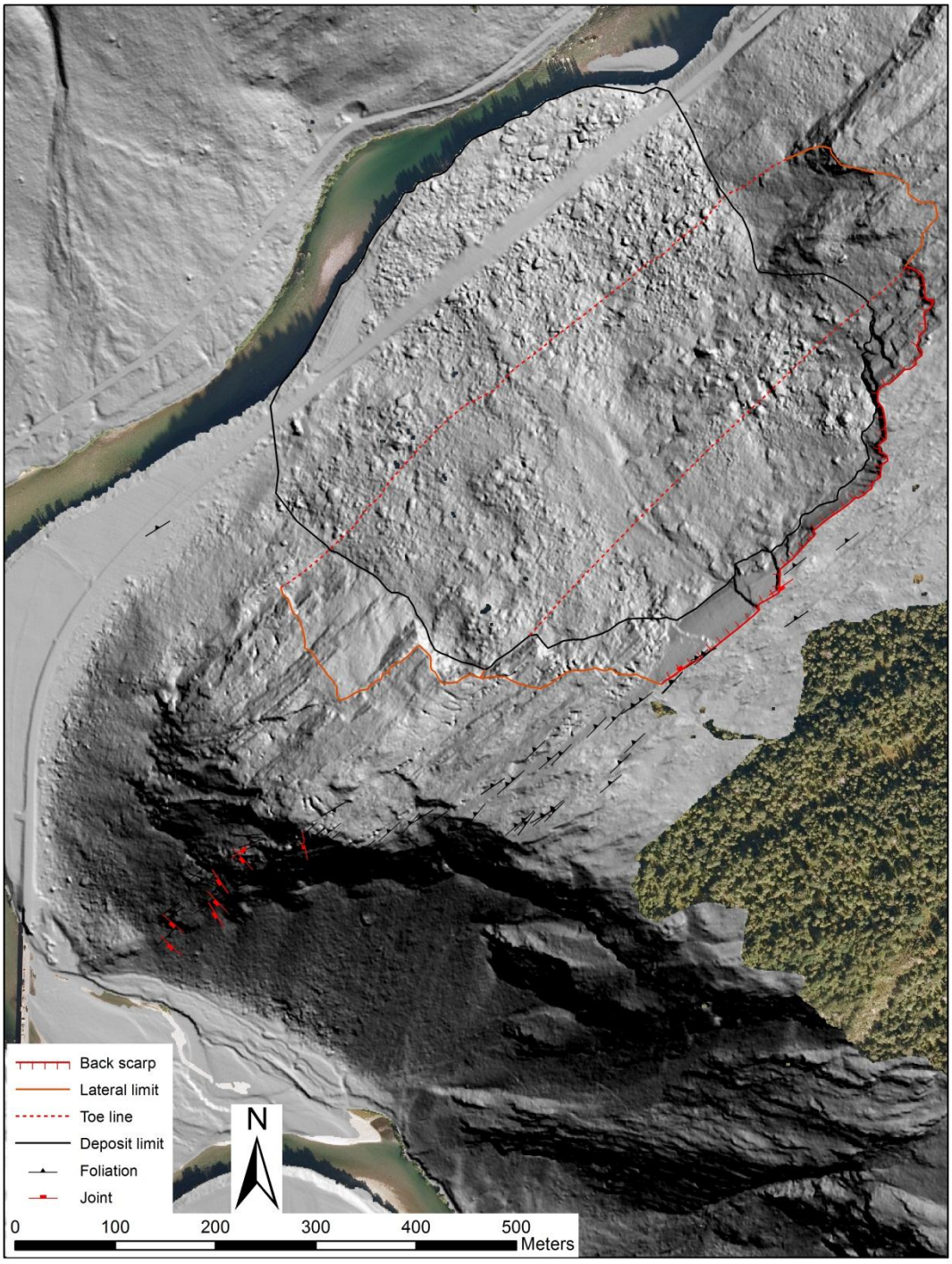

Figure 31 Contour lines of the historical rockslide at Ivasnasen, with also structural measurements that has been done by fieldwork in 2011 and 2012.

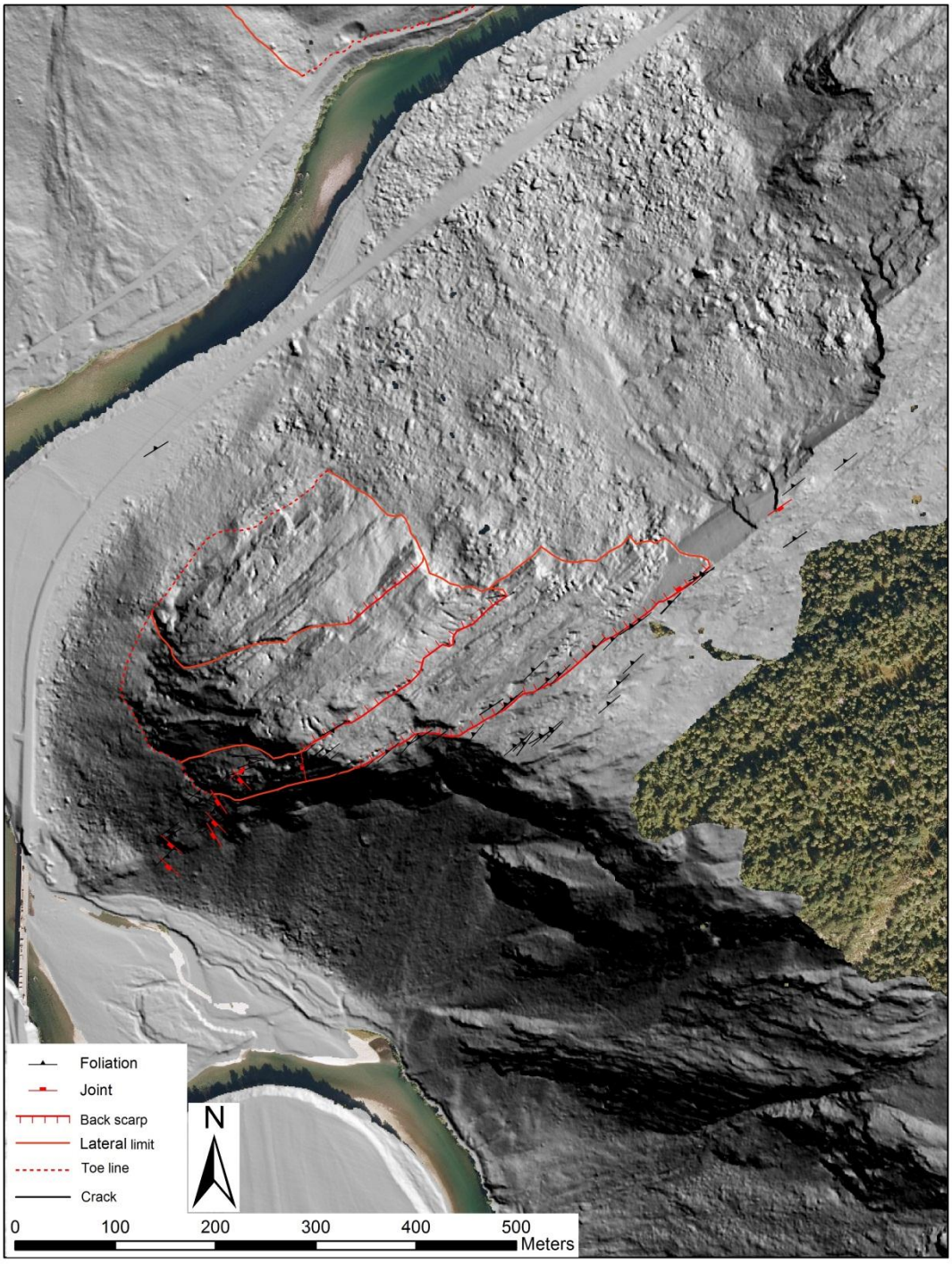

Figure 32 Contour lines for the unstable rock slope at Ivasnasen, structural measurements done by fieldwork are also shown at the map as foliation and joint.

Figure 33 is a set of pictures taken in the field, where they all shows sign of activity in the area, both the historical and the unstable part of Ivasnasen. Picture 1 and 2 is taken from the historical part. Picture 3 is in the zone between the historical and the unstable part. Picture 4 and 5 is from the lower part of the unstable area, and the last picture 6 is from the top of the unstable part. All the pictures are taken by the author.

- Picture 1 show a huge crack where the extensometer is set to measure if there are some movements. Smaller loose blocks can be seen down in the crack, and do represent sign of activity. But there is also vegetation growing in the crack. The vegetation represents that if there is some activity, it is not much. The extensometer that is placed here is placed on a good spot, and will hopefully give some meaningful observations in the future.
- Picture 2 shows the sliding surface for the historical rockslide, where it has 'cut' the remaining rock, and the 'eyes' in the augen gneiss is also visible with a closer look (see the remaining mass on the right in the picture).
- Picture 3 is a clearly visible crack that goes from the historical to the unstable part at Ivasnasen. It is covered by vegetation, so it is not critically active and moves a lot, but it is an indication that something is/has happened here. It might be that this is a result of the gravity when the historical rockslide went, as a result of gravity movement downwards.
- Picture 4 is taken from the bottom of the unstable part, and here it is clear that movement has caused the fractured of the rock. It is visible that different loose blocks are placed like this on different places and will fall out sooner or later.
- Picture 5 is taken in the same area as picture 4, and shows some large scale folding and how the folding does represent the fractures. Also here it is obvious that it is open cracks and that the blocks will fall out one day.
- Picture 6 is taken from the top of the unstable part, and shows some clear deep cracks. It was a number of cracks like this on the top of the unstable part.

All these pictures in figure 33 do represent activity in different scale, but it is important to be aware of these for the further analysis that is needed to be done before any conclusions are set.

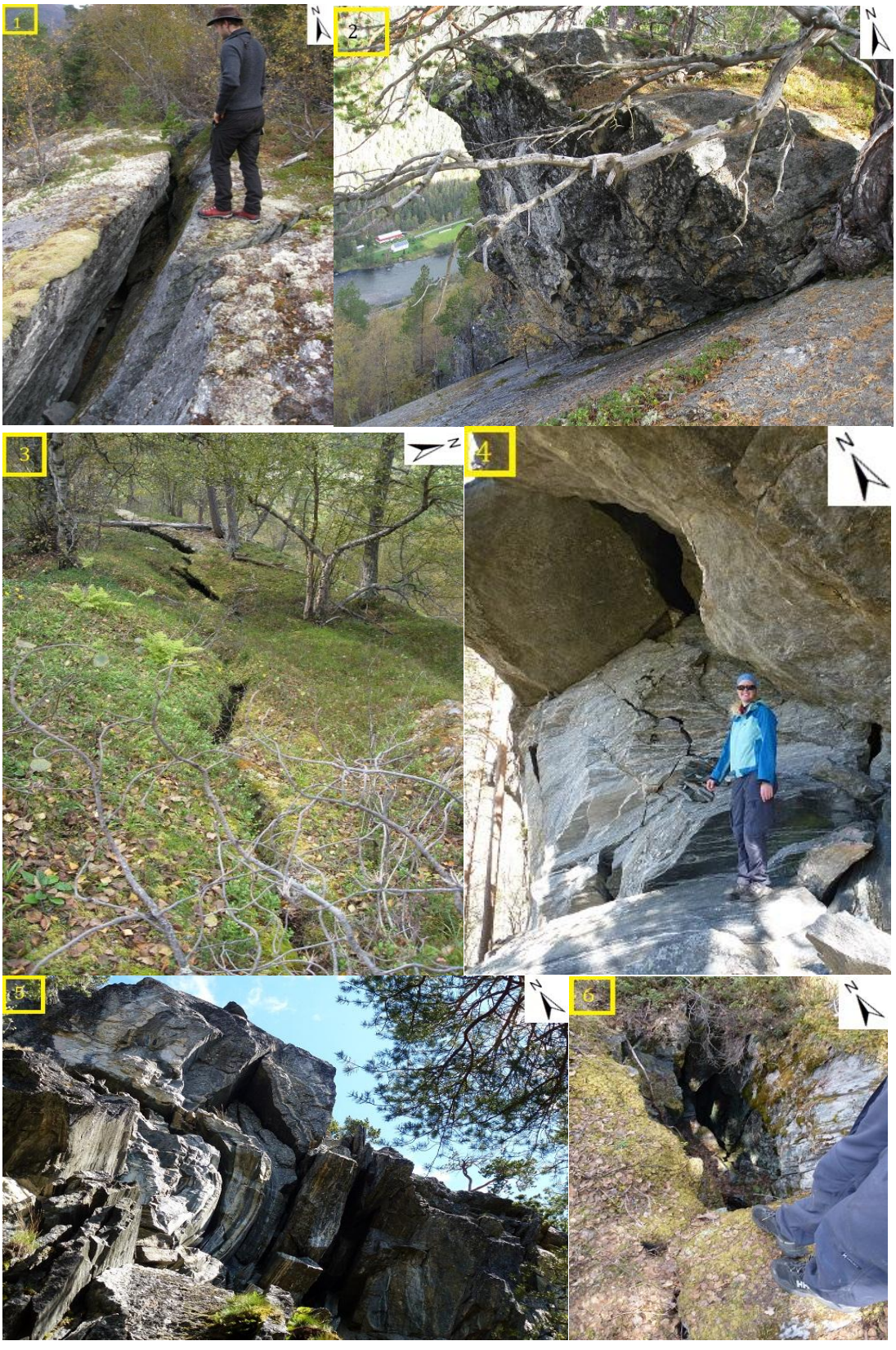

Figure 33 Picture 1 and 2 and is from the historical rockslide, picture 3 is in the middle of the historical and the unstable part, and figure 4,5 and 6 is taken from the unstable part at Ivasnasen. They all shows sign of activity with huge cracks and deformations. Pictures taken by the author.

5.2.1 Extensometer measurements

Two extensometer bolts were placed in 2010 to detect if there are some movements that represent activity, or not. How the extensometer bolt and the measurement work, please see chapter 4.10.

The back scarp was measured to have a length at 1520 meters at the position where the first extensometer bolt (EXT1) is placed. The measurement was done from the back scrap (the structural measurement established this). It is augen gneiss in this area where the back scarp is, and it seems like augen gneiss also can be found in the foliation. Since it is not any visible blocks between the back scarps and where the extensometer bolt is, it is likely to characterize this as the sliding surface. This was suspected and established by the structural analysis afterwards.

From table 5 the measurements from the extensometer bolts are listed. The measurements show no sign of activity in the time interval of one year, and this is as suspected. It was suspected that it would not have been registered any movement in one year. If there was registered any movement it would then have been classified as active. A one year interval is not enough to make conclusions. For making more specific results it should be followed up with more measurements.

Table 5 Extensometer measurements from 2010 and 2011, shows no sign of movement.

Point	East	North	Device position	2010 (mm)	2011 (mm)	Distinction
EXT1	506355	6936586	Eastern flank	7746.86	7744.92	-1.94
EXT2	506313	6936631	Eastern flank	6481.19	6477.29	-3.90

The run out length of the rockslide is defined to be in the bottom of the valley (as drawn in the DEM of 1meter, figure 31). The deposits cannot be detected on the other side of the river, just some large blocks in the middle of the river are visible, and this gives a good indication of the actual run out length.

There are several different sliding surfaces that are separated by vertical trend faces (see figure 33, picture 2). In the North Western part of Ivasnasen it has been observed a huge block that is still intact (same picture), but there are some worries since it has an open crack (fault gauche) behind in the contact zone to the sliding plane. The fault gauche has some crushed rocks, and it seems like it has been some activity here based on this. Based on this it was important to detect if there were some continuously deformation behind this huge block, and it was not. The deformation did reach quite far, but then it is not any visible traces further, and therefore it does not appear as active.

6.0 Kinematic analysis

The purpose of the kinematic analysis is to identify possible modes of slope failure. An overall purpose for the analysis is to define features that control the stability, such as a set or sets of discontinuities, or single feature such as a fault. To form a plane failure, the bedding must dip out of the face, or if it is a wedge failure then a pair of join sets must intersect (Wyllie and Mah, 2004).

The kinematic analyses in this master's thesis have been carried out by *Coltop3D* and *Dips*. For Ivasnasen the structural measurements that have been done during fieldwork are similar with the results from the LiDAR scan and airborne scan. The geology at Vollan is more complex. Because of the complexity it was necessary to split the area in smaller pieces and do the kinematical analysis on each area (figure 38). A kinematical analysis of rock slope failure modes by using a stereonet is really useful and quite easy to use. The analysis gives a quick answer of the potential failure modes. It is always important to keep in mind that even if the analysis indicates risk of failure, it is not necessarily that a failure will occur. Other factors than structural and friction angle may influence to increase stability too (see chapter 2.1 and 2.3).

In *Dips* each of the failure mechanism has been done by Goodmans criterions, (Rocscience, 2012).

- For planar failure a great circle of the topography is displayed with the different orientation for Ivasnasen and Vollan, and a daylight envelope has been drawn. The daylight envelope helps with the kinematical analysis, and any pole falling within this is kinematically free to slide if frictionally unstable. A pole friction cone is measured from the center of the stereonet and displayed, and any pole falling outside the cone represents a possible planar failure.
- For the toppling failure Goodman states that for slip to occur, the bedding normal must be inclined less steeply than a line inclined at an angle equivalent to the friction angle above the slope. This means that planes cannot topple if they cannot slide with respect to one another. A slip limit plane defines the critical zone for flexural toppling, and is derived from: topography angle – friction angle and the dip direction is equal as earlier. The critical zone for flexural toppling is the region between the slip limit plane, stereonet perimeter and the lateral limits (critical zone with respect to the dip direction of the slope). Each pole inside the critical zone represents a risk of flexural toppling.
- For the wedge failure the cone has been divided from: trend; dip direction + 180 degrees, the plunge; 90 – dip angle and the angle; 90 – friction angle. The critical zone for wedge sliding is the area inside the plane friction cone and outside the slope plane, and poles inside this zone represent a possible wedge failure. Wedges can also slide on a single joint plane. This might happen if one plane has a

more favorable direction for sliding and the second joint plane can act as a release plane instead of a sliding plane.

Each failure mechanism was tested for all the different sets. It has been found possibilities for both planar and wedge failure at Ivasnasen. At Vollan there are possibilities for flexural toppling, wedge and planar failure. For further details about each analysis for Ivasnasen and Vollan, please see chapter 6.1 and 6.2.

No lateral tolerance has been used for the failure mechanism analysis. The reason for this is that the topography is changing and it is not some clear structural sets in the area (especially for Vollan). The geology is complex and it is for a wide and huge area, it is not "just a road cut". It is bigger dimensions that need a bigger view of the whole area. Each analysis has been discussed under each site, and different options have been taken in concern.

For each different joint set it has been done a variability limit in degrees with help of Fischer's K. The variability of how precise the results are is represented by this, and is listed for each analysis.

6.1 Ivasnasen

During fieldwork and preparation of the scans (both terrestrial and airborne) it is visible that the sliding surface has a sort of a knick-point (marked with a red line in figure 34). This knick-point represents where it becomes steeper the higher up to the back scarp it is, an undulating topography. The red line shows the knick-point and that the angle becomes steeper. It shows a typically sliding surface, a planar slide failure function. The picture is adapted from Coltop3D.

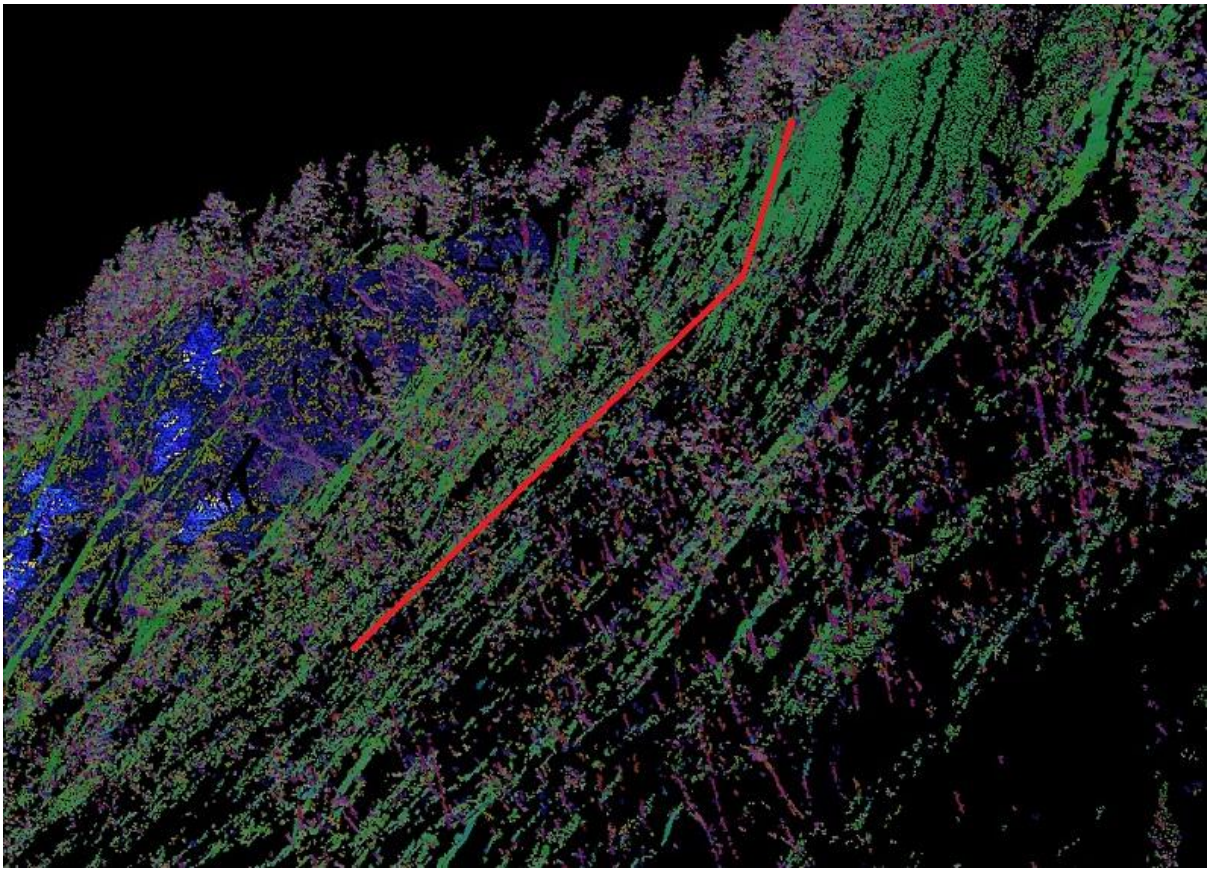

Figure 34 Illustrate the sliding surface where the angle becomes steeper (red line) to the edge of the back scarp.

The friction angle that has been used at Ivasnasen is from the tilt test that was done during a laboratory test during June 2012 (Dreiås, 2012). The results from the tilt test shows an average value for the basic friction angle, φb = 27,42 ±1 degree. Since the tilt test is done at samples from Ivasnasen where it is augen gneiss, there is likely to take in concern that there might be some rich biotite layers. For the failure mechanical analysis this was taken in concern and reduced the friction angle to be φb = 25. 25 degrees for the friction angle is common to use for kinematical analysis.

The kinematical analysis that have been done for the structural measurements from the fieldwork, is done by plotting all the structural measurements in the software Dips and then classify them by the different joint sets, as figure 35-37 shows.

For the LiDAR scans, both aerial and terrestrial scans, the kinematical analysis have been done first by Coltop3D. With Coltop3D the dip and dip direction was picked out by the different color sets and then the results have been added in the software Dips. The average values for each joint set have been used, so there are not as many different measurements as there are from the analysis that represents the fieldwork.

All the kinematical analyses that have been done at Ivasnasen (all three of them) are comparable. The structural analyses from fieldwork (figure 35) are much the same and are comparable with the terrestrial LiDAR scan from 2010 and 2011 (figure 36). The only different here is that the results with the LiDAR scans show three more joint sets than the one from the structural measurements done by fieldwork. It was expected that the LiDAR scans would show more different joint sets than the results from the fieldwork. This because of the difficulty to measure the different joint sets in field, due to the inaccessible area. This shows also the usefulness of LiDAR scans, that the structural measurements will give a better understanding of the site with the scans as a reference.

It has been used a topography for figure 36 that is a little different from the kinematical analysis that have been done for figure 35 and 37. The reason is that this is the area for the historical rockslide. The topography in this area with the historical rockslide (figure 36) is a little different from the unstable rock slope area (figure 35 and 37). This is the reason that the topography for the old rock slide has a dip direction/dip of 318/64, for the other analyses the topography has a dip direction/dip of 320/60. To be sure of the topography it was checked with the reconstruction of the area. It was decided to use this also for the field measurements since they include measurements for both the historical rockslide and the unstable rock slope.

Table 6, 7 and 8 shows the average joint sets, foliation, topography and what friction/wedge cone that is used. The representative analyses are showed in a figure (35-37 under each table).

Table 6 Joint sets, topography and other information from the structural analysis done by fieldwork.

Set	Dip	Dip direction	Angle	Variability limit (degrees)
Topography	60	320		
Foliation, S1	53	320		±13
Joint set 2	64	229		±17
Joint set 3	77	192		±13
Joint set 4	64	143		±15
Friction cone	90	90	25	
Wedge cone	90	90	65	

Figure 35 shows the results of the kinematical analysis that is done based on the fieldwork. It is both possibilities for wedge and planar failure. The stereonet shows all the plots, and it is visible that the main measurements are of the foliation.

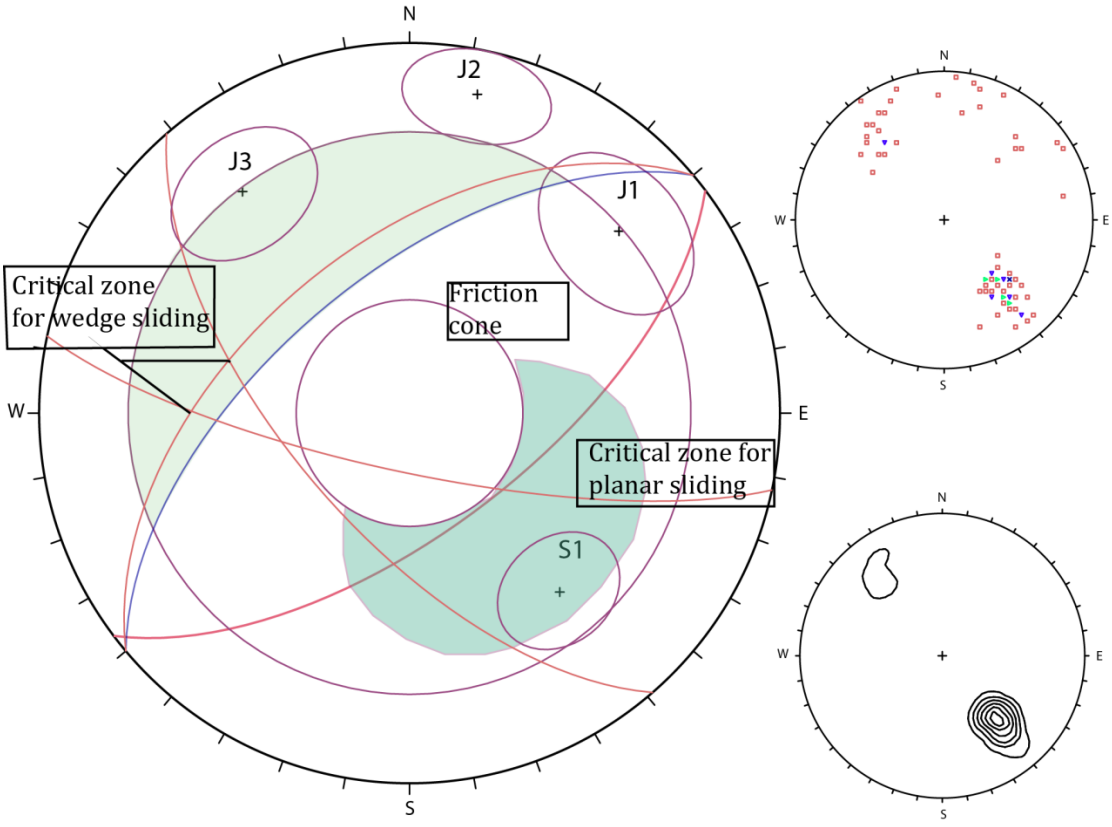

Figure 35 Kinematical analysis for the structural measurement from fieldwork at Ivasnasen, shows possibilities for both planar and wedge sliding.

Table 7 Joint sets, topography and other information from the structural analysis done by LiDAR scans (TLS, 2010 and 2011) of the scar.

Set	Dip	Dip direction	Angle	Variability limit (degrees)
Topography	64	318		
Foliation, S1	54	321		±10
Joint set 2	56	230		±10
Joint set 3	70	187		±10
Joint set 4	55	143		±10
Joint set 5	54	063		±10
Joint set 6	73	052		±10
Joint set 7	70	358		±10
Friction cone	90	90	25	
Wedge cone	90	90	65	

Figure 36 shows the results of the kinematical analysis that is done based on LiDAR scans from 2010 and 2011. This is the scans from the historical rockslide that are analyzed. It is both possibilities for wedge and planar failure. The stereonet shows an average value of the results from Coltop3D. It is more different joint sets than was found during fieldwork.

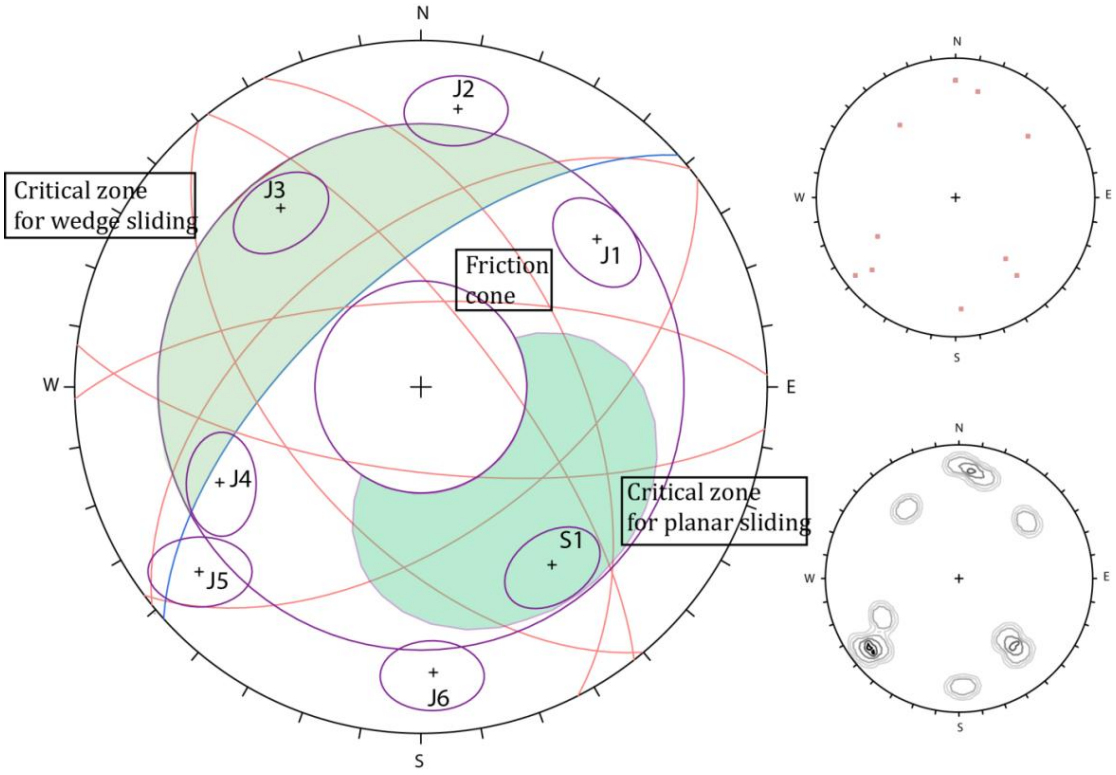

Figure 36 Kinematical analysis from LiDAR scans TLS 2010 and TLS 2011, shows possibilities for both planar and wedge sliding

Table 8 Joint sets, foliation and topography and other information from the structural analysis done by LiDAR scans ALS 2011 and TLS 2011.

Set	Dip	Dip direction	Angle	Variability limit (degrees)
Topography	60	320		
Foliation, S1	52	320		±10
Joint set 2	81	265		±10
Joint set 4	55	143		±10
Joint set 5	79	053		±10
Joint set 6	62	032		±10
Friction cone	90	90	25	
Wedge cone	90	90	65	

Figure 37 shows the results of the kinematical analysis that is done based on LiDAR (TLS and ALS) scans from 2011, both unstable and historical rockslide. It is both possibilities for wedge and planar failure. The stereonet shows an average value of the results from Coltop3D. It is also here more different joint sets than was found during fieldwork.

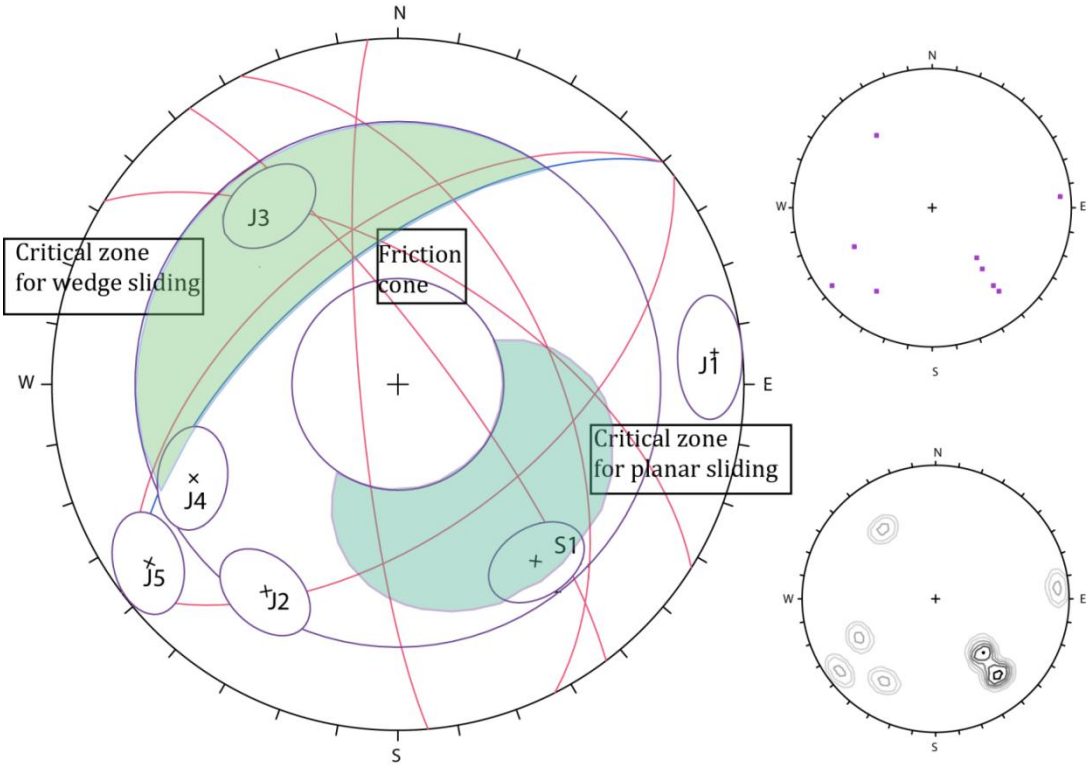

Figure 37 Kinematical analysis from LiDAR scans ALS 2011 and TLS 2010, shows possibilities for both planar and wedge sliding.

6.2 Vollan

For Vollan the geology is more complex, and it was not that easy to find a way to classify each joint set that gave a reasonable answer. To solve the complex geology it was decided to group the area in smaller groups to see if there were any relation or systematically differences in each area (see figure 38). For each smaller group that classified each area at Vollan all the structural measurements were put in different foliations and joint sets, and then calculated to an average. Since the foliation is the first index if an area is homogenous or not, this was the first to consider. This was done after all the structural measurements were put in a map (by using ArcMap) with different symbology for the foliations and the joint sets. From figure 38 it is also obvious that it is most structural measurements for the upper part of Vollan, but it seems like all the parts are representative after the kinematical analysis was done.

The dip direction/dip for the topography was chosen by the measurements that were done at the back scarp. It was decided to take one of the worst measurements and see how the analysis is related to this. This is a discussable way of doing it since they are in different lithology. But as can be seen as an example "the lower part", this does not influence the analysis since it does not result in any failure. Because of this it was decided to keep the same topography to get "the worst case" scenario out of all the analysis.

At Vollan all the kinematical analysis shows that all the failure mechanism might be representative in the area. When comparing all the analysis together we see that all except the lower part of Vollan might have a toppling failure mechanism. The wedge failure (marked with a black cross where it is in the critical zone for wedge sliding) is represented in all except the lower part of Vollan. Planar failure does occur, but is not as clear as the toppling and wedge failure. The analysis done of the part called "cabin area" is the most visual for planar sliding, and also the lower part of Vollan shows a tendency of planar failure. Where it is marked as wedge failure it is in a steep area, so the consequences will not be that big since it is that steep and the angle between are really low. The result of this will be that it is not much volume that will fail if a failure should occur.

After comparing the kinematical analysis of each area at Vollan, there might be likely to think that the lower part does not belong to the unstable part of the area. If this is the reality the toe line should be where the zone for the lower part starts. It is reasonable to think so, since the kinematical analysis does not show the same tendency for toppling and wedge failure as it does for the other parts. Anyway it is important to do some more analysis of the area to be sure of this hypothesis. But also due to the orthophotos this might be a good conclusion, based on the difference in structures that can be seen. The toe is drawn as far down as it is because it will have consequences all way down if the phyllite layer fails.

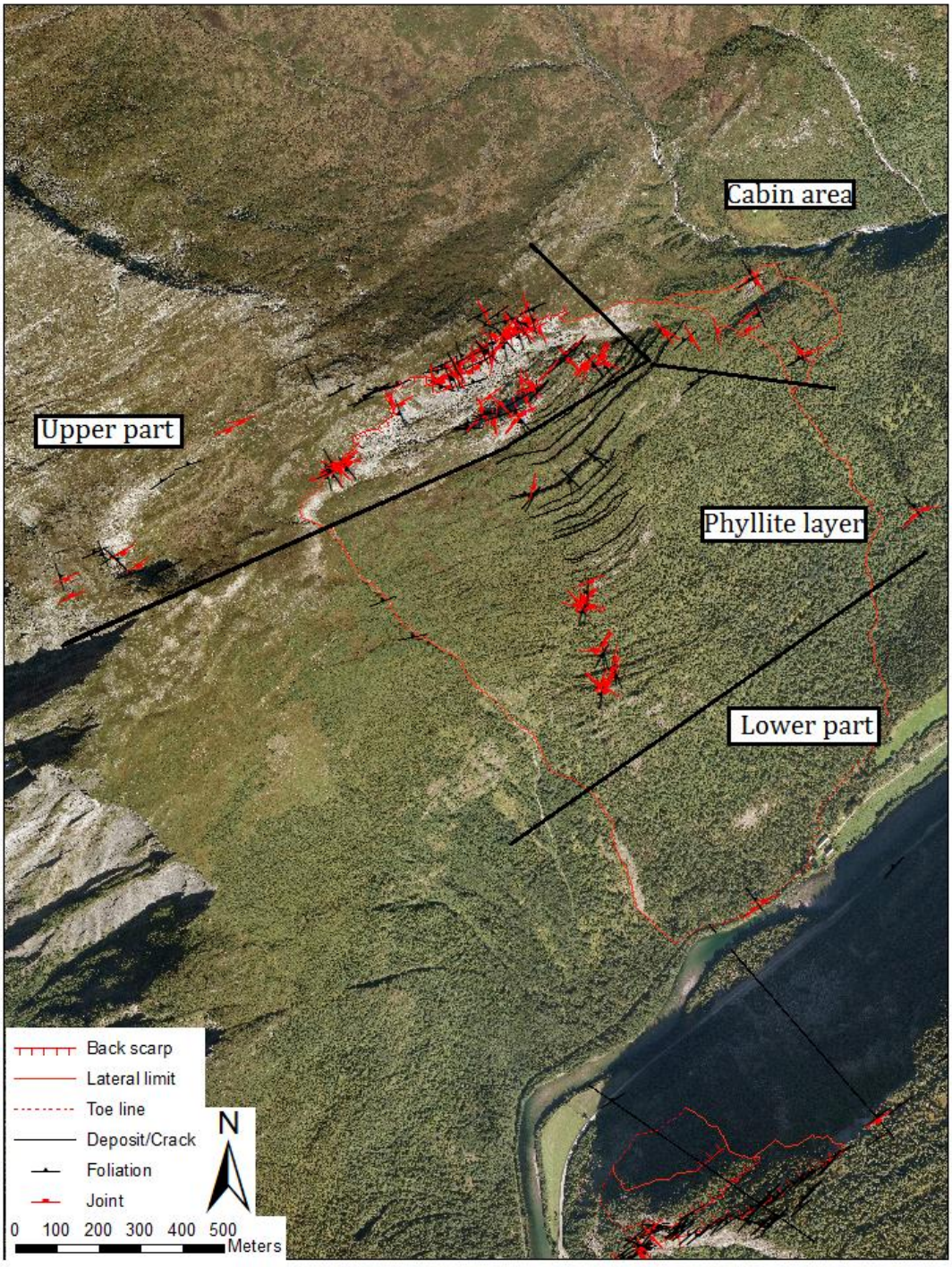

Figure 38 How Vollan is divided in the different areas, with the symbol that is rotated based of the structural measurements of how the dip/dip direction of the joints and foliation are.

Table 9 Joint sets, topography and other information from the structural analysis done by fieldwork, upper part.

Set	Dip	Dip direction	Angle	Variability limit (degrees)
Topography	84	152		
Foliation, S1	88	334		±10
Joint set 1	53	246		±14
Joint set 2	15	147		±10
Joint set 3	80	076		±16
Joint set 4	56	326		±16
Joint set 5	90	227		±10
Friction cone	90	90	20	
Wedge cone	90	90	70	
Toppling	64	152		

Figure 39 shows the results of the kinematical analysis that is done from the upper part of Vollan based on structural measurements from fieldwork. From the analysis it is toppling failure that is the major hazard, since the volume for wedge failure will not be of significance. The fieldwork support this analyses that the major treat here is toppling failure since the upper part is part of the back scarp, and it has been seen that toppling failure mechanism is dominating here.

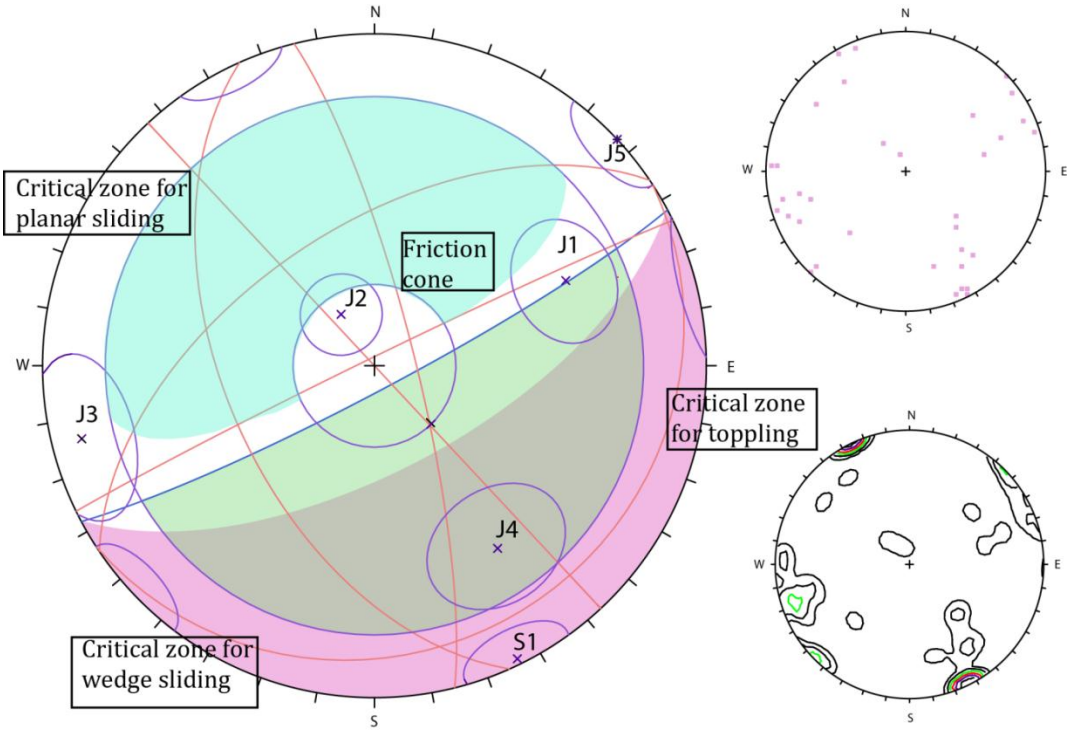

Figure 39 Kinematical analysis for the upper part of Vollan. Possibilities for planar, toppling and wedge failure.

Table 10 Joint sets, topography and other information about the area around the cabin at Vollan.

Set	Dip	Dip direction	Angle	Variability limit (degrees)
Topography	84	152		
Foliation, S1	66	159		±10
Joint set 1	55	227		±10
Joint set 2	29	286		±10
Joint set 3	78	310		±10
Friction cone	90	90	20	
Wedge cone	90	90	70	
Toppling	64	152		

Figure 40 shows the results of the kinematical analysis from the cabin area of Vollan based on structural measurements from fieldwork. From the analysis it is toppling failure and planar sliding that is the biggest treat here, since the volume of the wedge failure will be too small it is not critical. But it must be mention that it should have been some more measurements here to be sure.

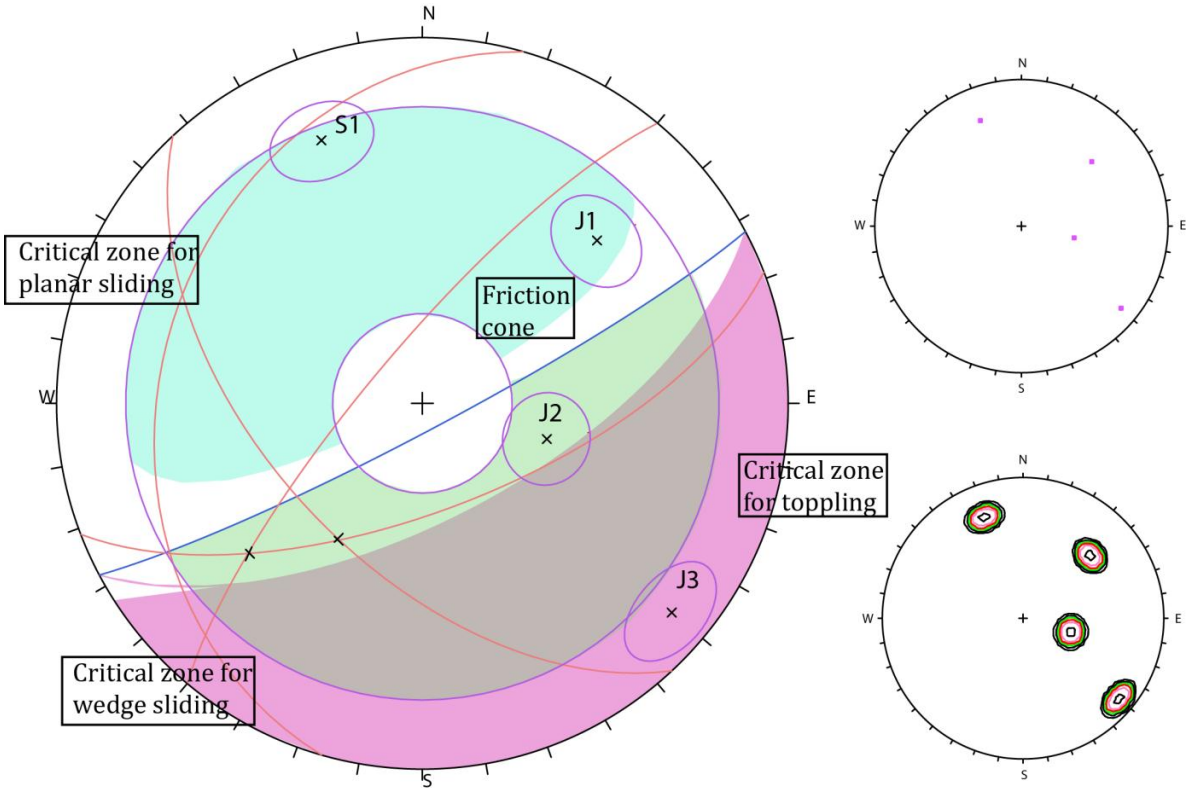

Figure 40 Kinematical analysis of the area around the cabin at Vollan. Possibilities for planar, toppling and wedge failure.

Table 11 Joint sets, topography and other information about the phyllite layer at Vollan.

Set	Dip	Dip direction	Angle	Variability limit (degrees)
Topography	84	152		
Foliation, S1	36	271		±10
Joint set 1	79	136		±10
Joint set 2	87	255		±10
Joint set 3	85	359		±10
Friction cone	90	90	20	
Wedge cone	90	90	70	
Toppling	64	152		

Figure 41 shows the results of the kinematical analysis that is done from the phyllite layer of Vollan based on structural measurements from fieldwork. From the analysis it is toppling failure that is the major treat here, since the volume of the wedge failure will be too small it is not critical, and the planar sliding do not exist in these measurements. But it must be mention that it should have been some more measurements here to be sure.

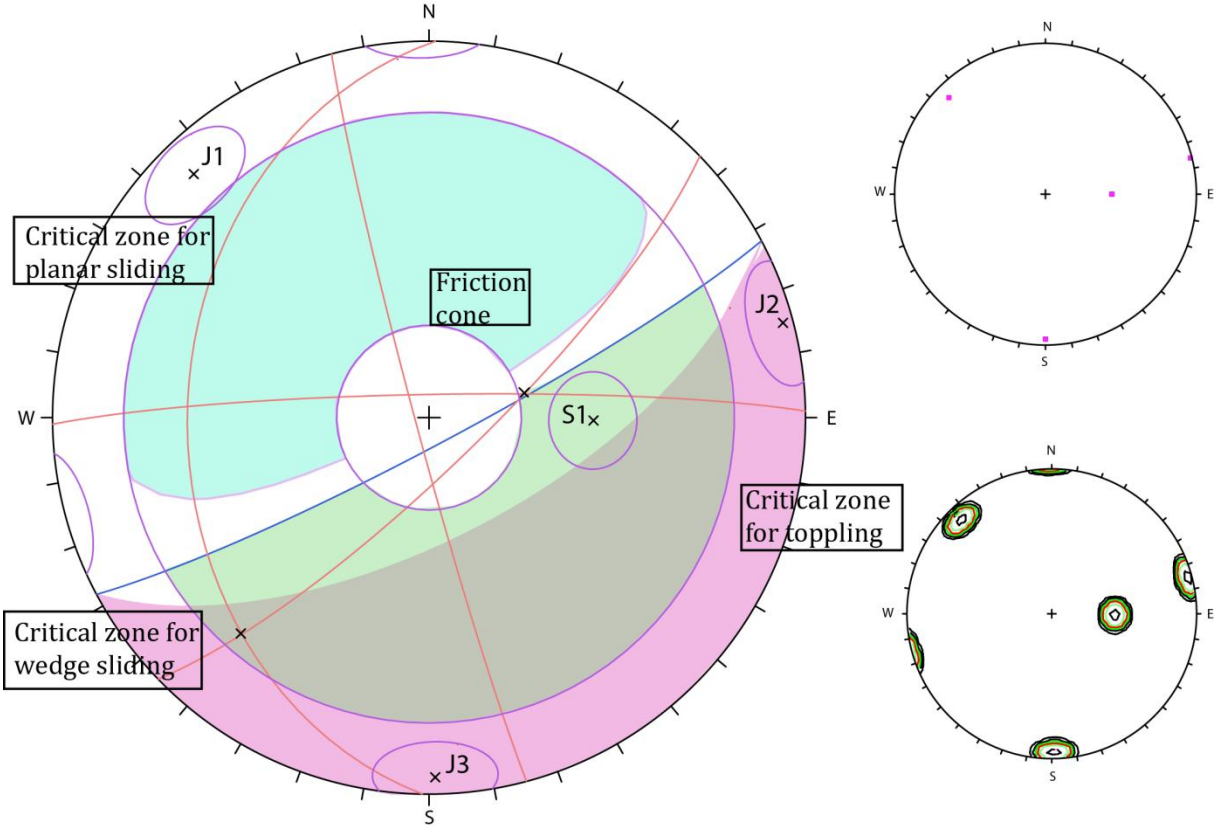

Figure 41 Kinematical analysis for the phyllite layer at Vollan. Possibilities for toppling and wedge failure.

Table 12 Joint sets, topography and other information about the lower part of Vollan.

Set	Dip	Dip direction	Angle	Variability limit (degrees)
Topography	84	152		
Foliation, S1	09	185		±10
Joint set 1	38	255		±10
Joint set 2	52	077		±10
Friction cone	90	90	20	
Wedge cone	90	90	70	
Toppling	64	152		

Figure 42 shows the results from the kinematical analysis that is done from the lower part of Vollan based on structural measurements from fieldwork. From the analysis it is no treat for any failure mechanism in this area. As discussed earlier this could support the theory that this is not part of the unstable area. But it must be mention that it should have been some more measurements here also to be sure.

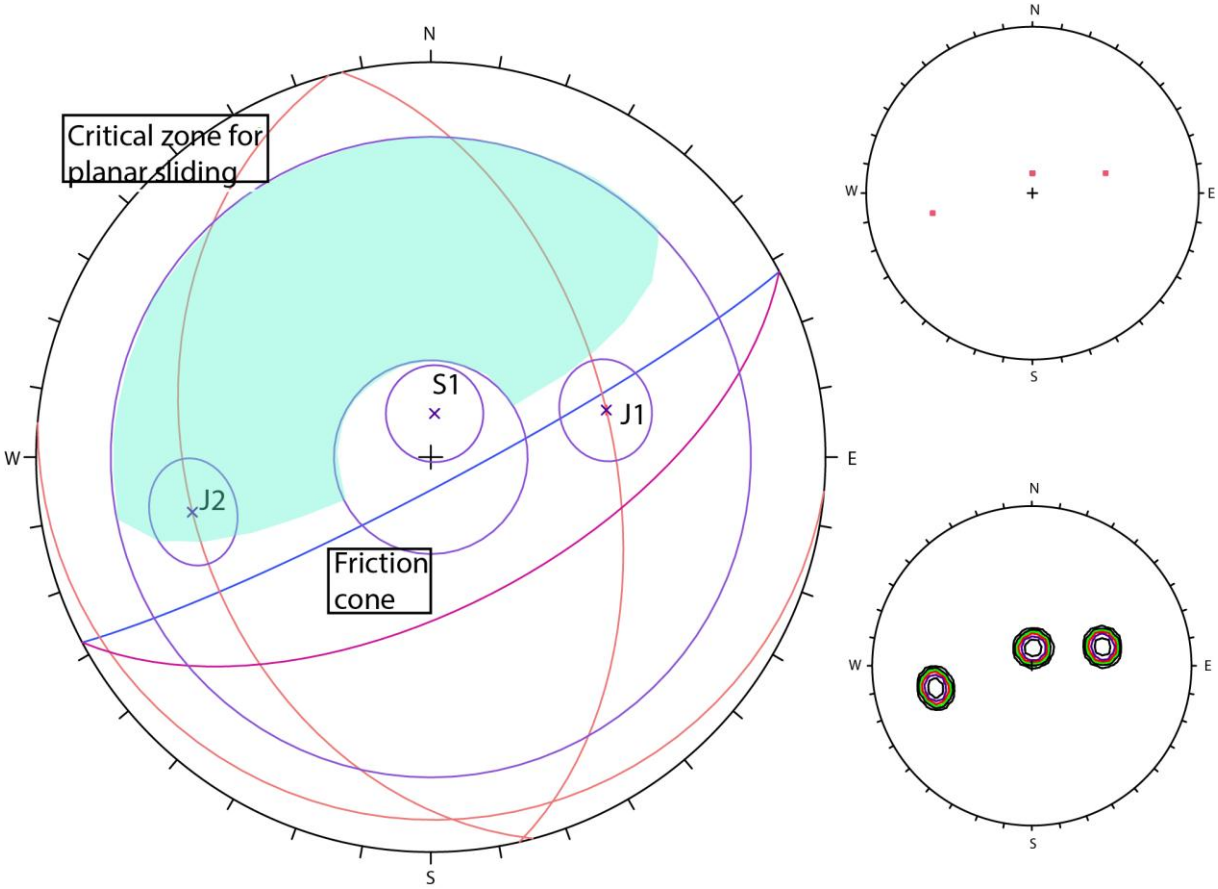

Figure 42 Kinematical analysis for the lower part of Vollan. No toppling or wedge failure can happen with this analysis, but there might be some planar sliding.

7.0 Laboratory analysis

7.1 X-ray diffraction (XRD)

The 24.04.2012 the XRD analysis was done for five different rock samples from both Ivasnasen and Vollan in the laboratory at NTNU, please see appendix 1. The analysis has been done at a *Bruker D8 ADVANCE. DIFFRACplus SEARCH software* in combination with the database *PDF-2* and the results that were suggested for the mineral faces for the samples are listed in table 1 (Drivenes and Sørløkk, 2012).

Table 13 XRD analysis of five different rock samples.

Sample		5, Meta-arcose	7, Gneiss	11, Quartzite	12, Augen-gneiss	13, Phyllite
Journalnumber		120139	120140	120141	120142	120143
Mineralgroupe	Mineral					
Quartz	Quartz	34	52	62	36	14
Glimmer	Mica	47	7			22
	Biotite			8	17	
	Phlogopite					15
Chlorite	Clinochlore	<1		1	<1	
Feldspar	Plagioclase	7	28	11	25	27
	Potassium feldspar	11	13	18	21	22
Amphibole	Actinolite					
Pyrite	Pyrite	<1	<1	<1		
Graphite	Graphite					1
Total		99	100	100	99	100

It is important to recalculate each mineral so they represent a value of 100% in total for the quartz, feldspar and plagioclase. This is needed to classify them further based on figure 43. Table 14 gives the values after analyzing and recalculated the results to 100% for the three minerals.

Table 14 Recalculation of the rocksamples (Woolley, 1996).

Sample		5	7	11	12	13
Journal number		120139	120140	120141	120142	120143
Recalculation		52%	88%	91%	82%	63%
	Mineral					
Quartz	Quartz	65,4	59,0	68,0	43,9	22,0
Alkali feldspar	Potassium feldspar	21,2	14,8	19,8	25,6	34,9
Plagioclase	Plagioclase	13,5	31,8	12,1	30,5	42,9

In the process of preparing of the samples for the XRD machine, it is important that the crushing of the samples down to dust so it is just fine-fine particles left and no bigger grains that can lead to a mistake. The micas are especially hard to crush since they are flakes and are not easy to observe either. There might also be that there are two times the values of glimmer, because of the peaks that is close to each other and may overlap (appendix 1). The quartzite does also contain less quartz than it normally does, but this could be errors in the preparations or other causes to that. The metamorphism for metamorphic rocks does often result in hard minerals and high intact rock strength, as the gneiss and quartzite that is found for this thesis (NBG and NFF, 2000).

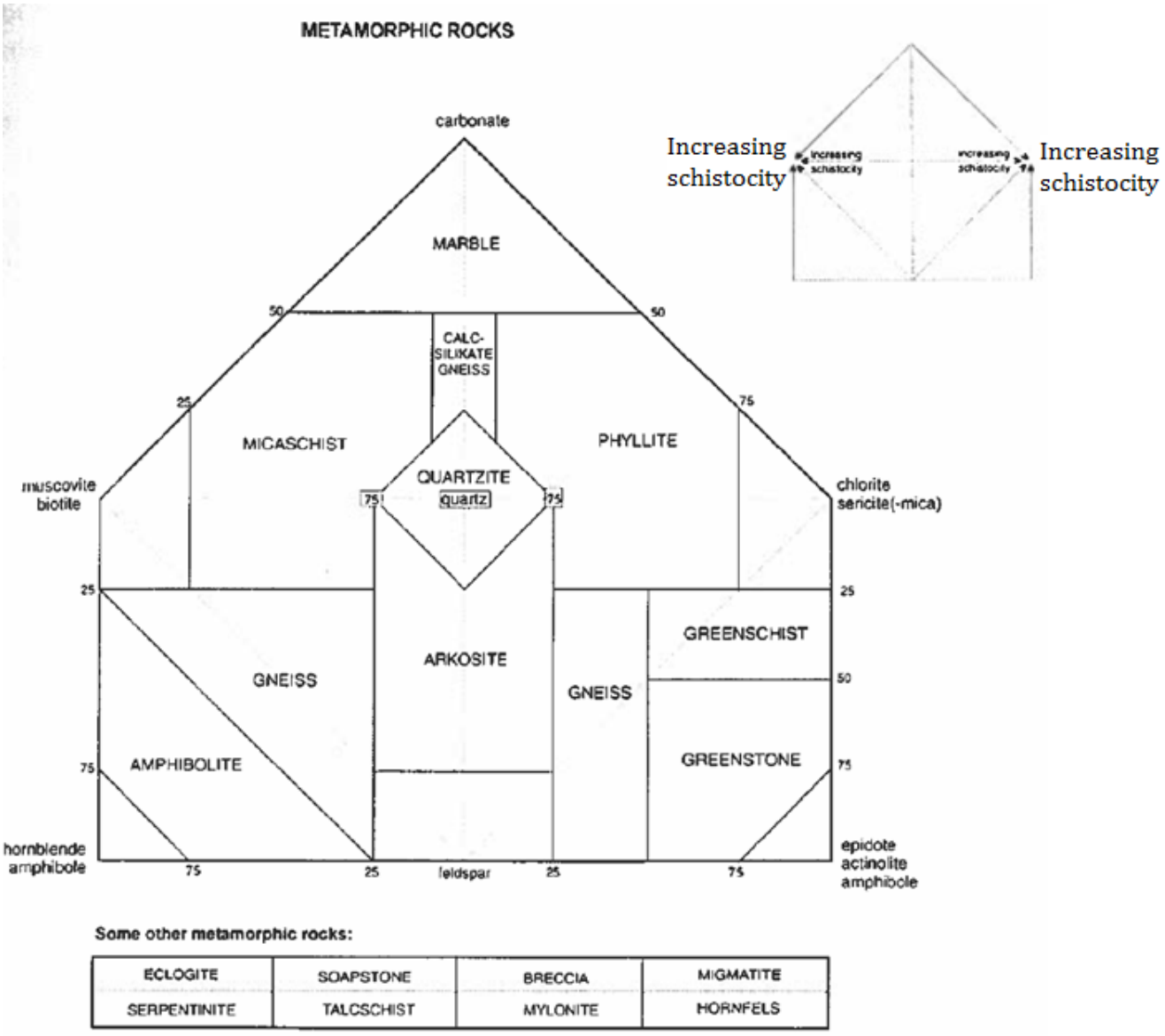

Figure 43 Simplified classification of metamorphic rocks from handbook 2 (NBG and NFF, 2000).

7.2 Rock mechanical testing

As a part of the subject "GEOL3093 –spesialpensum til masteroppgaven/særpensum" a week of laboratory experiment was done after another fieldtrip to Ivasnasen. The laboratory experiment, rock mechanical testing, could only be done from rock samples collected from Ivasnasen. This because of really difficult accessibility to pick up huge enough rock samples at Vollan. The laboratory experiment did follow the ISRM standards and the NTNU/SINTEF standards.

One huge block of augen gneiss was collected at Ivasnasen, and all the cores were drilled out of this. This gives a better result, since it is not necessary to consider if the weathering process is in different stages or not if there were different samples. It has been performed 6 different tests in the rock mechanical laboratory, these are:

- Uniaxial compressive strength
- Young's modulus
- Sonic velocity
- Tilt test
- Brazilian test
- Point load test

The results from the 6 different laboratory experiments have been presented in table 15. These results are the average from the entire test that was done, where it was done approximately 10 different tests for each experiment. The entire laboratory report can be found in (Dreiås, 2012).

Table 15 Results from the rock mechanical testing.

Test:	Normal:	Parallel:
Sonic Velocity (V)	3163m/s ±140	4179m/s ±27,6
Youngs modulus (E_{ci})	31GPa ±1,9	33GPa ±3,9
Poisson's ratio (υ)	0,11 ±0,06	0,13 ±0,08
Uniaxial compressive strength (σ_{ci})	72,4MPa ±4,5	78,3MPa ±14,6
Fracture angle	$16,2^0$ ±3,4	Fracture angle = $18,6^0$ ±1,7
Brazilian (σt)	12,9MPa ±1,5	13,22MPa ±2,2
Point load test (σp)	9MPa ±0,9	5MPa ±0,8
Tilt test (ϕb)	27,42 ±0,5	

Normally there are a bigger difference between the normal and the parallel bedding. In this case since the rock is an augen gneiss the error here might be the foliation of the core sample, and if there were some small invisible cracks in the cores. Anyhow all of the experiments are representative and useful in further investigation of the site.

It would have been interesting to do the same tests at Vollan as well, but since the site is so high up (1010m.a.s.l) it was impossible to carry out huge enough samples to do the tests on. The author tried to carry out rock samples, but got to know afterwards in the laboratory that these samples were too small. The possibility to pick up the rocks with a helicopter was discussed, but the conclusions were that it was still too difficult to get out huge enough rock samples. Since the site at Ivasnasen is close to the main road, it was easier to pick up some loose blocks that were close to the road. A weathering process has started for blocks that are picked up like this, but this has been taken in concern for the analysis.

8.0 Ante-Rockslide Topography (ART) and volume estimations

The procedure to reconstruct the topography with the SLBL procedure for ART reconstructed and deposits:

1) First reconstruct the landslide and define the limits for the unstable area with polylines in ArcGIS (figure 51 and 52). For getting more precise lines, it was used ArcScene to see the area and the lines in 3D. This is done by working through the vectors and gives the angle of intersection between.
2) Start to reconstruct the topography in Polyworks by using polygones to build up the surface of the rockslide area limits. To use the information further it is important to import the polygones as 'raster'-files after the reconstruction.
3) For the SLBL it is needed to define some fixed points, this is done by setting the hole area to be = -1, and everything else (around) = 1. Ended up with two fixed points for the historical landslide and three different fixed points for the unstable area; 1) first scenario, 2) second scenario and the last 3) for the third scenario.
4) Export the data that can be read in SLBL to ASCII (grid text format); raster to ASCII.
5) Input ASCII files to CONEFALL for all fixed points. ASCII files are standard input and output files in the software CONEFALL.
6) Output CONEFALL with an ART reconstruction and deposits. ART is the reconstruction of the topography and for the unstable area. It is easy to see where the rock mass is thickest since the red color describes where it is the thickest part.

Figure 44 and 46 show the reconstruction and construction of the topography for the historical rockslide and the unstable part of Ivasnasen. Figure 44 have two different scenarios, where scenario 1 represents the "newest" part and scenario 2 represent the whole part. During the reconstruction it was found traces that can relates to that it has been two historical rockslides in the area. The solutions in figure 44 give a picture of the amount of each of them. Figure 46 is the unstable part of Ivasnasen and shows three different scenarios. Scenario 1 is the "worst case" scenario, and the total volume of masses will be biggest if this scenario happens. Fix point 1 represent the colors (green and purple) in each scenario (figure 44 and 46) the values outside the areas. Fix point -1 represent the representative measured area. These fix point are set like this, so they can represent the area that is of further interest, please see point 3) in the listed SLBL procedures.

The ART that represent the reconstruction of the deposits and the thickness of the rock masses is shown in figure 45 and 47. The red color represent where the deposits/masses are thickest, and the results make sense due to the fieldwork that has been done.

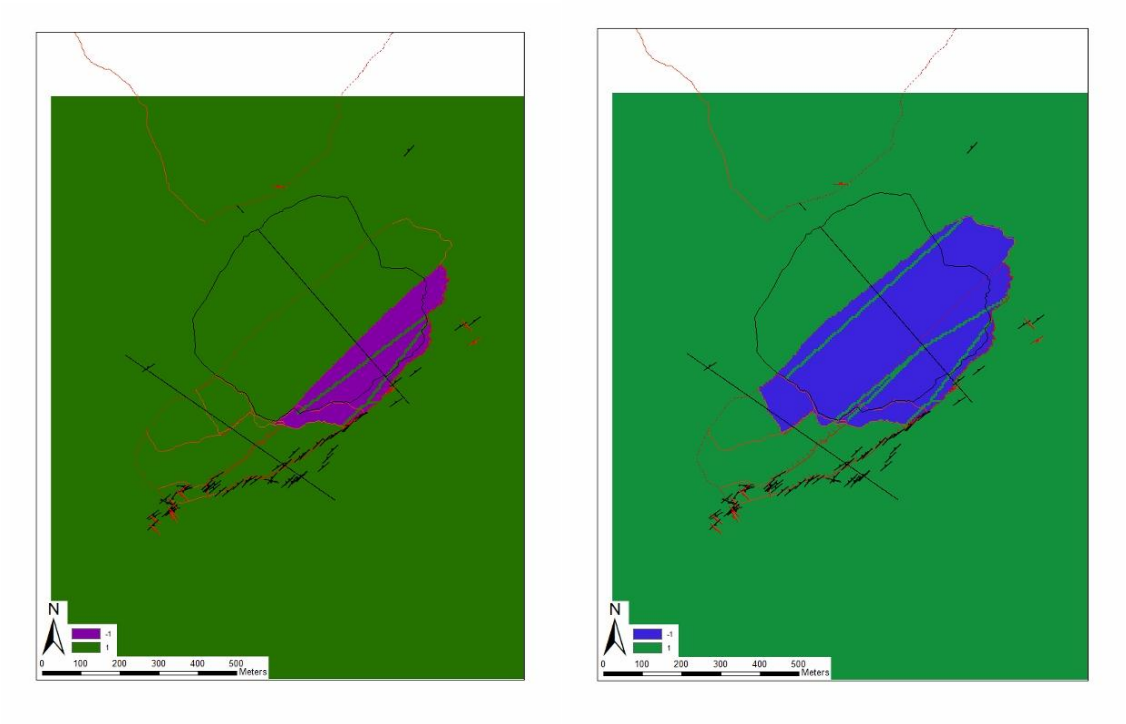

Figure 44 Reconstruction of the topography for the old historical landslide at Ivasnasen. Left: scenario 1 -the upper part. Right: scenario 2 -the whole part. It is likely to think that part 1 is the youngest part that has slide out. Purple (left) and blue (right) correspond to fixpoint -1 (marked area) and the green color correspond to fixpoint 1 (everything around).

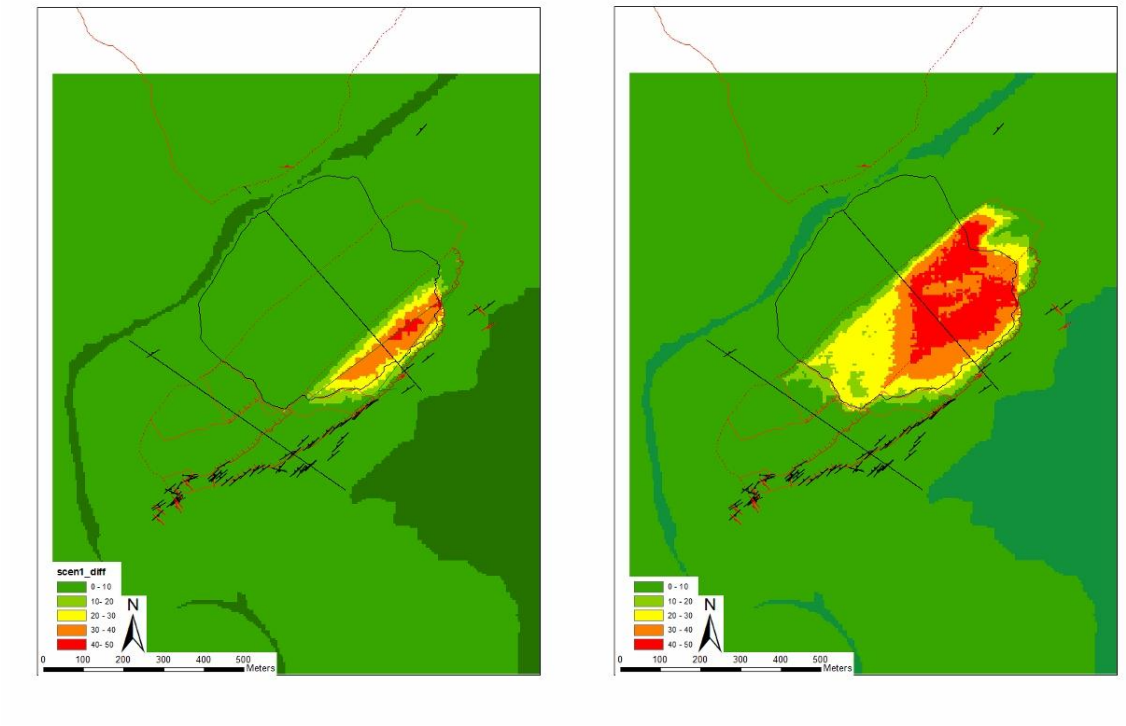

Figure 45 ART reconstruction of the historical landslide scenario 1 (left) and scenario 2 (right), where the red color represents the thickest part of the deposits.

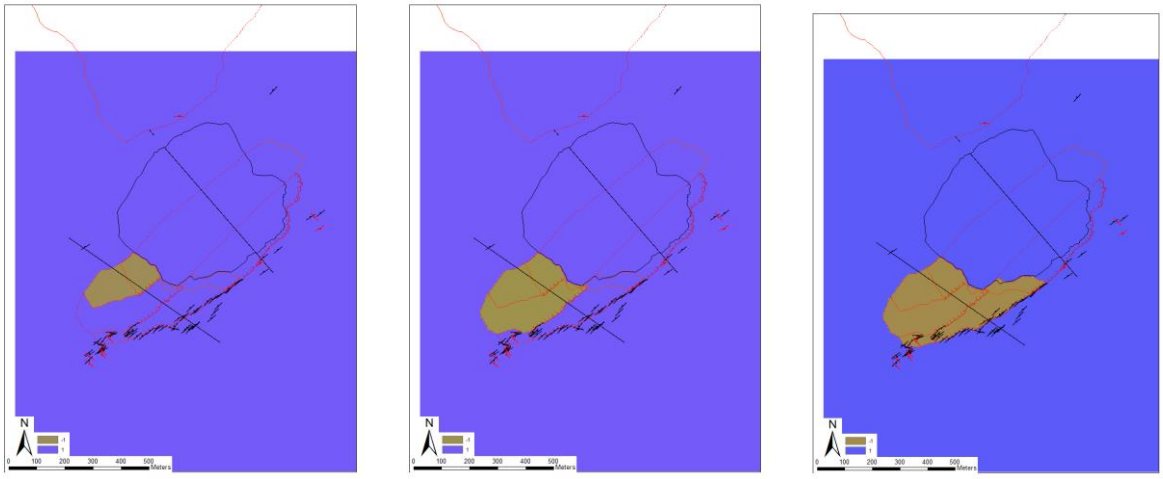

Figure 46 The unstable area at Ivasnasen, classified as scenario 3 (left), scenario 2 (middle) and scenario 1 (left). All of the scenarios shows how the area has been classified. The color brown represent the fixpoint -1 and the purple represents fixpoint 1.

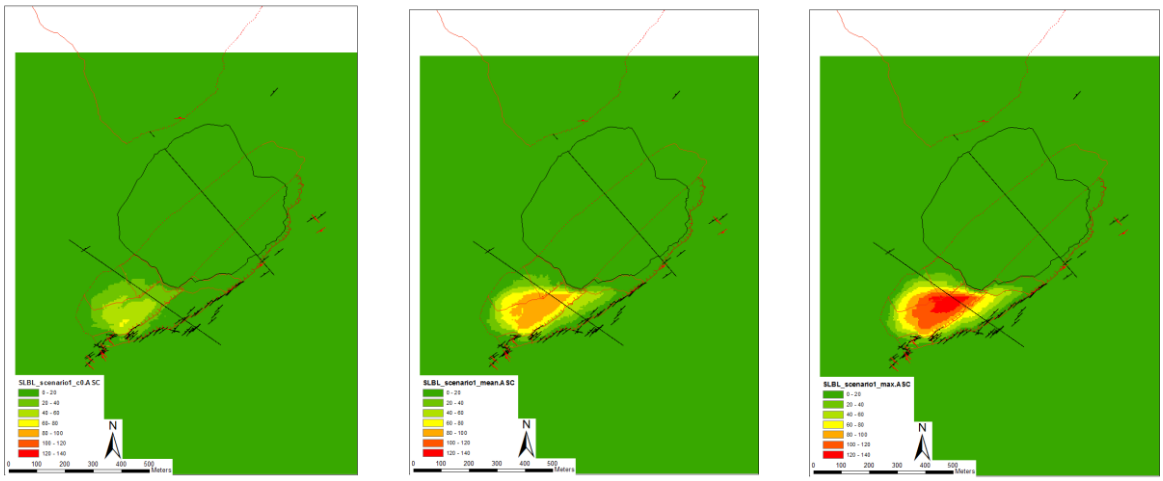

Figure 47 The thickness of the rockmasses for each scenario, scenario 3, scenario 2 and scenario 1.

Figure 48 and 49 shows where the profiles have been drawn for the historical rockslide and the unstable part at Ivasnasen. From these two lines the investigations for the topography was picked out. Figure 48 is the historical rockslide and shows each scenario (1 and 2) and also the deposits area. Figure 49 is the unstable part of Ivasnasen and describes how the part is classified in each scenario (1, 2 and 3). For the historical rockslide it was visible that it most likely has been two rockslides happened to different time periods. The reason for this is that it was visible traces of another back scarp (figure 48, light orange 0, 1, 0 layer). With the visible traces of another, older, back scarp it is reasonable to think that it has been two events. This will be discussed further under chapter 10 (discussion).

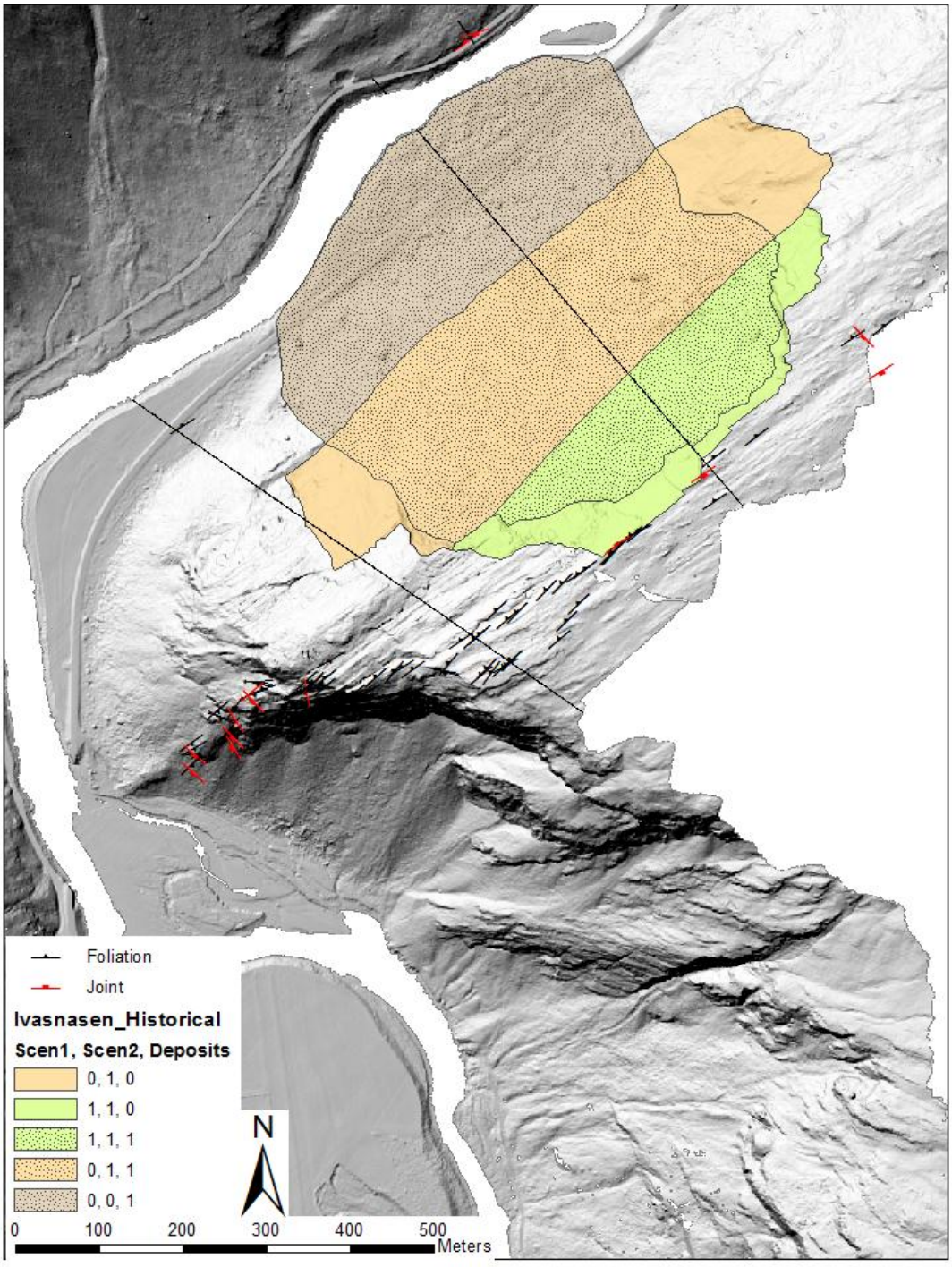

Figure 48 Shows the historical part of Ivasnasen and how it is groped. The black line shows where the profile is taken from. For the historical landslide it has been drawn two different back scarps (0,1,0 and 1,1,0) this symbolize two different happenings, and will be discussed further.

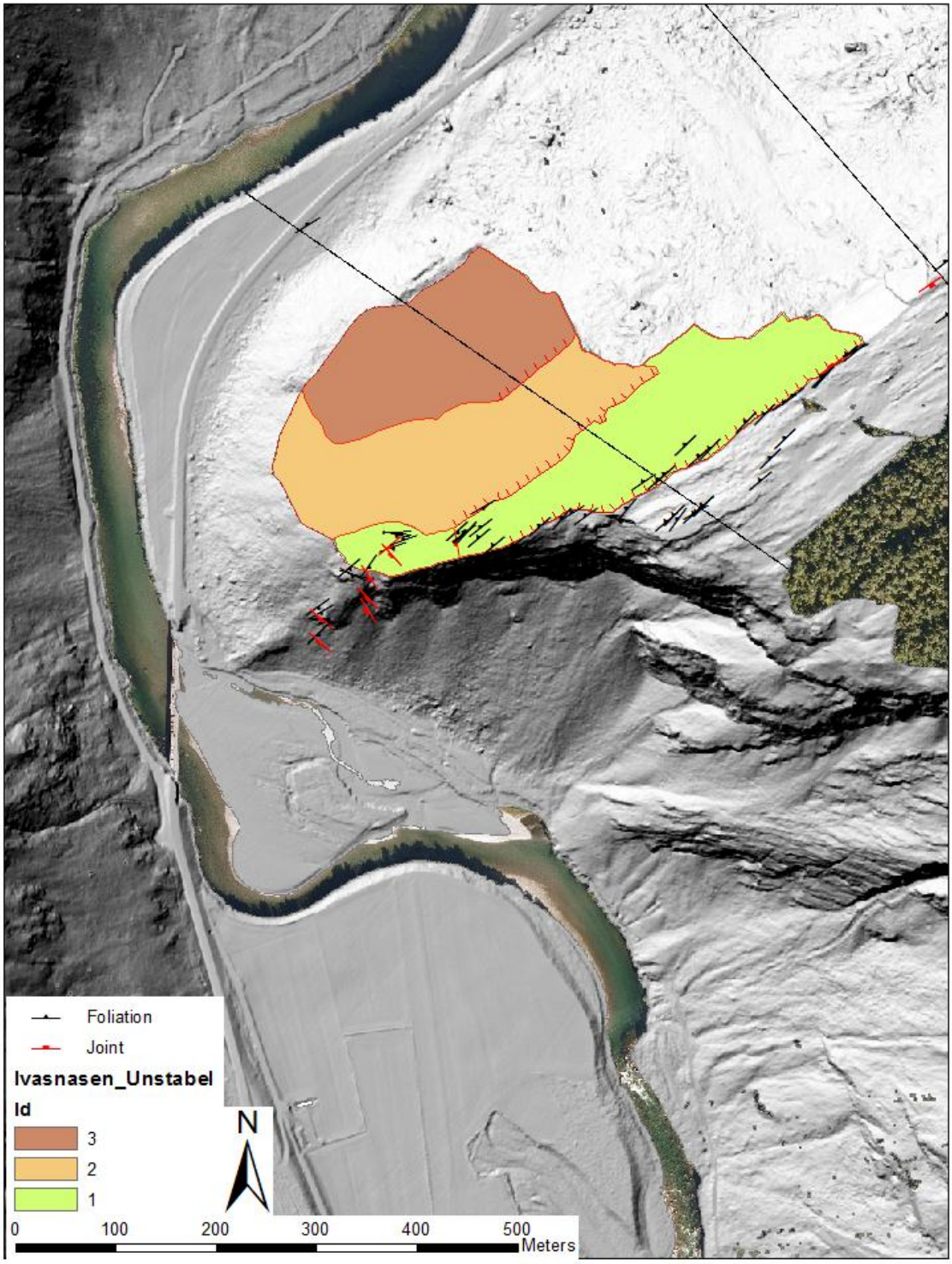

Figure 49 Shows the unstable part of Ivasnasen and how it is groped. The black line shows where the profile is taken from. The colors represent the three different scenarios.

Figure 45 and 47 describes the lowest interface between the bedrock and the deposits, and this gives the maximum thickness of the deposits for the historical rockslide at Ivasnasen. Thereafter the SLBL algorithm is used in the software CONEFALL to get the height different between the straight line and the maximum deposits (figure 50), and then the volume calculations can be done. The same was done for the unstable rock slope. Since there are several different scenarios for the unstable area it is more illustrating to show it for the historical one. The maximum height = 55m and maximum angle = 42 degrees of the deposits were measured and used for the volume calculations. The thick black line in figure 50 shows todays topography. If we combine the two lines that have been drawn above and under the topography line we get the maximum thickness of the deposits. From this an average thickness of the deposits are found, which is multiplied by area of the landslide to find the volume. A curvature (c) represent a tolerance value, and this leads to a second degree curve (Jaboyedoff et al., 2004d) as a convex or concave surface. To decide the curvature parameters, difference of height of 0m and 55m in length of the quadrat was measured, see equation 4 (Jaboyedoff and Derron, 2005):

$$\Delta c = \pm \left(\frac{4 h_{max} \Delta x^2}{L^2} \right) \qquad \textit{Equation 4}$$

h_{max} = Difference between curvature value zero (c=0) and interpreted thickness of deposits/reconstructed topography

Δx = Grid cell size

L = Length of profile

The curvatures are estimated from equation 4 and listed below in table 16. Figures 53 and 54 shows the results for each calculated curvatures and the chosen paths.

Table 16 Calculations of the curvature

	Min	Mean	Max
Historical rockslide	0,016325	0,020406	0,024487
Unstable, scenario 1	0	-0,029562	-0,059124
Unstable, scenario 2	0	-0,033375	-0,066750
Unstable, scenario 3	0	-0,088757	-0,177515

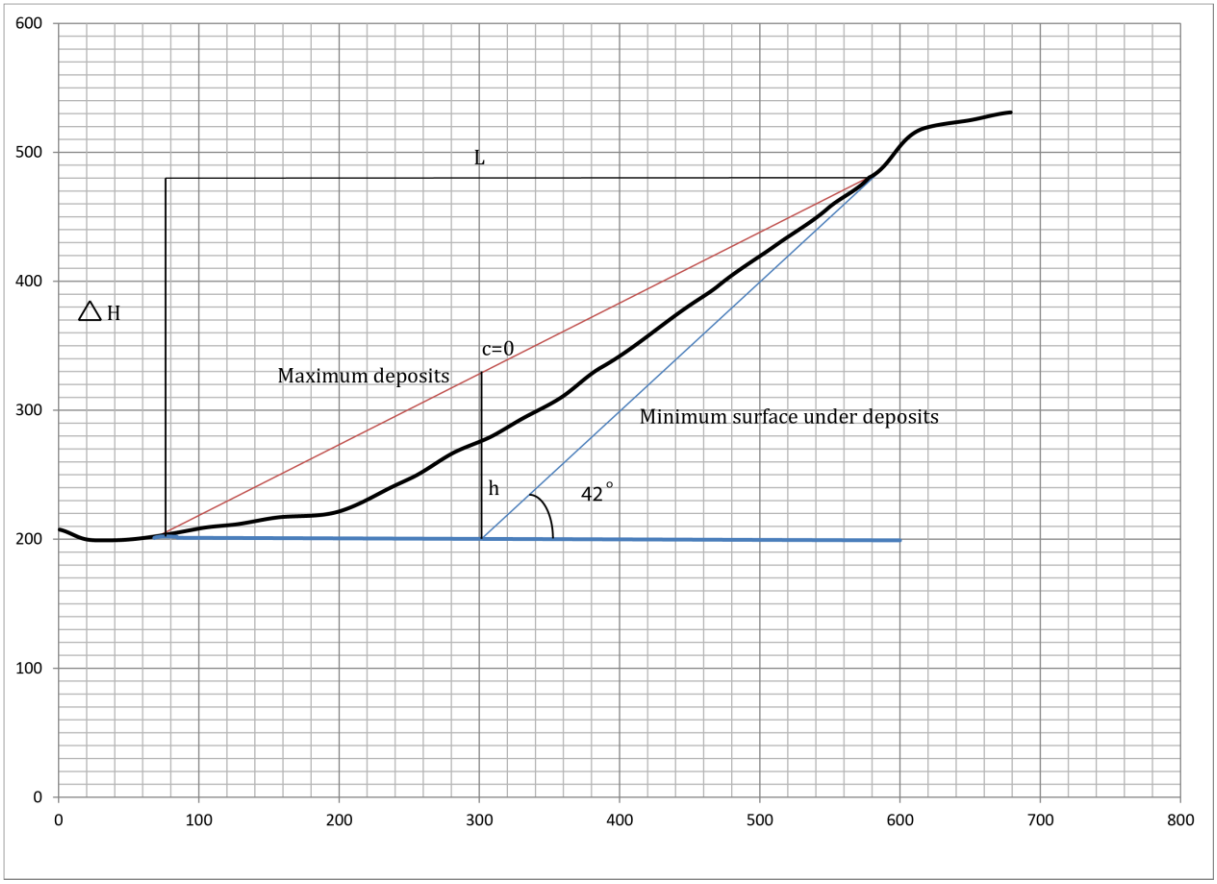

Figure 50 Illustration of how the maximum angle and depth were foud. This is from the topography for the historical rockslide at Ivasnasen. The same procedure were done for the ustable area at Ivasnasen.

8.1 Interpretations of results

The software CONEFALL is using the text grid files (ASCII) for the DEM (DEM for the deposit volume estimations and the inverted DEM for the ART reconstruction) and the source points (deposits polygons and ART polygons) (Jaboyedoff and Labiouse, 2003). After CONEFALL has run the different profiles the software gives out average estimated curvatures (min, max and mean). These curvatures are then added to ArcGIS. The values for the curvatures for the reconstructed ART and the deposits areas (see figure 45 & 47) can then be used to estimate the final volume for the historical and unstable area at Ivasnasen. Zonal statistics in ArcGIS are used for the volume estimations. The zonal statistics summarize the values of raster with the zones of another dataset and reports the results to a table (see table 17-18). The zonal inputs are the polygons that are made based on the sketches that is made in ArcGIS and transformed to polygons (figure 51 and 52).

A SUM table summarizes the height difference between the input rasters and the volume of each polygon. It is calculated by multiplying the SUM from the zonal output table with the DEM cell size, see equation 5:

$$V = SUM * 5m * 5m \qquad \textit{Equation 5}$$

To get a good estimate for the calculated volume for the historical rockslide it is important to have the difference between the topography before and after the rockslide. It is therefore important to also add the volume for the deposits. Please see appendix 2 for all the information of the used values.

Table 17 Volume calculations for the reconstructed topography with the deposits for the historical rocklide at Ivasnasen. Scenario 1 represent the whole area and scenario 2 the upper part of the rockslide.

	Volume
Scenario 2	5237265,8 = 5,2 Mm^3
Scenario 1	1223329,2 = 1,2 Mm^3

Table 18 Volume calculations for each scenario for the unstable rock slope at Ivasnasen. All three scenarios are presented, and all three shows a minimum, mean and maximum scenario.

	VOLUME
Scenario 1, c0	2088675 = 2,1Mm^3
Scenario 1, mean	3981250 = 4,0Mm^3
Scenario 1, max	5395325 = 5,4Mm^3
Scenario 2,c0	1104200 = 1,1Mm^3
Scenario 2,mean	1867800 = 1,9Mm^3
Scenario 2, max	2784850 = 2,9Mm^3
Scenario 3, c0	113875 = 0,1Mm^3
Scenario 3, mean	319075 = 0,3Mm^3
Scenario 3, max	633925 = 0,6Mm^3

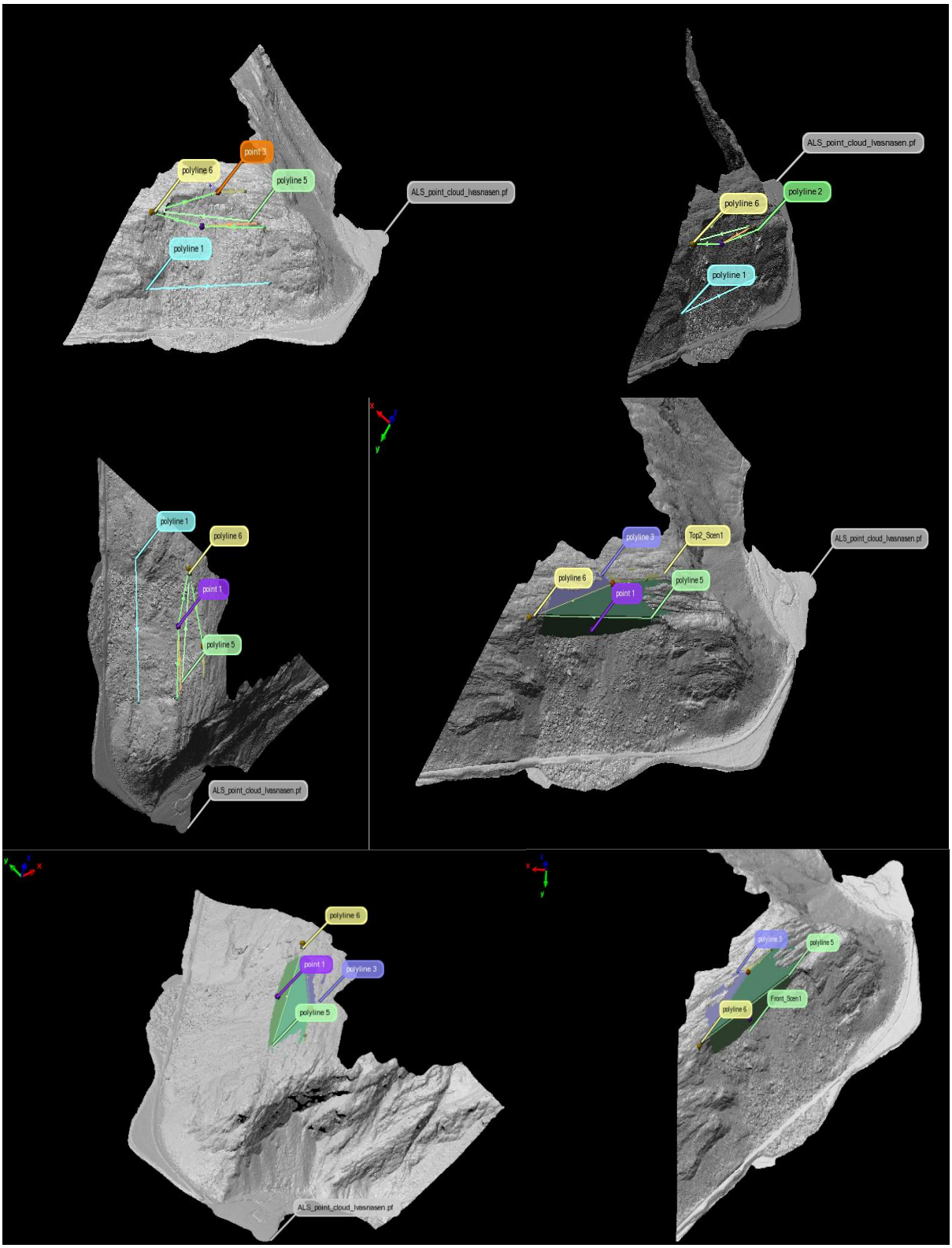

Figure 51 Polylines that have been drawn in PolyWork to reconstruct the historical rockslide at Ivasnasen.

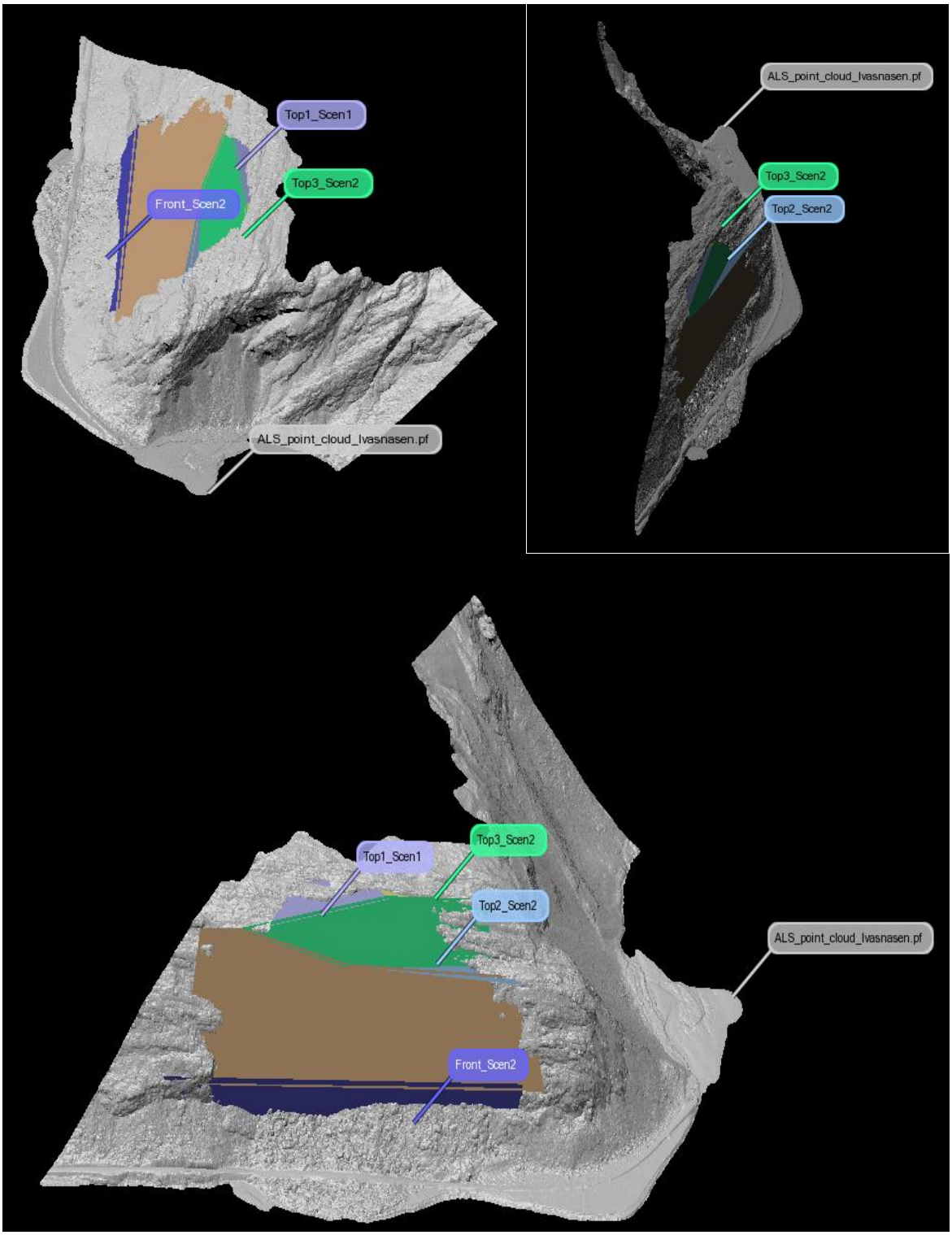

Figure 52 Results of the reconstructed topography for the historical rockslide at Ivasnasen. As it can be seen they fit really well with today's topography and is therefore representative to the historical topography.

Figure 53 shows in a graph of the reconstructed topography for the historical rockslide at Ivasnasen, where it is shown the reconstructed topography for scenario 1 and 2. Both of these scenarios fit each other well, and it is possible to conclude that it seems to be a good reconstruction. Since scenario 1 is the newest scenario, it is this scenario that has been used for further numerical analysis of the rockslide. The graph also shows three different results for the deposits, as minimum, mean and maximum deposits. The results for the deposits are representative and none of them seems to be completely wrong. None of the deposits goes extremely low or above today's topography. The relations between them are not big, and they can all be a good guess of the thickness of the deposits.

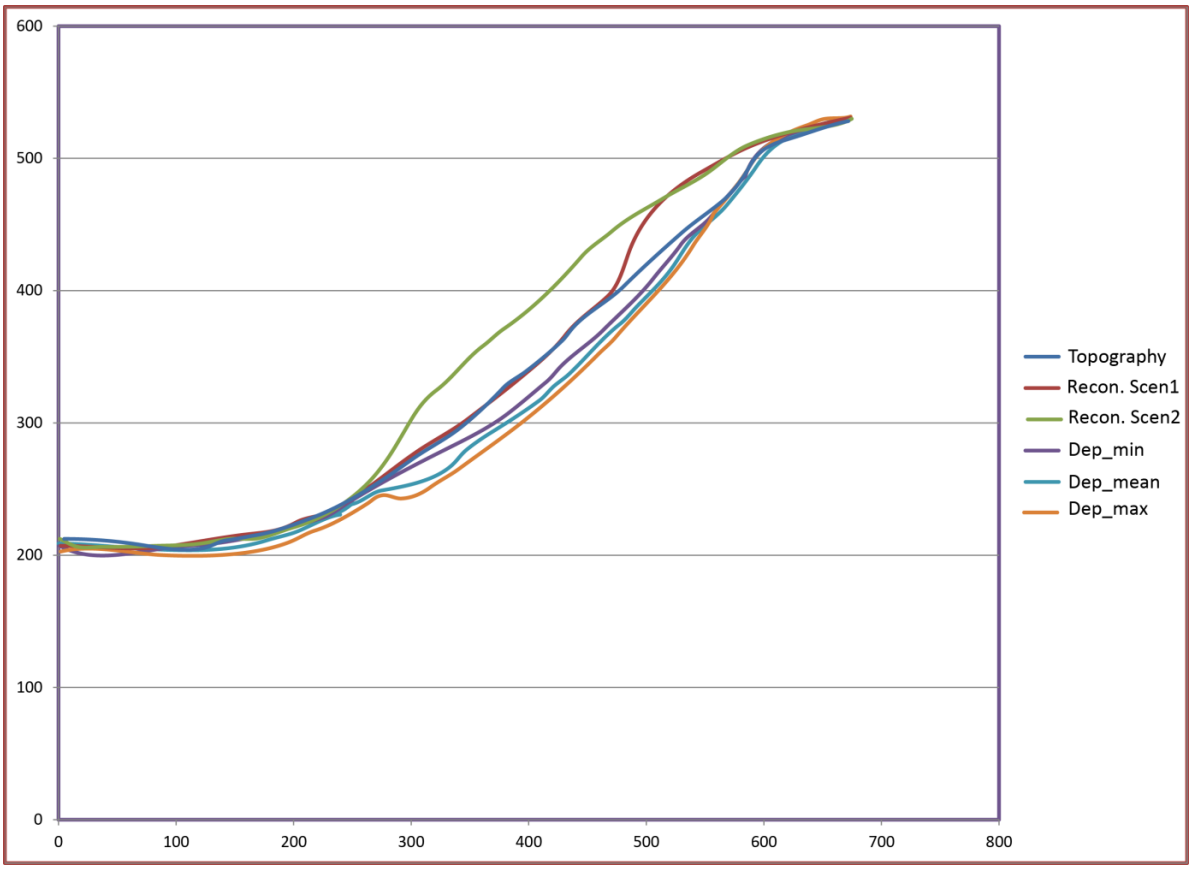

Figure 53 Reconstruction of the topography for the historical rockslide at Ivasnasen, and also the results from the depth of the deposits. For the results of the depth deposits, there are none of them that seem to be completely wrong, so none of them have been favouristed. For the reconstruction it is two options, reconstruction for scenario 1 (where it is only the upper part) and there are the reconstructions for the entire part (scenario 2), both fits well.

Figure 54 illustrates each scenario for the unstable part of Ivasnasen, and how it looks like after a possible failure. The chosen scenarios that the author find most probable to happen are marked with a thicker line than the rest that also is dashed. It is difficult to decide which one that is the most correct one, but it was important to choose one scenario that seems to follow the topography and to think of how it might look after a rockslide.

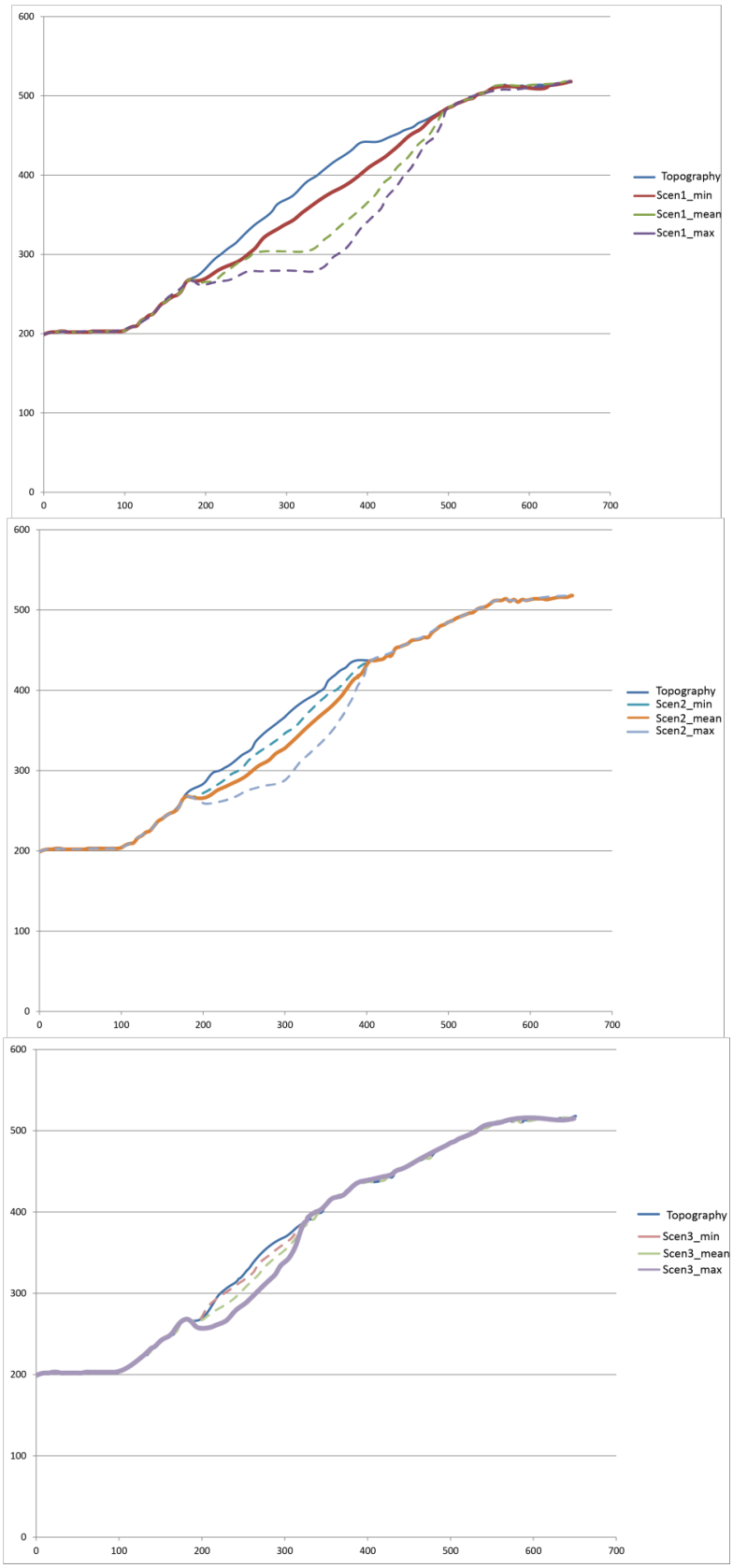

Figure 54 All the threes different scenarios from the unstable rockslope at Ivasnasen.The most likely happenings in each scenario are marked with a thicker line than the rest that is also dashed. It seems like the topography (blue line) get up before it flattens out, the reason for this is a "knick" in the topography that gives this illustration.

Table 19 gives an overview of the different chosen paths (figure 53 and 54) and the volume estimates for these. The volume calculations for the unstable rock slope are for those paths that most likely will occur if a rockslide failure will happen at Ivasnasen (marked with a thicker line in figure 54). The table shows also the volume estimations for the two scenarios for the historical rockslide. Each scenario is picked out from table 17 and 18 where the volume calculations for each scenario are listed. As describe earlier, scenario 1 will be "the worst case scenario" for the unstable part so it is natural that this also represent the biggest amount in volume.

Table 19 Volume estimations for the each chosen scenario for the historical rockslide and the unstable slope at Ivasnasen.

	Volume
Historical, Scenario 1	5237265,8 = 5,2Mm^3
Historical, Scenario 2	1223329,2 = 1,2 Mm^3
Unstable, Scenario 1, min	2088675,0 =2,1Mm^3
Unstable, Scenario 2, mean	1867800,0 =1,9Mm^3
Unstable, Scenario 3, max	633925,0 = 0,6Mm^3

All the calculated rockslide volumes were the final step of the SLBL analysis. The calculated volume for the historical rockslide is 5,2Mm^3 for the entire area and 1,2Mm^3 for the upper part. The volume estimation for the entire area fits well with the estimations Saintot et al. (2008) did measure.

For the unstable part at Ivasnasen there has been picked out these three different scenarios that is listed in table based on figure 54 to be the most reliable numbers of the volume that might fail. Table 19 shows the biggest volume to be 2,1Mm^3 for the unstable rock slope. If it has been the reality that it is two back scarps at Ivasnasen, then it is likely to think that if the unstable part also will fail, then the unstable part also will go in different "parts". This is also due to the cracks that have been seen in the elongation of the historical back scarp. It is therefore more natural to think that if a failure will occur, then scenario 3 or 2 will go first and in the end scenario 1. Scenario 1 is therefore set to be "the worst-case scenario".

9.0 Numerical analysis

Numerical analysis contains evaluating bigger amounts of data. Where numerical analysis is more recent development in slope stability analysis than earlier, when the more traditional limit equilibrium method was used.

The numerical analysis has in this thesis been used for the area of the reconstructed and the constructed topography at Ivasnasen.

Shear Strength reduction (SSR) is a method that Phase^2 uses to determine the Strength Reduction Factor (SRF) of a slope. The SRF is equivalent to the factor of safety (see chapter 2.3). An analysis with the SSR method is run for a series of increasing trial factors of safety (f) until failure occurs. According to Wyllie and Mah (2004) an equation for the cohesion (c) and friction angle (φ) are reduced for each trial:

$$c_{trial} = \left(\frac{1}{f}\right) c \qquad \textit{Equation 6}$$

$$\emptyset_{trial} = \tan^{-1}\left(\frac{1}{f}\right) \tan\varphi \qquad \textit{Equation 7}$$

Phase^2 and the SSR method reduce the shear strength until the slope becomes unstable. The critical SRF is the value at failure and is the last stage of the model anyhow many stages the model consist of (Rocscience, 2011). What has been done in this thesis is to restrict the stability analysis to a special area with adding an SSR search area (see figure 56).

9.1 Assessment on input parameters

Based on recommendations from Wyllie & Mah (2004) figure 55 illustrates the recommendations on model size to avoid artificial boundaries. Boundaries are either real or artificial, where real boundaries in slope stability problems that are usually stress free, and correspond to the natural or excavated ground surface. In reality the artificial boundaries does not exist. It is two types of artificial boundaries and these are prescribed displacement or prescribed stress. The prescribed displacement boundaries inhibit displacement in either the vertical or the horizontal direction, or both. Prescribed stress boundary is also called a “constant stress boundary” and is most likely where

slopes are cut into areas where the topography rises behind the slopes. Usually the prescribed displacement boundaries represent the conditions either in the base of the model (fixed in both the vertical and horizontal direction), and in the toe of the slope (displacement near the toe are inhibited only in the horizontal direction). Normally there are no significant differences with the respect to the results for these two types of artificial boundaries conditions. To get the model in equilibrium it is important that the magnitude for the horizontal stress for the prescribed stress boundary, must match the assumptions regarding initial stress (Wyllie and Mah, 2004).

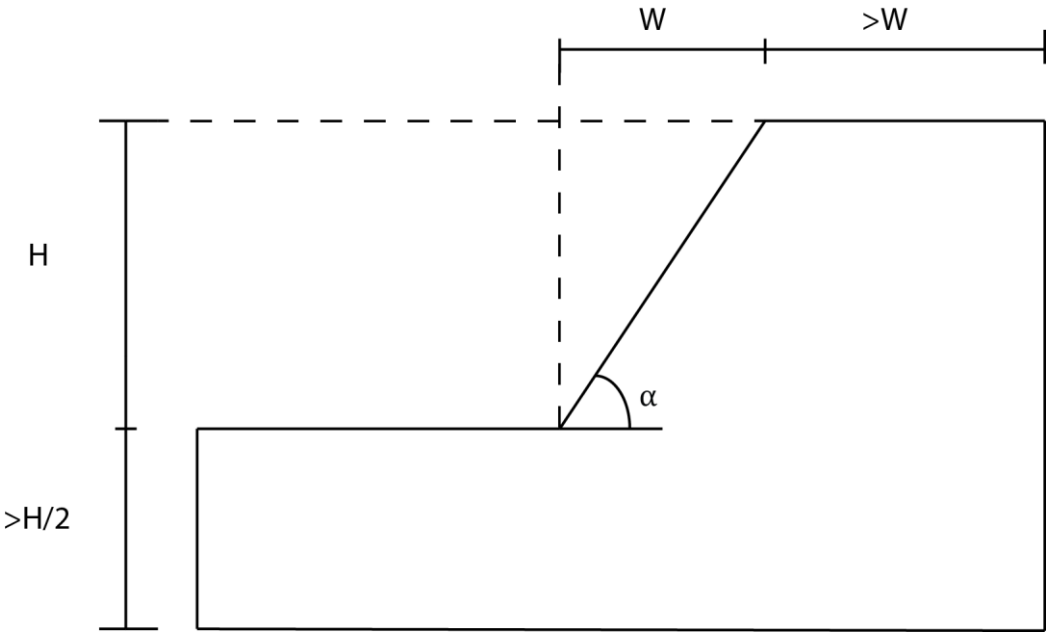

Figure 55 Recommendations for locations of artificial far-field boundaries in slope stability, model is from Wyllie and Mah (2004)

These boundary conditions have been used to analyze the historical rockslide and the unstable slope at Ivasnasen (Rocscience, 2011, Grøneng, 2010, Sandøy, 2012):

- That the surface of the model is free to move in all directions.
- To allowed deformation and prevent stress concentration the left and the right vertical boundaries are allowed to move in the vertical (y) direction, but not in the horizontal (x) direction.
- See figure 56 where the boundaries has changed directions in the lower corners (zoomed in at the small picture left top corner), where they can move horizontally but the bottom line is locked vertically.

The locations from where the profiles for the final profiles (figure 56) used in Phase^2 is illustrated as a black line in figure 48 and 49. The profiles is reconstructed and constructed with a combination of the two softwares ART from SLBL and Polyworks. Figure 56 shows the reconstructed topography for the historical rockslide on the top

(dark pink) and the constructed topography for the unstable slope of Ivasnasen below (light pink).

Rocscience (2011) recommend building up the mesh with 800 elements, so this is done. It has also been used a mesh set up with 6-node triangles, and this is based on recommendation from Hammah (Hammah et al., 2006).

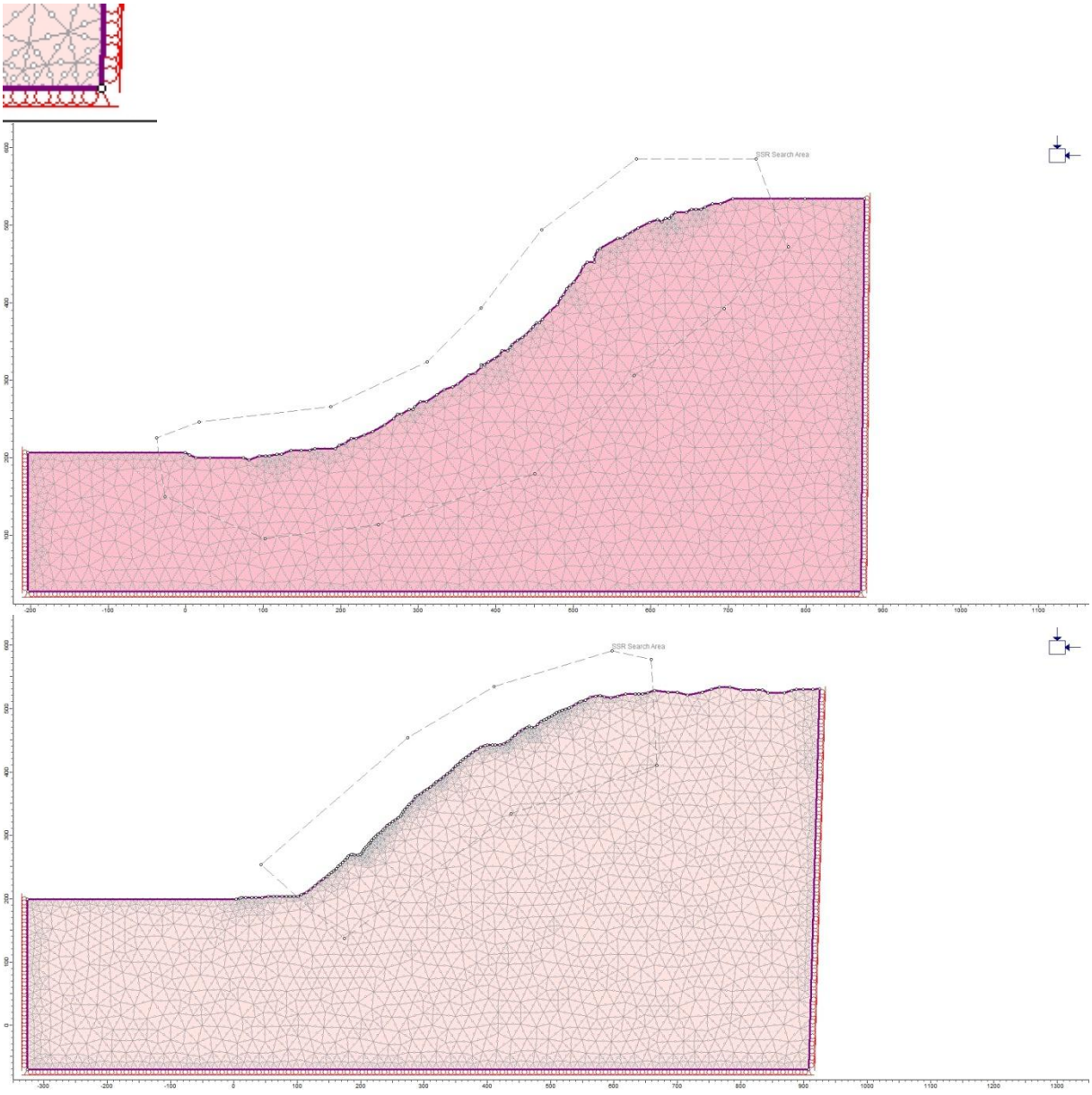

Figure 56 Top; profile of the rebuilded topography of the historical rockslide at Ivasnasen. Below; the topography of the unstable slope. This are the final profiles that have been chosen for Phase². The grey boxes, or dashed lines, shows the SSR search area. Left top corner is a zoom-in of the corners, to show the different directions for the lower corners in the profiles.

9.2 Modeling

9.2.1 Failure criterions

Based on Rocscience (2011) it was decided to use the failure criterion after Hoek (2007). This describes the strength and deformation capability for rock mass in modeling. A classical linear Mohr-Coulomb criterion is the most applied (Hoek, 2007c) with the equation:

$$\tau = c + \sigma_n \tan\varphi \qquad \textit{Equation 8}$$

τ = Shear stress

c = Cohesion

σ_n = Normal stress acting

φ = Friction angle of the material

The software, Phase^2, do also allow us to use the non-linear empirical Hoek-Brown failure criterion. This failure criterion is more suitable for predicting failure of rock masses compared to the classical linear Mohr-Coulomb criterion (Hammah et al., 2004). The equation for the generalized Hoek-Brown criterion for jointed rock mass is (Hoek, 2007c):

$$\sigma'_1 = \sigma'_3 + \sigma_{ci}\left(m_b \frac{\sigma'_3}{\sigma_{ci}} + s\right)^a \qquad \textit{Equation 9}$$

σ'_1 = minimum effective principle stress at failure

σ'_3 = maximum effective principle stress at failure

σ_{ci} = uniaxial compressive strength of the intact rock mass

m_b = value of the Hoek-Brown constant m for the rock mass, given by $m_b = m_i e^{\left(\frac{GSI-100}{28-14D}\right)}$

s & a= constant factors, depending on the rock mass properties, given by:

$$s = e^{\left(\frac{GSI-100}{28-14D}\right)}$$

$$a = \frac{1}{2} + \frac{1}{6}\left(e^{\frac{-GSI}{15}} - e^{\frac{-20}{3}}\right)$$

9.2.2 Hoek-Brown to Mohr-Coulomb criterion

The Hoek-Brown criterion should not be used when one of the discontinuity set is significantly weaker than other, or if a few discontinuities dominate the rock mass. The Hoek-Brown criterion assumes isotropic rock mass and therefore needs to be applied in a rock mass with sufficiently number of closely spaced discontinuities. The discontinuities must have similar surface characteristics and isotropic failure behavior, (Hoek, 2007c).

For this master thesis a Hoek-Brown criterion is used because of the unknown basal surface for the historical rockslide, and the criterion suits best the fractured rock mass at Ivasnasen. It is important to use the same criterion for the historical rockslide and the unstable part to get a best comparable result. There have been some difficulties to do the SSR analyses in Phase^2 based on the input parameters (m_b, s and a) with Hoek-Brown criterion. But according to Hammah et al. (2004) the generalized Hoek-Brown criterion can still be used if the parameters are converted into the Mohr-Coulomb failure envelope using RocLab, and then applying the equivalent cohesion and friction angle in the standard SSR. There have also been some troubles to obtain the friction angle and the cohesion. This because of the so-called active friction angle is not a constant, but depending on the actual normal stress level, (Nilsen, 2000). The normal stress needs to be calculated before the cohesion and friction angle may be determined, is because of the non-linear relationship between shear strength and normal stress, (Nilsen et al., 2011).

Table 20 shows how the parameters at Ivasnasen have been converted in the Hoek-Brown criterion, by RockLab. The table shows how "*the non-linear relationship is taken into consideration with the 'Instantaneous Mohr-Coulomb' that is calculated in RocLab"*, (Loftesnes, 2010, Sandøy, 2012). RocLab gives out an estimate for the peak strength parameter for the specific normal stress. An equation for the mean value for the normal stress is given by the equation:

$$\sigma_n = \gamma z \cos \alpha_{slope} \qquad \textit{Equation 10}$$

γ = rock mass unit weight

z = overburden basal surface

α_{slope} = basal surface angle

In this case of Ivasnasen it has been reconstructed an overburden range from around 10 to 45 meter for the historical rockslide and around 30 meters for the unstable part. The SLBL showed an average dip of 42^0 and a density of 2800kg/m^3. This results in a normal stress of 0.2-1.0MPa, with a mean value of 0.6MPa.

Table 19 gives the parameters that are used in RocLab, both the input and the output parameters. The peak cohesion and friction angle is based on the Hoek-Brown parameters. The geological strength index (GSI) is set to be 58, and is based on the recommendations in RocLab. A GSI of 60 is described as: "*very blocky, interlocked, partially disturbed mass with multi-faceted angular blocks formed by 4 or more joint sets*". Since there has not been done any analysis with JCS (joint surface compressive strength) with Smith hardness the GSI was decided to use the parameter that describes the rock mass and the surface (good) quite well. The intact rock parameter (m_i) is found from Rocscience. Because a gneiss has a m_i of 28±5, it was decided to set it as 23, since it is an augen gneiss with rich biotite layers, (Hoek, 2007b). The disturbance factor (D) expresses the mechanical stresses (e.g weathering, erosion and glaciation) the rock mass might have been exposed to and the parameter is chosen after recommendations from Loftenes (2010) and Sandøy (2012). The value of D is set to be equal 0.5 after the recommendations. This make sense since a smooth blasting have a value of D=0.7, (Hoek, 2007b). According to Rocscience (2011) it was chosen a granite with tectonic shear zone, schistose and broken granite, disintegrated rock and gouge to see witch parameter for the C_{peak} and φ_{peak} that was the best option in this case, (Hoek, 2007c).

Table 20 Input parameters to estimate Hoek-Brown criterion parameters for Phase².

	Parameters	Symbol	Values	Source
Input	UCS, Uniaxial compressive strength	σ_{ci} (MPa)	72,44	Laboratory test
	Intact rock parameter	m_i	23	Hoek (2007b)
	Geological strength index	GSI	58	RocLab estimations appendix 3
	Disturbance factor	D	0,5	Loftenes (2010) & Sandøy (2012)
	Young's modulus	E_i (GPa)	31,16	Laboratory test, appendix 1
	Mean normal stress	σ_n (MPa)	0,6	Estimation based on equation 10
Output	Deformation modulus	E_m (MPa)	8472,15	RocLab estimations, appendix 3
	Peak friction angle	φ_{peak} (^{0})	42	Recommendations Rocscience(2011)
	Peak cohesion	C_{peak} (MPa)	0,24	Recommendations Rocscience (2011)
	Tensile strength	σ_t (MPa)	-0,094	RocLab estimations, appendix 3

9.2.3 Elastic and plastic material in the modeling

Phase² make it possible to choose if the material is elastic and/or plastic for slope stability. For this the Hoek-Brown and Mohr-Coulomb uses the peak strength to describe failure, where the elastic rock mass describe the failure and the plastic rock mass describe the residual values. The modeling made of Ivasnasen is run both with an elastic-plastic model and with different strain-softening reduction of both cohesion and friction angle of 10, 20 and 30% of the peak values (figure 63-74 and table 24). The numerical analyses were run with all these different percentage of the peak values to get the best possible fit for the modeling.

9.2.4 Structural settings

The orientations of the discontinuities has a major influence on slope stability, (Wyllie and Mah, 2004). Phase² do allow us to include the joint networks in the analysis, but since the software only do the analysis there are joint sets who is excluded in the analysis (J1, J2,J4, J5 and J6). It is only the foliation S1 and the joint set J3 that is included in the numerical analyses based on this. The foliation S1 is the main discontinuities set at Ivasnasen. J3 do not occur that often as S1 so the J3 joint network is therefore analyzed with a wider spacing than the S1.

There has not been done any analysis with Smith hardness, and it is therefore hard to do any calculations to get the instantaneous cohesion (c_i) and friction angle (φ_i) for the joint sets. The average dip angle for each discontinuity set measured during fieldwork has therefore been used. The tensile strength and peak cohesion are the same as analyzed for the augen gneiss. The input parameters for the joint networks are shown in table 21.

Table 21 Input parameters to Phase² for the joint networks.

Normal stress: 0,6MPa	**S1**	**J3**
Shear strength (MPa)	0.094	0.094
φ_i (^{0})	53	77
c_i (MPa)	0.24	0.24

Joint normal- and shear stiffness parameters are also parameters that can be added for the joint sets, and these describes the joints elastic behavior by joint normal (K_n) and shear (K_s) stiffness, please see equation 11-14.

$$K_n = \frac{E_i \times E_m}{L\,(E_i - E_m)} \qquad \textit{Equation 11}$$

$$K_s = \frac{G_i \times G_m}{L\,(G_i - G_m)} \qquad \textit{Equation 12}$$

$$G_m = \frac{E_m}{2(1+v)} \qquad \textit{Equation 13}$$

$$G_i = \frac{E_i}{2(1+v)} \qquad \textit{Equation 14}$$

The stiffness is estimated in the equation from the rock mass modulus (E_m), the intact rock modulus (E_i) and the average joint spacing (L). $G_m$is the rock mass shear modulus, and G_i is the intact rock shear modulus.

Equations 11-14 gives the calculated values listed in table 22 with the results for the normal and shear stiffness, S1 is the foliation and J3 is the joint set. It was tested with a Poisson's ratio at 0.13 who was the average value that was measured during laboratory analyses, but this was too low for the numerical modeling when calculating the K_n and K_s. It was therefore decided to use the highest value measured in the laboratory, also based on recommendations from Hoek (2007c). According to Panthi (Panthi, 2012), 0.13 was a good number to use for the Poisson's ratio, this will be discussed further in chapter 10, (discussion). It was decided to use the numbers based on Hoek (2007c) because of lack of time.

Table 22 Calclulated parameters from equation 11-14.

	S1	**J3**
Poisson's ratio (v)	0,24	0,24
2 (1+v)	2,48	2,48
G_m (MPa)	3416	3416
G_i (MPa)	12565	12565
E_m (MPa)	8472	8472
E_i (MPa)	31160	31160
L (m)	5	10
K_n (MPa/m)	2327	1164
K_s (MPa/m)	938	469

9.2.5 Stresses

According to Wyllie & Mah (2004) the in situ stresses are often neglected in slope stability analysis. There are several reasons for this but some is that the limit equilibrium analysis cannot include the effect of stresses in the analyses. Analyses have also been performed mostly on soils and not for rocks and the in situ stresses for rock masses are not routinely measured. This makes the in situ stress rate more limited. Slope failures are gravity driven, so the effects of in situ stress are therefore characterized as minimal (Wyllie and Mah, 2004).

There has not been done any in situ stress measurement for Ivasnasen. It is natural to believe that a redistribution of stress along the slope has occurred during valley excavation from previous glaciation. Since there is not any data of how thick the ice was during glaciation at Ivasnasen it is not possible to convict a numerical model of the elastic rebound and stress redistribution by glacial melt. It is also assumed that the load of the ice is much smaller than the load of overburden rock masses.

Wyllie and Mah (2004) says that slope failures are gravity driven and Rocscience (2011) that gravity field stress option is used when an in-situ stress field varies with depth and is regularly used for surface or surface excavation.

A vertical component is used in a relaxed environment where the rock mass behaves elastic (ASTM, 1967, Sheorey, 1994):

$$\sigma_v = \gamma \times z \qquad \textit{Equation 15}$$

σ_v = vertical component
γ = unit weight
z = depth

The horizontal component of stress is calculated based on the vertical component, by assuming that the subsurface rock is homogenous, isotropic (same intensity in all directions), linear-elastic and no tectonic forces active present (example folding, faulting or shrinking in earth's crust). The stability analysis is determining of the stress in rock, (ASTM, 1967). The horizontal stress is expressed in Myrvang (Myrvang, 2001):

$$\sigma_h = \left(\frac{v}{1-v}\right)\sigma_v \qquad \textit{Equation 16}$$

σ_h = horizontal component

v = Poisson's ratio

σ_v = vertical component

For the augen gneiss at Ivasnasen this assumed to have an average stress ratio of σ_h=0.11 x σ_v. This is a low ratio for Norwegian conditions, so it was decided to take the highest value of the Poisson's ratio from the laboratory report (Dreiås, 2012). The stress ratio for the horizontal component is now: σ_h= 0,32 x σ_v, it is still low for the Norwegian conditions, but they are analyzed and expected to be low because of the short distance between the shear zone and slope surface (Myrvang, 2001). The Poisson's ratio will be discussed further in chapter 10.

9.2.6 Water

There is a professional discussion of how the water pressure and pore pressure do influence the slope stability. The influence of water pressure has a thorough understanding but the understanding of the influence for pore pressure is not so well. The presence of water in a slope reduces the shear strength of the rock mass due to the decreased value of σ'_n acting on the discontinuity surfaces. Water increase the erosion and weathering processes and act as a driving force in near vertical tension cracks. The most common method is to specify a water table in Phase^2 is by adding a piezometric surface (Wyllie and Mah, 2004).

If the area is described to be "low precipitation areas" the precipitation during a year is less than 20 inches per year. Areas that receive more than 50 inches per year are considered "high precipitation areas". Both water and freeze/thaw cycles contribute to the weathering and movement of rock materials. The impact of these can be interpreted from knowledge of the freezing conditions at each site (Hoek, 2007a).

For the case of Ivasnasen, the hydrological situation has not been studied and there has not been observed any daylight dikes or small rivers close by the rockslide area. But the area around Ivasnasen is a so-called marsh area that contains and keeps a lot of water for a longer period. The marsh area reach all over the area, and this may result in a higher pore pressure than normal. Since it does not exist any information about the historical event, like when and how it went it is difficult to tell if there has been a lot of water seepage at the time when the rockslide failed. For the unstable part the marsh area might have an influence, same with heavy rainfall and freeze/thawing conditions. Based on measurements from yr.no (yr, 2012) shows a precipitation of 680mm for one year measurements (2011-2012) at Oppdal, please see appendix 4. Oppdal is close to Gjøra and is therefore representative for the precipitation measurements. Measurements of 680mm/year do classify this area as a middle high precipitation area.

For the numerical analysis in Phase^2 all the consideration if it was a dry slope, moderately saturated (normal groundwater table), medium saturated (medium groundwater table) or if it was extremely saturated (high groundwater table) has been done.

9.2.7 Earthquake

Due to Rocscience (2011) an earthquake load can be added in Phase[2]. In this case it is not done, since the date of the event is not set and the critical SRF did go below 1 without this load. It was tested, and the results were concluded not to have much influence of an earthquake load. It was therefore decided not to include these results.

The effect of an earthquake can be modeled as a permanent vertical body force. The load is defined by entering a horizontal or/and vertical seismic coefficient. Where the seismic force, F_s, is given by:

$$F_s = kW_{FE} \qquad \textit{Equation 17}$$

W_{FE} = weight of each finite element

k = seismic coefficient

9.2.8 Summary of input parameters for both Ivasnasen slope models

Table 23 gives a list of all the used parameters for the numerical modeling at Ivasnasen, both the historical rockslide and the unstable rock slope. The groundwater table has been added as a trigger factor and is tested with high, medium and low groundwater table.

Table 23 Input parameters in Phase² for Ivasnasen.

General settings and input parameters in Phase² , version 8.01, for Ivasnasen			
Analysis type:	Single stage model: Plane strain		
SSR Stop criteria	Square root energy		
Maximum numbers of iterations	500		
Tolerance	0.001		
Convergence type	Absolute energy		
Mesh Type	Graded		
Element type	6 noded triangles		
Default number of nodes on external	300		
Boundary conditions	Bottom: restrain y Left: restrain x Right: restrain x Top (surface): free restrain Lower corners: restrain x,y		
Stresses Gravity	Unit weight: 0.0028 Total stress ratio ($\sigma_H/\ \sigma_v$) in plane: 1.2		
	Total stress ratio ($\sigma_h/\ \sigma_v$) out of plane: 0.6		
	Locked-in-horizontal stress (both in and out of plane): 0		
S1, foliation	Dip/dip direction 53/320, 40m spacing		
J3, joint set	Dip/dip direction 77/192, 80 m spacing		
Failure Criterion	Mohr Coulomb, elastic-plastic models		
Young's modulus, E_i, laboratory (MPa)	31160		
Deformation modulus, $E_{m,}$, RocLab (MPa)	8472		
Poisson's ratio, v	0,24		
Peak values, from RocLab, φ_{peak} (^{0})	Material: 42	S1: 53	J3: 77
c_{peak} (MPa)	0,24	0,24	0,24
σ_t (MPa)	-0.094	-0.094	-0.094
Normal stiffness, $K_{n,}$ (MPa/m)	S1: 2327	J3: 1164	
Shear stiffness, K_s, (MPa/m)	S1: 938	J3: 469	

The models where tested for when the critical SRF become lower than the critical value that is 1,0. For the calculations given for each scenario, please see appendix 3.

9.3 Interpretation of results

The numerical analyses were first done with no join set added. Figure 57 shows the total long term displacement for the historical rockslide and 59 for the unstable rock slope, both with no joint sets added. For figure 57 is the present topography also drawn in the historical rockslide model. This shows that the present topography correlate really well due to where the highest displacement is, and where the failure did occur. Both figures are with no groundwater table and no joint set, and these will all be included in other figures. The critical SRF is 1.64 for the historical rockslide and 1.67 for the unstable. The figure does also show a bigger total displacement with 0.08meters for the historical rockslide and 0.06meters for the unstable part.

Figure 58 and figure 60 shows the long term maximum shear strain for both areas. If we compare these figures to figure 57 and 59 it is clearly a similarity to those two, the connected maximum shear strain are marked with a red dashed line. For the historical rockslide the dashed maximum shear strain is comparable to the present topography. Please notice that the SRF for the unstable slope is higher for the maximum shear strain than the total displacement, the reason for this is to highlight the area better.

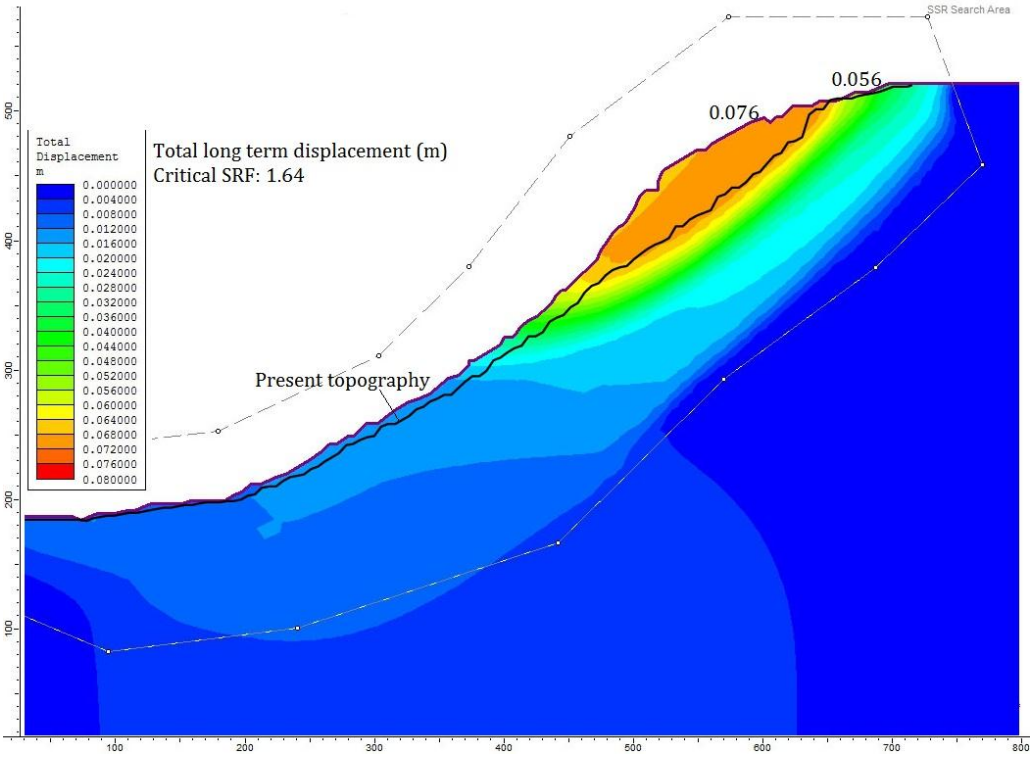

Figure 57 Total long term displacement historical rockslide, marked with present topography, critical SRF=1.64.

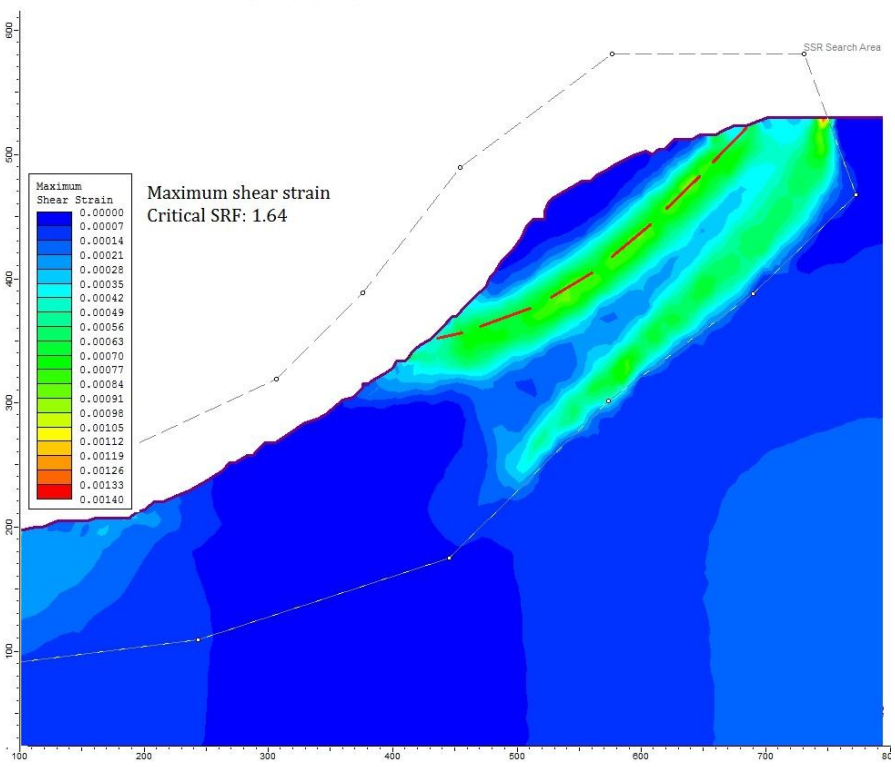

Figure 58 Maximum shear strain for the historical rockslide with no joints, critical SRF=1.64.

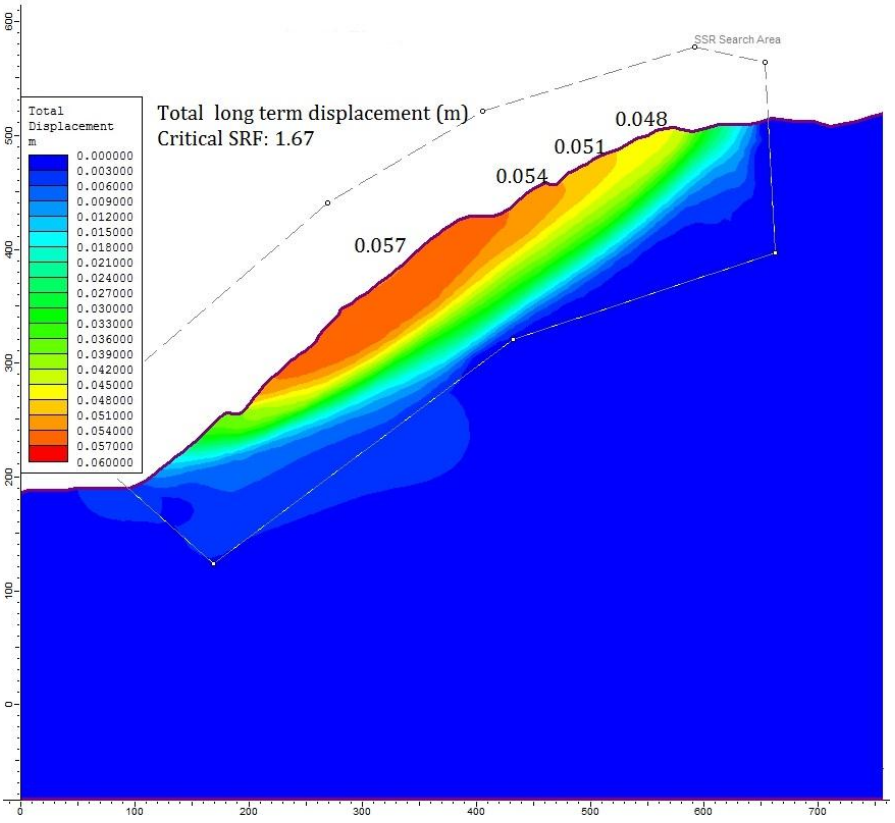

Figure 59 Total long term displacement for the unstable slope, critical SRF=1.67.

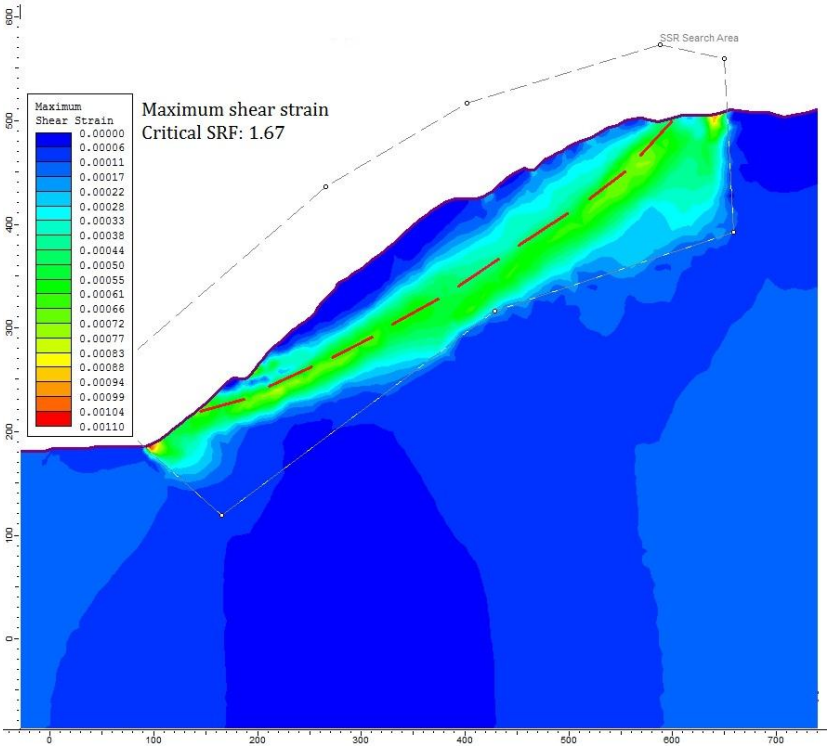

Figure 60 Maximum shear strain for the unstable slope with no joints, critical SRF=1.67.

The strain softening analyses, figure 63-74 include a parameter of study the rock mass and discontinuities of residual friction angle, φ_{res}, and cohesion, c_{res}. The influence of the groundwater table was tested. Data for the year for the rockslide does not exist and it is therefore unknown how the precipitation in this period was.

The reconstructed topography for the historical rockslide and the constructed topography for the unstable rock slope of Ivasnasen were modeled with the same input parameters. They were all tested with a high, medium and low groundwater table. Table 24 shows the results for each percentage of the different water tables. For the high groundwater table the critical SRF value became below 1.0 at 10% of the residuals value of peak. For the medium groundwater table the critical SRF value became below 1.0 at 20% of the residuals value of peak. For the low groundwater table the critical SRF value became below 1.0 at 30% of the residuals value of peak. It was decided to test the slopes properly, and this is the reason why so many values of the residual values of peak were chosen. Please see appendix 3 for all the measured residual values. Figures 63-74 illustrates when the SRF value is below 1.0 modeled with high, medium and low groundwater table for the maximum shear strain and the total displacement for each value.

Due to the results from table 24 with the illustrating figures 63-74 it is shown that groundwater table has a huge influence on reducing the SRF. It has also been tried to add earthquake load, but this did not have as much influence of the stability compare to

the groundwater. It was decided not to include the load of earthquake, especially because the date of the rockslide is unknown and the groundwater table had the biggest influence.

Table 24 Calculations for each ground water table and the representative critical SRF value.

	SRF:	
High groundwater table	Historical:	Unstable:
0%	1.15	Unknown
5%	1.1	Unknown
10%	**0.91**	**0.9**
Medium groundwater table		
15%	1.14	1.16
20%	**0.95**	**0.96**
Low groundwater table		
25%	1.06	1.07
30%	**0.98**	**0.97**

Figure 61 and 62 summarize the results of how much impact of decreasing the friction angle or the cohesion had on the SRF. The tendency is for the unstable rock slope that a reduction in friction angle gives a 75% reduction in SRF and 48% reduction in SRF with a reduction of the cohesion. For the historical rockslide the tendency is the same, but here it is a reduction in the SRF with 80% with reducing the friction angle and 56% for the cohesion. With this analysis it is shown that it is the friction angle that reduces the SRF most, but the cohesion reduces it much too. This shows that it is comparable to the real-life situation, since both the friction angle and cohesion reduces the SRF significantly. Table 25 and 26 shows the calculations for the figures.

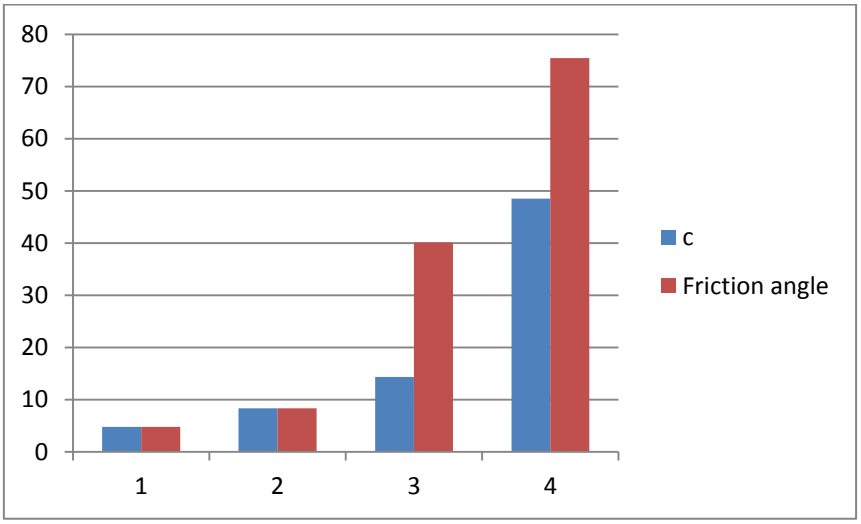

Figure 61 The results of the analysis of how much impakt of decreasing the friction angle or the cohesion had on the SRF for the unstable rock slope.

Table 25 Input parameters to figure 61, unstable rock slope; the friction angle is constant 42 degrees during the modeling for the cohesion, and the cohesion is constant 0.24 during the modeling for the friction angle.

c:	%:	SRF:
0,24	0	1,67
0,204	15	1,59
0,168	30	1,53
0,12	50	1,43
0	100	0,86
angle:	%:	SRF:
42	0	1,67
35,7	15	1,59
29,4	30	1,53
21	50	1
0	100	0,41

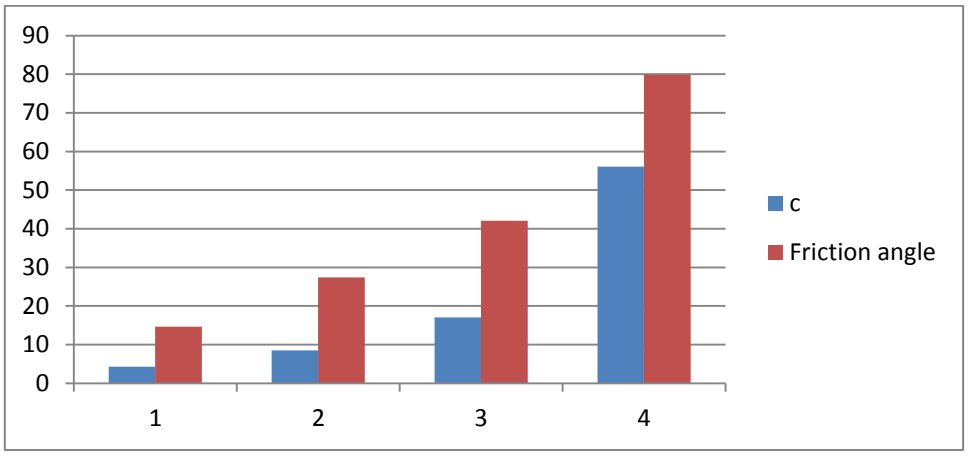

Figure 62 The results of the analysis of how much impakt of decreasing the friction angle or the cohesion had on the SRF for the historical rockslide.

Table 26 Input parameters to figure 62, historical rockslide; the friction angle is constant 42 degrees during the modeling for the cohesion and the cohesion is constant 0.24 during the modeling for the friction angle.

c:	%:	SRF
0,24	0	1,64
0,204	15	1,57
0,168	30	1,5
0,12	50	1,36
0	100	0,72
angle:	%:	SRF:
42	0	1,64
35,7	15	1,4
29,4	30	1,19
21	50	0,95
0	100	0,33

9.3.1 Historical rockslide modeling

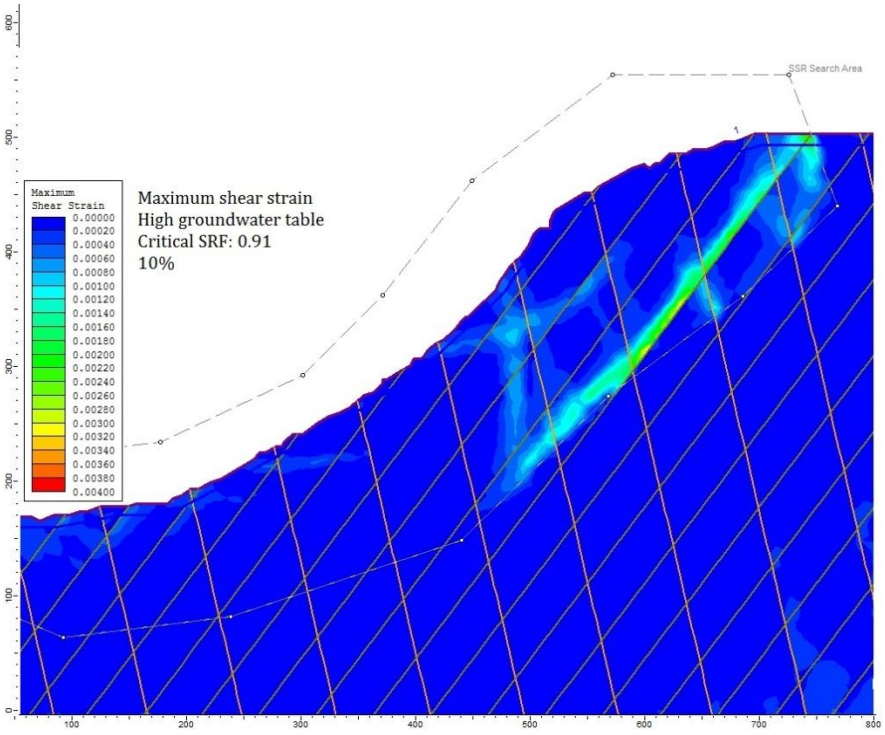

Figure 63 Maximum shear stain for the historical rockslide with high ground water table, critical SRF=0.91 with 10% reduction in residual values.

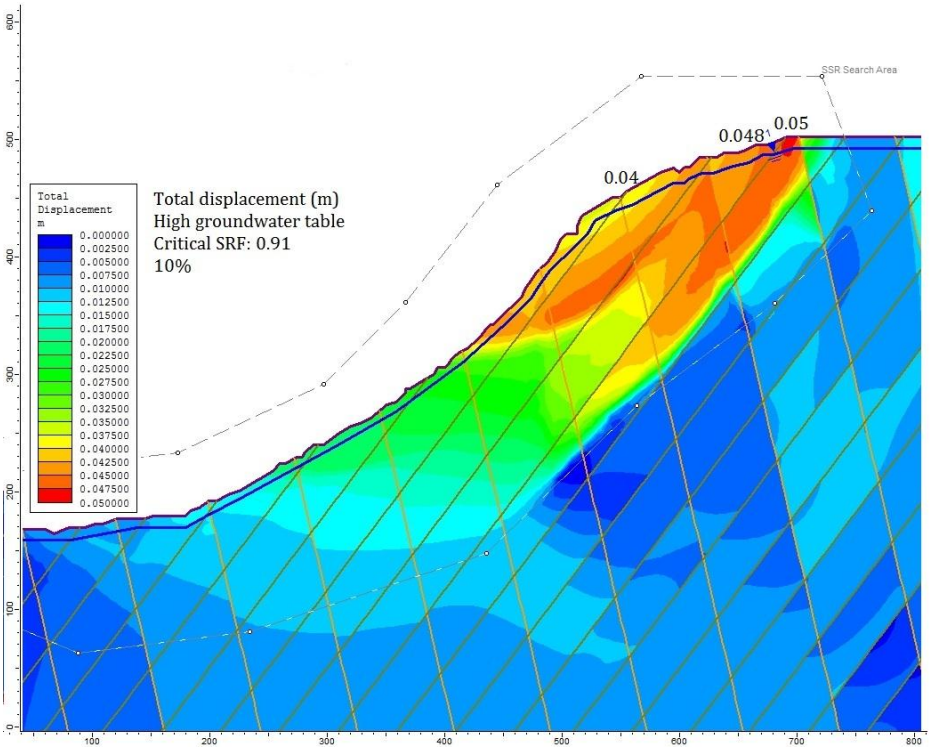

Figure 64 Total displacement for the historical rockslide with high ground water table, critical SRF=0.91 with 10% reduction in residual values. It is marked the values for the total displacement at the figure.

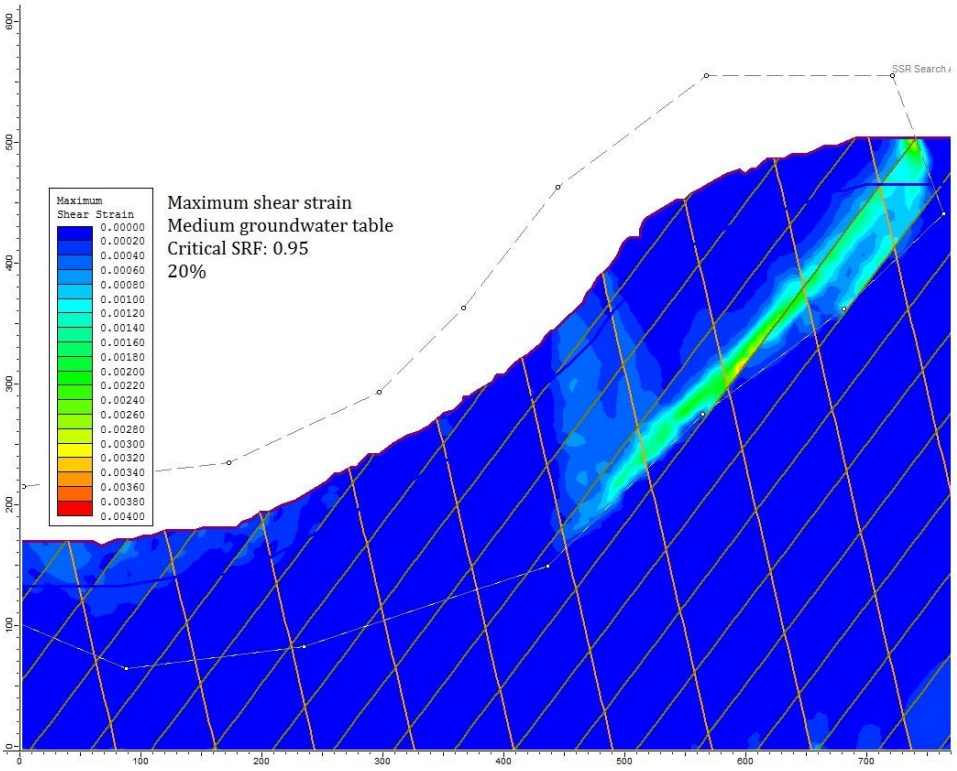

Figure 65 Historical rockslide, medium ground water table, critical SRF=0.95 with 20% reduction in residual values.

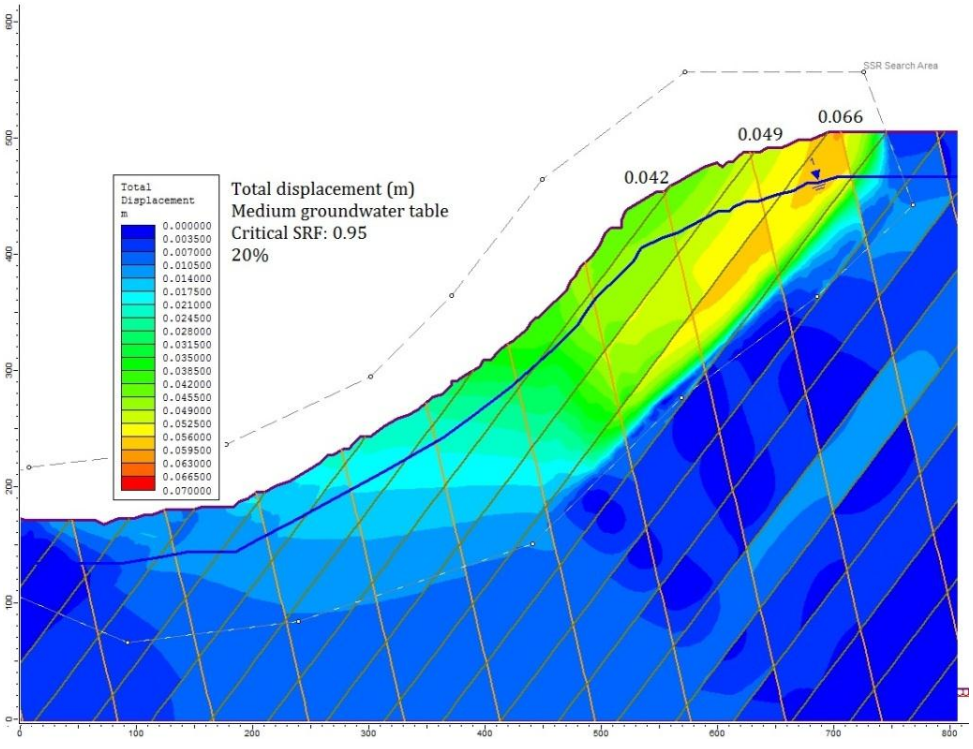

Figure 66 Total displacement for the historical rockslide, medium groundwater table, critical SRF=0.95 with 20% reduction in residual values. It is marked the values for the total displacement at the figure.

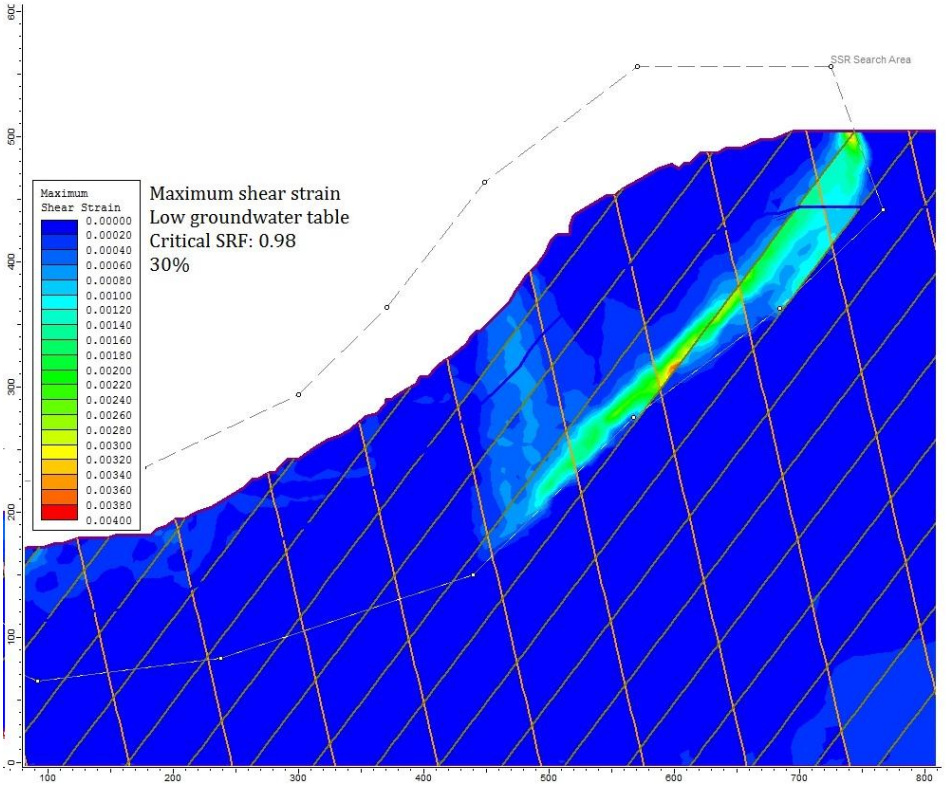

Figure 67 Historical rockslide, low ground water table, critical SRF=0.98 with 30% reduction in residual values.

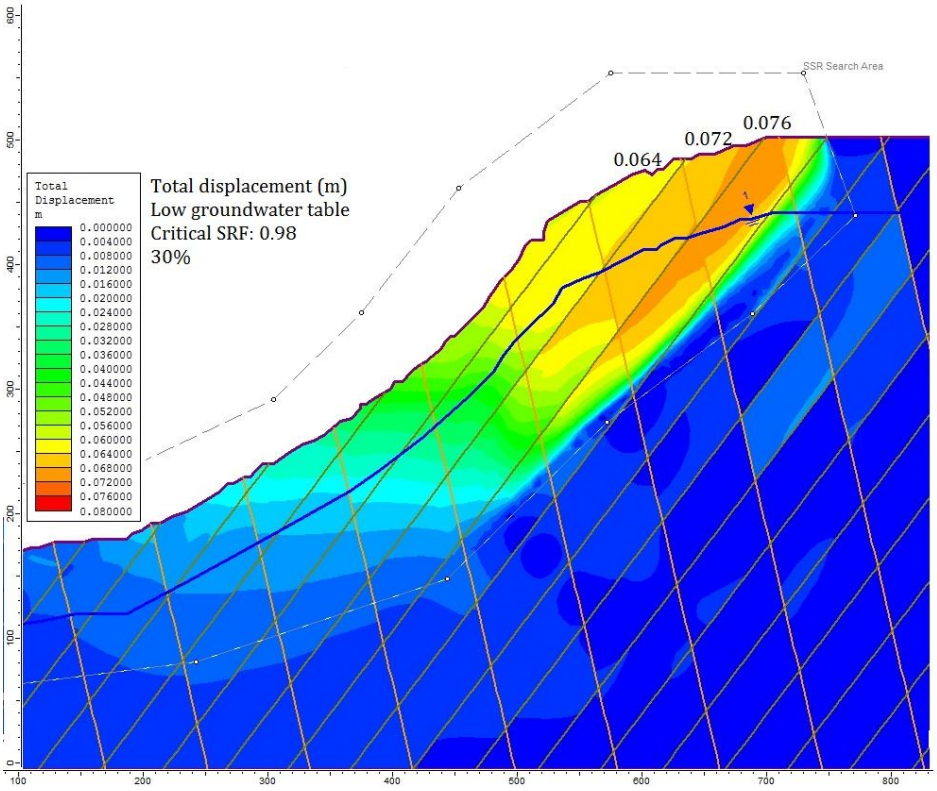

Figure 68 Total displacement for the historical rockslide, low groundwater table, critical SRF=0.98, with 30% reduction in residual values. It is marked the values for the total displacement at the figure.

9.3.2 Unstable rock slope modeling

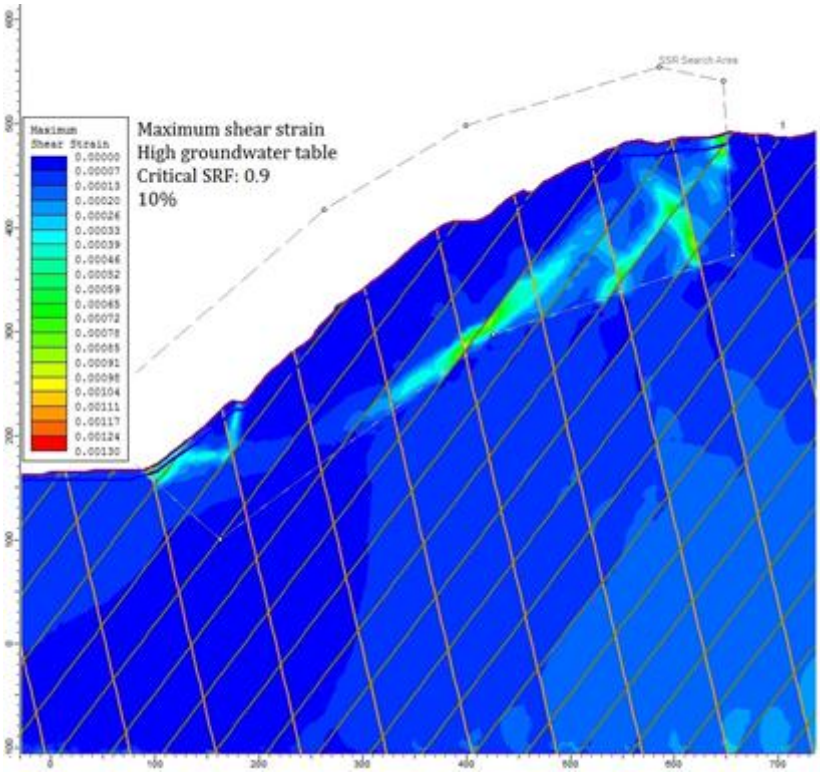

Figure 69 Unstable slope, high ground water table, critical SRF=0.9 with 10% reduction in residual values.

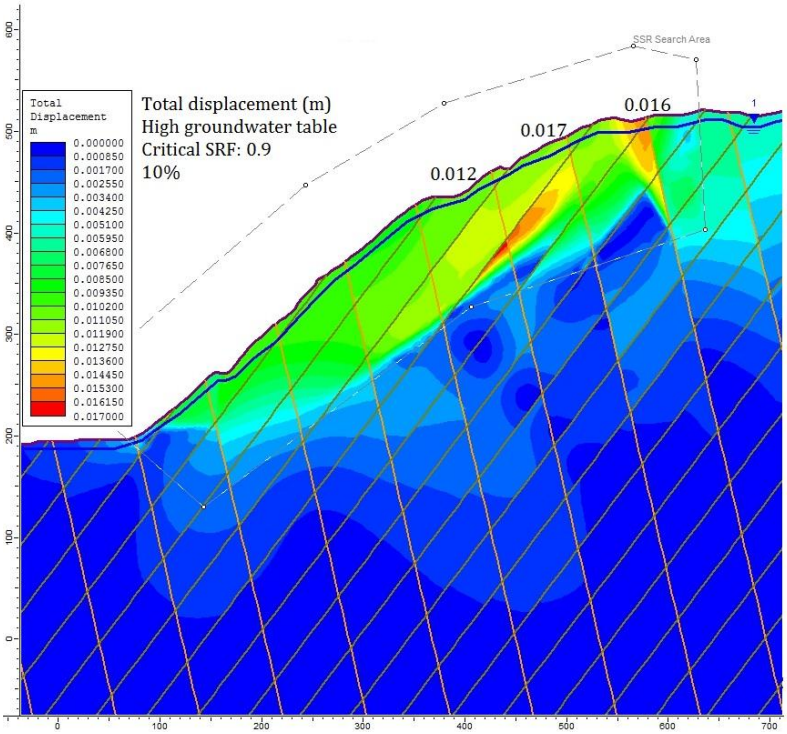

Figure 70 Total displacement for the unstable slope, high ground water table, critical SRF=0.9 with 10% reduction in residual values. It is marked the values for the total displacement at the figure.

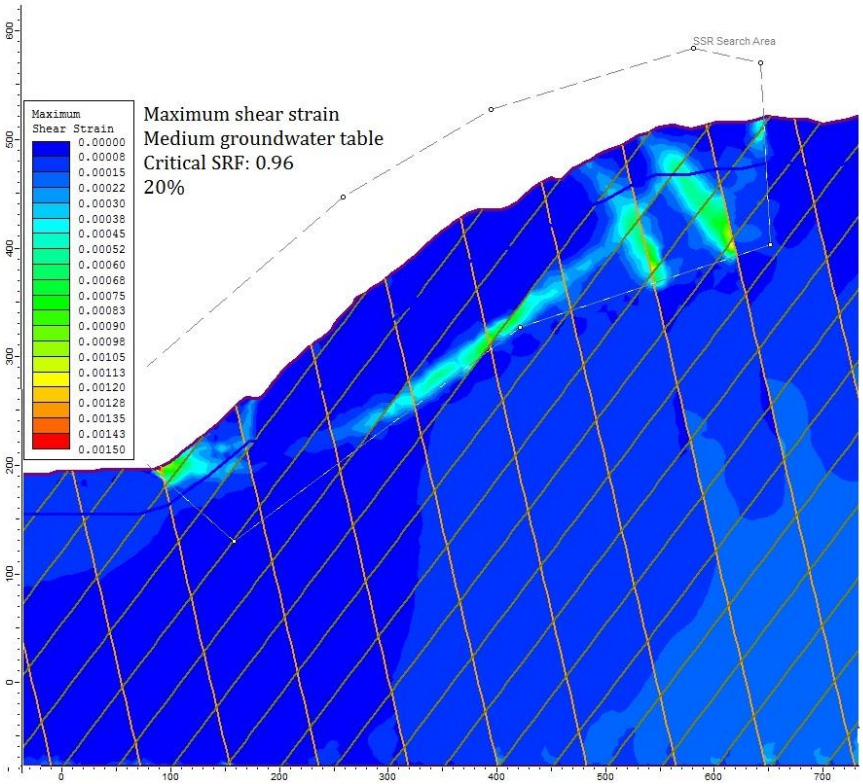

Figure 71 Unstable slope, medium ground water table, critical SRF=0.96 with 20% reduction in residual values.

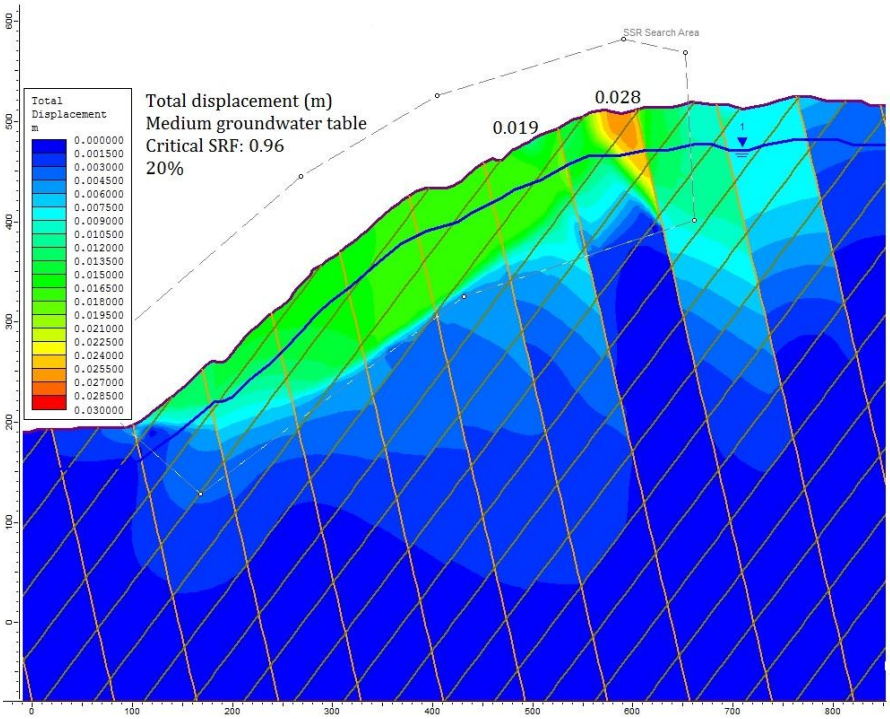

Figure 72 Total displacement for the unstable slope, medium groundwater table, critical SRF=0.96 with 20% reduction in residual values. It is marked the values for the total displacement at the figure.

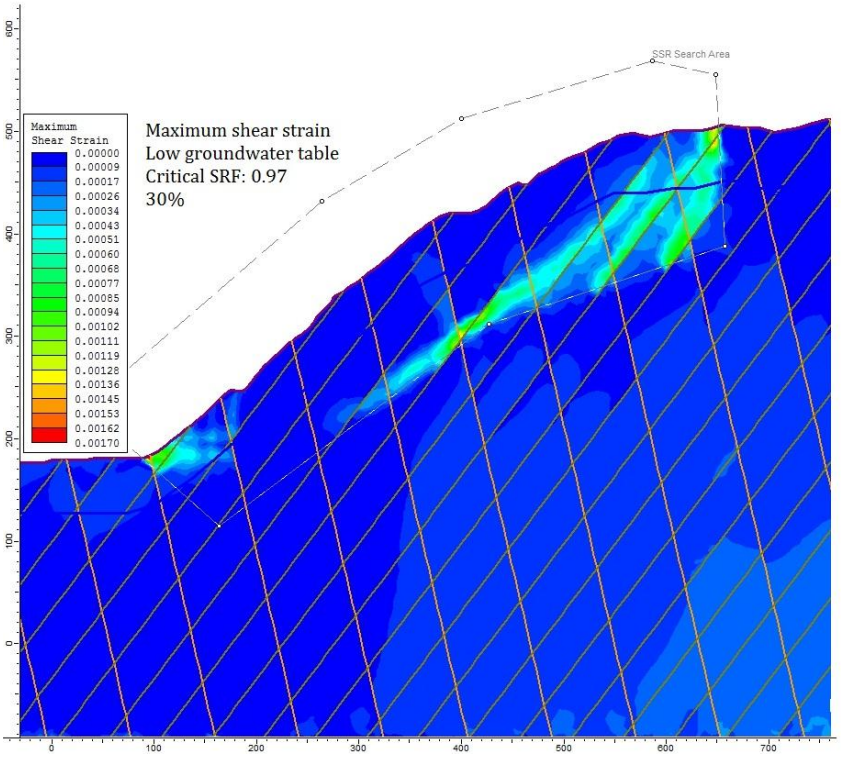

Figure 73 Unstable slope, low ground water table, critical SRF=0.97 with 30% reduction in residual values.

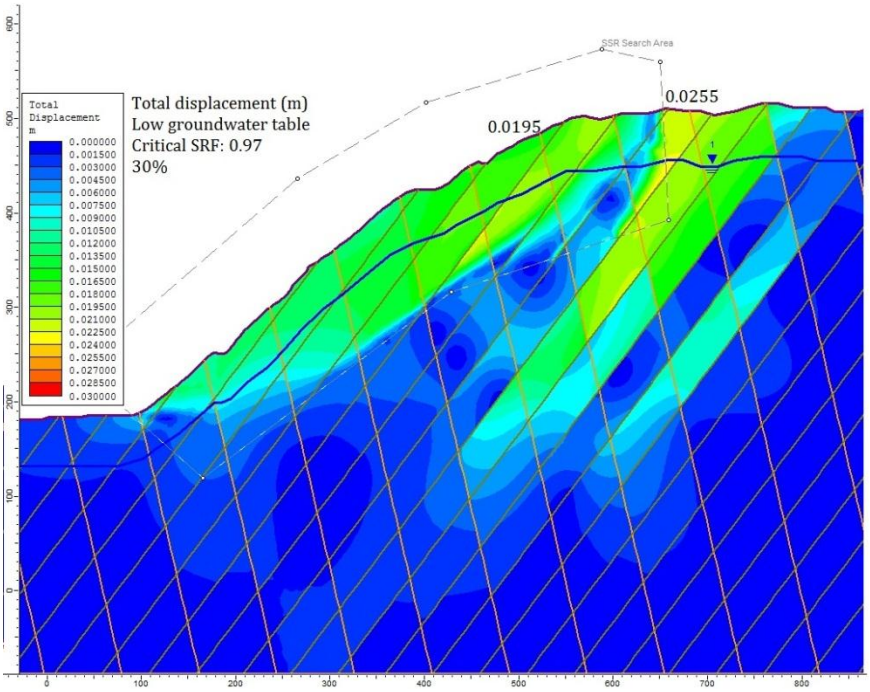

Figure 74 Total displacement for the unstable slope, low groundwater table, critical SRF=0.97 with 30% reduction in residual values. It is marked the values for the total displacement at the figure.

10 Discussion

The geology for the area around Gjøra is quite complex. The geological profile that has been produced during this thesis is just from the valley where Ivasnasen and Vollan are located. Due to the geological profile that has been drawn, the quartzite that if found at the back scarp of Vollan belongs also to a huge synclinal that goes deep. The geological profile is based on fieldwork and the available geological map (Røros&Sveg, 1989) that exists. Based on limited geological data of the area it is not possible to tell how deep the augen gneiss at Ivasnasen goes, same with the quartzite and phyllite at Vollan. To get a better understanding of the entire geology there would have been better to have a profile that covers a bigger area, but since there are not any detailed geological bedrock map of the area it was hard to give a better profile.

New advanced technology has been used in this thesis, and the results based of this are of really good quality. The use of LiDAR scans in this thesis show that the technique is very useful in steep and inaccessible areas such as Ivasnasen. With help of the scans it was found more joint sets than it was during fieldwork. During fieldwork it was found 3 different joint sets (J1, J2 and J3) and the foliation (S1), and with the LiDAR scanner it was found 3 more joint sets (J4, J5 and J6). This is important information when doing the kinematical analyses. It is, of course, important to do fieldwork also to get a better opinion by yourself of the geology and the structures, and to get structural measurements that can prove that the scans are correct. In this case the scans and the fieldwork were comparable, and this makes the analyses even more trustworthy and informative. Extensometer bolts and GPS monitoring have also been used in order to get better knowledge of other possible movements at Ivasnasen or Vollan. In this case it has not been observed any movement for none of the sites. It is important to do continuously measuring over a longer period than what has been done here, for getting a better knowledge of the reality. Really slow movement as it seems to be at Vollan needs to be measured during a longer period than this. The GPS monitoring shows there is no significant movements at Vollan, but if the time interval had been longer the conclusion might have been another. The speed of a very slow movement is <1.6m/year and an extremely slow movement is <60mm/year, so then more measurements are needed to get some good indications. Since there has been seen a lot of huge cracks at Ivasnasen, there should have been discussed if other extensometer bolts should be placed out in different places. Extensometer bolts are easy to use and give a good impression of the movement. If more extensometer bolts have been placed in different places it might lead to valuable information.

Core logging would have given useful information both at Ivasnasen and Vollan because of the complex geology, groundwater table and also the really slow movement process that might take place at Vollan. With this it would have been easier to detect if there is an ongoing really slow movement process or not, and also how high the groundwater table is. A piezometer could have been added after getting the knowledge about where

the groundwater table is running, and this would have given meaningful information for further analyses.

The SLBL outputs from CONEFALL are used to evaluate the chosen curvature (figure 53 and 54, chapter 8.1). It was difficult to choose the one that seems to be the best fit for the unstable area, especially since it is not known how it will look in the future if the unstable part fails. For the historical rockslide, none of them seems to be completely wrong and could all be possible scenarios. During the analyses it has been discovered that it most likely have been two events at Ivasnasen, since there are visible markings in the topography that might look like this. These where discovered during the work with a 3D model in ArcScene. Based on this makes it difficult to choose just one of the scenario in figure 53, since it in reality seems like there has been two. The modeled two scenarios are representative for the outputs from CONEFALL. Discovering the two back scarps for the historical rockslide at Ivasnasen gives valuable information for the unstable slope. This because it might predict that also the unstable part might take place in different scenarios, especially since the traces for the eventually first event at Ivasnasen do have traces in elongation of the back scarp to the scenario as is marked with scenario 2 for the unstable slope. During fieldwork it was found rich biotite layers in the augen gneiss at Ivasnasen. It is likely to believe that there are zones at Ivasnasen where the biotite layers are richer than other zones, and that it might have been one of these in the gouge for the back scarp. But it can also has been that small changes in the topography have resulted that "just" this part at Ivasnasen failed, and not the entire part that includes the present unstable rock slope.

Kinematical analysis of the area shows a main structural failure mechanism at Vollan to be toppling failure, and for Ivasnasen planar failure. There is registered a possibility for wedge failures both for Vollan and Ivasnasen. It is more likely that a wedge failure can happen at Ivasnasen compare to Vollan, since the eventually failure for wedge sliding at Vollan will be in a really small scale. During fieldwork it has been registered some failure that can represent wedge failure at Ivasnasen, but this is not the main treat here, and it is the planar failure that will make the biggest damages. A planar failure is often related to water entering the sliding surface and fill the vertical tension cracks. This can cause an atmospheric pressure where the sliding surface daylights in the slope face. Normal stress will act at the surface and failure can occur (Wyllie and Mah, 2004). At Ivasnasen where it is a marsh area, this is a likely situation that can happen. Based on measurements from the webpage yr.no (yr, 2012) shows a precipitation of 680mm for one year measurements (2011-2012) close to Gjøra. Measurements of 680mm/year do classify this area as a middle high precipitation area (508mm/year low and 1270mm/year high). Presence of water reduces the stability of a sliding surface of 10%. Based on this precipitations data it is obvious that this will have an influence of Ivasnasen and Vollan (Wyllie and Mah, 2004). For Vollan it could be that the really slow movement is a result of the toppling failure in the quartzite for the back scarp, and that the load of the rock masses affects the phyllite layer below. It is more likely to believe that it is linked to the thrust, where the phyllite layer have taken a lot of displacement

since all the "ridges" have been displaced above the layers and the "ridges" seems to be the result. It is three types of really slow movement, and they are classified as seasonal, continuous and progressive movements. It might be that Vollan is a combination of all these. The seasonal movement is within the depth of soil and depends of seasonal changes in soil moisture and temperature. The continuous movement depend on the shear stress is continuously and exceeds the strength of the material. The progressive movement is where the slopes are reaching the point of failure, as other types of mass movement (USGS, 2006). The depth of the soil and the shear stress are important analysis that must be done to get a better conclusion about Vollan.

The chosen volume estimations for Ivasnasen seem to make sense, since they all matches today's topography. For the historical rockslide the results matches the results that has been presented from Saintot et al (2008). The result that is presented is based on the reconstruction and construction of the basal failure surface from SLBL. The volume estimate shows a volume of the historical rockslide to be 5.2Mm^3 for the entire area and 1.2Mm^3 for the upper part. The unstable part have a smaller volume that is estimated to be 0.6Mm^3 for the smallest part (scenario 3), 1.9Mm^3 for the middle part (scenario 2) and 2.1Mm^3 for the entire area. The volume estimations for the unstable part are based on the scenarios that the author has picked out to be the most likely ones. Of course if "worst-case-scenario" should be mentioned as a possibility, then it would have been 5.4Mm^3 for the entire part. It is unlikely that all this will fail in one based on the two back scarps for the historical rockslide that is in elongation with the unstable rock slope. Also based on the graphs that represent the different volumes, it is not likely that a failure will fail like that. All the values that is measured and chosen are huge and do all represent the category "rock avalanche".

The results of the different analysis are never better than the input of the model. For the numerical simulations of actual conditions within a rock slope it will always subject to errors and uncertainties deriving from input parameters, model setup or weakness in the model itself. It is important to be aware and detect such limitations, and it is useful to reduce uncertainties by parameters studies and detect what influence they might have on the stability. For Ivasnasen the largest uncertainty is the shear zone strength input parameters, since these are not measured in-situ. It is also a limited availability on representative literature data and knowledge of the actual slope conditions. Therefore the input parameters and the fracture set are assumed to have as good quality as possible. The input parameters are based on literature and fieldwork, this does clearly introducing some uncertainty. For all the figures that have been modeled in Phase^2 (figure 57-74) has been measured with the maximum shear strength and the total displacement. The maximum shear strength is areas that are likely to constitute the failure surface within the rock masses, after evaluating them based on the critical SRF values it gives a probable sliding plane.

Based on the analyses that have been done in Phase^2 it is most likely to think of the figures with high groundwater table and 10% reduction of the residual values (figure

63&64 for the historical rockslide and figure 69&70 for the unstable rock slope) as the most correct ones. This is due to the marsh area and the precipitation conditions. The marsh area keep the water seepage for a longer period and the water pressure can be build up. The hydrogeological conditions are not investigated, so the location for the water table in the model is not correct. It is not correct that the groundwater table goes as a linear line either. In the modeling it has been tried with different height for the groundwater table to get better result. The groundwater table should therefore have been measured. This first by core logging and see in which area the groundwater table was highest and then add piezometers to get a better knowledge about the pore pressure and the reality. When adding the water table in Phase^2 the software does not allow us to model the water table to follow the joint networks, since normally this is the reality. This is also a weakness. When the water is assumed to fill the pores within the rock, this will not be the case when modeling and the water will only affect the effective stresses within the slope as a whole.

The Poisson's ratio was measured to have an average value of 0.11 in the laboratory, and a highest value of 0.24. Based on different personal and theoretical recommendations (Hoek, 2007b) it was decided to use the highest value of 0.24. Unfortunately this depends of whom that gives the advices. My supervisor K. Panthi, told me on a briefing just before delivering that the average value was a good number to use. The numerical modeling takes a lot of time to do, so it was tested with a Poisson's ratio with an average of 0.11 and it was observed that this did not have so much influence of the SRF. It was unfortunately not time to do all the numerical modeling all over, but this should be mentioned if other numerical modeling will be done for further analysis at Ivasnasen.

Phase^2 does just allow us to measure the slope instability in 2D. This must be one of the main sources of errors. If the software would allow doing the analysis in 3D it would have made the modeling much more reliable. This because for the sake of Ivasnasen there were joint sets that could not be added in the modeling, and these joint sets do also affect the instability. The joint sets that have been added to the model are the undulating foliation, (53/320) and joint set, J3 (77/192). Therefore in this case there are uncertainties regarding stresses, displacements and rock mass fracturing that is not parallel to the analyzed profile.

The total displacement for the historical rockslide is higher than it is for the unstable rock slope. When the biggest long term total displacement has been found to be 0.076m for the historical rockslide, it is found to be 0.057m for the unstable rock slope. This can be related to the total volume estimations that have been done for Ivasnasen, since the difference are 3.1Mm^3 for the biggest scenarios for each sites. The total displacement for the historical rockslide does fit the present topography, and it makes the results therefore trustworthy. How big the total displacement has been is uncertain, since 0.076meter is not a huge displacement. This might have been enough if there was a rich biotite layer that daylighted the slope and made it unstable. For the part that is left (the unstable rock slope) the total displacement is even smaller, but if it is the same

conditions as it for the historical rockslide, with a rich biotite layer this might also be enough. Anyhow, fieldwork shows that it is sign of activity, but the uncertainty is about if it all will fail or just a small part. Due to figure 54 with all the scenarios for the unstable part, it seems like it is profile 2 (scenario 2) that is the one that fit the curvature for the displacement for the models in Phase[2]. It makes sense that profile 2 might be the first to fail, since this is the one that is in elongation with the oldest event of the two back scarps for the historical rockslide.

Modern technologies to analyze rock slopes stability do have their strengths and weaknesses. It does not matter if the analyses are done with different softwares or numerical modeling techniques, because they all will always give some unwanted effects. But if the analyses are used as they should be, as a tool to get a better understanding, then they is useful and give a better knowledge of the sites.

The present tendency is to talk about climatically changes, and these are definitely a threat when it comes to slope stability. How the changes has come into being, if there is human made or a natural cycle is another discussion and will not be taken here, but the fact is that the changes are a reality. With these climatically changes it will results in a warmer climate that can cause consequences for the slope stability. The listed trigger mechanisms (chapter 2.1) for landslides, shows that the climate is an important trigger factor. Where the freeze and thaw process occur more often, also with heavier precipitation, flooding, rapid snow melting, water and groundwater pressure can increase. The climate changing can also result in stronger winds. If all these and more processes occur more often as a result of climatically changes, they will all be a threat for increasing and damaging landslides.

The risks these unstable rock slopes can cause in the area around Gjøra seems to be limited. It is a river (Driva) flowing at the bottom of the valley, but it seems like it is not deep enough that a huge tidal wave can be created. It is possible that the river can be dammed up and this can cause a crevasse that can be threatening for the inhabitants down in Gjøra. The road (road 70) that goes through the area is not so busy, so it is not likely that a vehicle will be hit by a block fall, but it can cause damages to the infrastructure (the road, bridge). It is fortunately not many inhabitants in the area, and it is just the farm below Vollan that is directly threatened of the unstable rock slopes. To get a better knowledge and a better opinion about the risk and threat in the area, it is recommended that a more detailed study with another topic should be done.

11 Conclusion

This master thesis uses fieldwork and laboratory data to analyze the Ivasnasen rockslide and the unstable rock slopes at Ivasnasen and Vollan.

When it comes to Ivasnasen and Vollan, they are located in steep areas and both have the angle of gradient that is representative for a major failure. Ivasnasen does represent volume estimates that classify the unstable part as a potential rock avalanche. Any volume estimations have not been done in this thesis for Vollan, but the area is clearly big enough to be classified as a potential rock avalanche area as well. This is because a rock avalanche is estimated to have a volume of more than $0.1Mm^3$ (NGI). It is important to do follow-up and further analysis on each site to get a better understanding of them, and get to know more precise about the actual movements. Movements that results in failure might go really slowly until they suddenly fail. At Vollan there might be that the GPS monitoring will show a significant movement in about 10 years from now on, but it is not significant for a short period of just two years, that is the existing period for the GPS monitoring data today.

The precipitation in the area is quite big, and this might affect the instability for Ivasnasen and Vollan, on both sides of the U-shaped valley. Further analyses should be done, especially at Vollan, since this is a really huge area with a complex geology that is needed to be studied in detail.

The following key points are meant to give a better understanding for the mechanisms related to the historical event and the unstable parts, and can be used for similar large-scale rockslides or other unstable rock slopes:

- By using modern GIS software, SLBL (Slope Local Base Level) and Polyworks it is possible to get a realistic reconstruction and construction of the topography. It is thereafter possible to get a volume estimate.
- ART (The Ante-Rockslide Topography) is favorable to use in combination with SLBL and PolyWorks technics to get as precise topography and volume estimations as possible.
- It is useful to do the reconstruction and construction of the topography before starting the numerical modeling, since the final profiles must be used in Phase^2.
- With help of the ART and SLBL in combination with PolyWork the historical rockslide has been estimated to have a volume of $5.2Mm^3$ for the whole part and $1.2Mm^3$ for the upper part. For the unstable part it has been calculated and chosen a volume of $0.6Mm^3$ for the smallest scenario, $1.9Mm^3$ for the medium scenario and $2.1Mm^3$ for the largest scenario.
- It is useful to use Phase^2 to get an impression of possible failure surfaces, but it is important to use different methods since Phase^2 only does a 2D modeling. There

are uncertainties regarding input parameters and the individual geological interpretations.

- During fieldwork and laboratory testing a bigger amount of biotite is found for the analyses for Ivasnasen. It is likely to think that it was a rich biotite layers in gouge-filled joints for Ivasnasen that might have been a trigger factor for the failure.
- Numerical modeling shows that the historical failure at Ivasnasen could not have failed without the presence of a high groundwater table. Since not any historical sources about when and how the precipitation was during this period existing, this is a suggestion of the situation.
- Since the modeling in Phase^2 do include the foliation, and it seems during fieldwork that this is the most important for the slope stability, the results is representative even it is in 2D. But it would have been interesting to see how the modeling would have been in 3D.

12 Recommendation

Even though Ivasnasen and Vollan have been studied in detail during this master thesis, there are still further analysis and investigations that is required for further work. This thesis has covered much, but it was not time to do everything. The suggestions for further work are listed below:

- DEM of 1meter that covers the entire area, especially to get a better knowledge of the area around Vollan. The DEM of 10meter that is used is not detailed enough.
- More GPS monitoring over a longer period for Vollan. This should be done to detect if there are some movements in the ground or not.
- Place out more extensometer bolts over different parts at Ivasnasen. This is an easy and handy way to quickly get an understanding of the activity for the unstable rock slope.
- LiDAR scan of the unstable part at Ivasnasen for a longer period, with just a year interval it was not detected any block fall or movement, but the results of this might be different if there are more datasets to compare.
- Airborne LiDAR scans of Vollan should be done, so the same analysis could be done at Vollan as it has been for Ivasnasen.
- Use of Smith-hammer in-situ, for getting the correct parameters of the joints.
- A model setup for numerical analyses which include all the joint sets. This may be done by calculating joint set properties based on a combination of discontinuities and intact rock properties.
- Numerical modeling of Vollan.
- Use piezometer to get a better knowledge about the pore pressure and the groundwater table.
- Measuring the resistivity of the rock masses with help of geoelectrical measurements.
- Analysis with thin section in microscope.
- Risk analyses of the area.

References

ASTM, A. S. F. T. A. M. 1967. Determination of stress in rock. *Library of congress catalog card number,* 67-26104.

BESL, P. J. & MCKAY, N. D. 1992. A method for registration of 3-D shapes. *IEEE Transactions on Pattern Analysis and Machine Intelligence 14,* 2**,** 239-256.

BJORDAL, H. E. A. 2011. Sikring av veger mot seinskred. *VD rapport Vegdirektoratet,* Nr.32**,** 78.

BLIKRA, L. H. & NEMEC, W. 1998. Postglacial colluvium in western Norway; depostional processes, facies and palaeoclimatic record. *Sedimentology,* 45.

BRAATHEN, A., BLIKRA, L. H., BERG, S. S. & KARLSEN, F. 2004. Rock-slope failures in Norway; type, geometry, deformation mechanisms and stability. *Norwegian Journal of Geology,* 84**,** 67-88.

BRÜCKL, E. P. 2001. Cause-Effect Models of Large Landslides. *Natural Hazards,* 23 (2)**,** 291-314.

CHAN, R. K. S. & LAU, T. M. F. 2007. Slope Safety System and Landslide Risk Management in Hong Kong. *Geotechnical Engineering Office, Civil Engineering and Development Department, Hong Kong SAR, China*.

CONFORTI, C. 2005. Terrestrial Scanning Lidar Technology applied to study the evolution of the ice-contact image lake (Mont Blanc, Italy). 9th Alpine Glaciological Meeting**,** 1-5.

COUTURE, R. 2011. Landslide Terminology National Guidelines and Best Practices on Landslides. *Geological Survey of Canada open file 6824*.

CRUDEN, D. M., HU, Z. Q. & LU, Z. Y. 1993. Rock Topples in the Highway Cut West of Clairvivaux Creek, Jasper, Alberta. *Canadian Geotechnical Journal,* 30**,** 1016-1023.

CRUDEN, D. M. & VARNES, D. J. 1996. Landslide types and processes.

DALSEGG, E., RØNNING, J. S., TØNNESEN, J. F., SAINTOT, A. & GANERØD, G. V. 2010. Geologisk og geofysisk kartlegging av Gikling, et ustabilt fjellparti i Sunndalen, Møre og Romsdal. NGU.

DERRON, M.-H., JABOYEDOFF, J. & BLIKRA, L. H. 2005. Preliminary assessment of rockslide and rockfall hazards using a DEM (Oppstadhornet, Norway). Natural Hazards and Earth System Sciences 5**,** 285-292.

DRAMIS, F. & SORRISO-VALVO, M. 1994. Deep-seated gravitational slope deformations, related landslides and tectonics. *Engineering Geology,* 38**,** 231-243.

DREIÅS, G. M. 2012. Laboratory report -Projected laboratory methods for rock slopes.

DRIVENES, K. & SØRLØKK, T. 2012. XRD-analysar av 5 prøve av bergartsmateriale.

DØRUM, E. 1989. *Storofsen i 1789* [Online]. http://www.rise.no/norsk/historie/storofsen.htm.

EIKEN, T. 2011. Rapport om Deformasjonsmålingar i potensielle fjellskred. Universitetet i Oslo: Institutt for geofag.

ELGIN, M. 2005. Creating and using digital elevation models. *Beca International Consultants Ltd.*

EVANS, S. G., HUNGR, O. & CLAGUE, J. J. 2001. Dynamics of the 1984 rock avalanche and associated distal debris flow on Mount Cayley, British Columbia, Canada; implications for landslide hazard assessment on dissected volcanoes. *Engineering Geology,* 61 (1)**,** 29-51.

GEE, D. G. 1975. A tectonic model for the central part of the central part of the Scandinavian Caledonides. *American Journal of Science* 275-A**,** 468-515.

GIRAUD, A., ROCHET, L. & ANTOINE, P. 1990. Process of Slope Failure in Crystallophyllian Formations. *Engineering Geology,* 29**,** 241-253.

GOGUEL, J. 1978. Rockslides and Avalanches. *Developments in Geotechnical Engineering***,** 693-706.

GOODMAN, R. E. & BRAY, J. W. 1976. Toppling of rock slopes. *American Society of Civil Engineers,* 2**,** 201-234.

GORUM, T., GONENCGIL, B., GOKCEOGLU, C. & NEFESLIOGLU, H. A. 2008. Implementation of reconstructed geomorphologic units in landslide susceptibility mapping: the Melen Gorge (NW Turkey). . *Natural Hazards,* 46**,** 323-351.

GRØNENG, G. 2010. Stability Analyses of the Åknes Rock Slope, Western Norway. *NTNU, Department of Geology and Mineral Resources Engineering,* 2010:30.

HAMMAH, R. E., CURRAN, J. C. & CORKUM, B. 2004. Stability analysis of rock slopes using the finite element method. *Eurock 2004 & 53rd Geomechanics Colloquium*.

HAMMAH, R. E., YACOUB, T. E., CORKUM, B. C. & CURRAN, J. 2006. A comparison of finite element slope stability analysis with conventional limit equilibrium investigation. *Proceedings of the 58th Canadian Geotechnical and 6th Joint IAH-CNC and CGS Groundwater Specialty Conferences Saskatoon, Saskatchewan, Canada.*

HENDERSON, I. A. & SAINTOT, A. 2007. Fjellskredundersøkelser i Møre og Romsdal.

HOEK, E. 2007a. *Analysis of rockfall hazards* [Online].

HOEK, E. 2007b. *Rock mass properties* [Online]. www.rocscience.com.

HOEK, E. 2007c. Shear strenght of discontinuities. *Rocscience, Practical rock engineering,* Avaliable online at http://www.rocscience.com.

JABOYEDOFF, M., BAILLIFARD, F., COUTURE, R., LOCAT, J. & LOCAT, P. 2004c. New insight of geomorphology and landslide prone area detection using Digital Elevation Model(s). *Lacerda, W.A., Ehrlich, M., Fontoura, A.B. & Sayão, A. (eds), Landslides: Evaluation and Stabilization.,* London: Taylor & Francis.**,** 191-198.

JABOYEDOFF, M., BAILLIFARD, F., COUTURE, R., LOCAT, J. & LOCAT, P. 2004d. Toward preliminary hazard assessment using DEM topographic analysis and simple mechanical modeling by means of sloping local base level. . *Lacerda, W.A., Ehrlich, M., Fontoura, A.B. & Sayão, A. (eds), Landslides: Evaluation and Stabilization.,* London: Taylor & Francis.**,** 199-205.

JABOYEDOFF, M., BAILLIFARD, F., DERRON, M.-H., COUTURE, R., LOCAT, J. & LOCAT, P. 2005. Modular and evolving rock slope hazard assessment methods. *Landslides and Avalanches: ICFL 2005 Norway. London: Taylor & Francis Group.***,** Pages 187–194 of: Senneset, K., Flaate, K. & Larsen, J. O. (eds).

JABOYEDOFF, M. & DERRON, M. H. 2005. A new method to estimate the infilling of alluvial sediment of glacial valleys using a sloping local base level. *Geogr. Fis. Dinam. ,* Quat. 28**,** 37-46.

JABOYEDOFF, M. & LABIOUSE, V. 2003. Preliminary assessment of rockfall haard based on GIS data. *South Africa Institute of Mining and Metallurgy, Johannesburgh, South Africa,* 10th International Congress on Rock Mechanics ISRM 2003 - Technology roadmap for rock mechanics.**,** 573 -578.

JAEGER, J. C. & COOK, N. G. W. 1968. Time-dependent effects (2nd ed.). *John Wiley & Sons Inc.*

KEAREY, P. 2001. *The new penguin dictionary of geology,* London, Penguin Books.

KEEFER, D. L. 1992. The susceptibility of rock slopes to eartquake-induced failure. *Proceedings of the 35th Annual Meeting of the Assoc. og Eng. Geologists, CA***,** 529-538.

KÖTHE, R. 2000. Definitions: DTM etc. Scientic landscapes.

LOFTESNES, K. 2010. Svaddenipun, Rjukan - Stability analysis of potentially unstable mountainside. *Department of Geology and Mineral Resources Engineering. NTNU, Trondheim*.

MENG, X. 2012. Landslide. *Encyclopedia Britannica.* http://www.britannica.com/EBchecked/topic/329513/landslide/251485/Types-of-landslides?anchor=ref875531.

METZGER, R. & JABOYEDOFF, M. 2008. R. Metzger, M. Jaboyedoff. 10.

MORA, P., BALDI, P., CASULA, G., FABRIS, M., GHIROTTI, M., MAZZINI, E. & PESCI, A. 2003. Global Positoning Systems and digital photogrammetry for the monitoring of mass movements: application to the Ca'di Malta landslid (northern Apennines, Italy). *Engineering Geology,* 68 (1-2)**,** 103-121.

MYRVANG, A. 2001. Bergmekanikk. *nstitutt for geologi og bergmekanikk, NTNU, Trondheim.*

NBG & NFF 2000. Engineering geology and rock engineering, Handbook no. 2. *Norgwegian Group for Rock Mechanics and Norwegian Tunnelling Society*.

NGI. *Tre typer steinskred* [Online]. www.ngi.no. Available: http://www.ngi.no/no/Utvalgte-tema/Skred-og-skredfare/Skredkategorier/Tre-typer-steinskred/.

NGI. 2012. *Skredbane* [Online]. http://www.ngi.no/upload/Utvalgte%20tema/Skred/sikring%20og%20tiltak/skredbane.jpg.

NGU. 2012. *Berggrunnskart* [Online].

NILSEN, B. 2000. New tends in rock slope stability analyses. *Bulleting Eng Geol Env 58***,** 173-178.

NILSEN, B. & BROCH, E. 2009. Ingeniørgeologi -berg, grunnkurskompendium. *NTNU, Institutt for geologi og bergteknikk, Trondheim*.

NILSEN, B., LINDSTRØM, M., MATHIESEN, T. K., HOLMØY, H. K., OLSSON, R. & PALMSTRØM, A. 2011. Veileder for bruk av Eurocode 7 til bergteknisk prosjektering. *in bergmekanikkgruppe, N. (Ed.)***,** 7.

NILSEN, O. & WOLFF, F. C. 1989. Geologisk kart over Norge, berggrunnskart RØROS & SVEG, 1:250 000. *Norges geologiske undersøkelse*.

NORDGULEN, Ø., ANDRESEN, A., RAMBERG, I. B., BRYHNI, I., NØTTVEDT, A. & RAGNES, K. E. 2007. The Western Gneiss Region, in: . *Geological Society of Norway,* The Making of a land - Geology of Norway**.,** 112-118.

OPPIKOFER, T. 2009. Detection, analysis and monitoring of slope movements by high-resolution digital elevation models. *Faculty of Geosciences and Environment Université de Lausanne (UNIL), Lausanne*.

OPPIKOFER, T. & JABOYEDOFF, M. 2008a. Åknes/Tafjord project: Analysis of ancient rockslide scars and potential instabilities in the Tafjord area & Laser scanner monitoring of instabilities at Hegguraksla. *Institute of Geomatics and Analysis of Risk, University of Lausanne, Lausanne, Switzerland.,* IGAR report IGAR-TO-009.

OPPIKOFER, T., JABOYEDOFF, M. & 2008B 2008b. Åknes/Tafjord project: Structural analysis and displacement measurement of the Åknes rockslide by terrestrial laser scanning. . Institute of Geomatics and Analysis of Risk, University of Lausanne, Lausanne, Switzerland.

OPPIKOFER, T., JABOYEDOFF, M. & KEUSEN, H.-R. 2008a. Collapse at the eastern Eiger flank in the Swiss Alps. . *Nature Geoscience,* 1(8).

OPPIKOFER, T., JABOYEDOFF, M., PEDRAZZINI, A., DERRON, M.-H. & BLIKRA, L. H. 2012. *High-resolution digital elevation model analysis of rock slope failures in Tafjord (Norway): Part 1 - Past rockslides and rock avalanches* [Online]. www.terranum.ch: IGAR. [Accessed 2012 2011].

OYAGI, N., SORRISO-VALVO, M. & VOIGHT, B. 1994. Introduction to the special issue of the symposium on deep-seated landslides and large-scale rock avalanches. *Engineering Geology,* 38**,** 187-188.

PANTHI, K. 2012. *RE: Personal communication for this thesis.*

RAMBERG, I. B., BRYHNI, I. & NØTTVEDT, A. 2007. *Landet blir til: Norges geologi*.

ROALD, L. A. 2008. *De største flommene i Norge* [Online]. http://www.yr.no/nyheter/1.6233304: NRK. [Accessed 25.09.2008.

ROBERTS, D. & GEE, D. G. 1985. An introduction to the structure of the Scandinavian Caledonides I. 55-68.

ROCSCIENCE. 2011. *Phase2, online user manual* [Online]. http://www.rocscience.com/products/3/Phase2.

ROCSCIENCE. 2012. *Tutorial Dips* [Online]. http://www.rocscience.com/downloads/dips/webhelp/tutorials/Dips_Tutorials.htm: Rocscience inc.

SAINTOT, A., BOHME, M., REDFIELD, T. & DAHLE, H. 2008. Field studies of unstable slopes in Sunndalen Valley.

SANDØY, G. 2012. Back-analysis of the 1756 Tjellefonna rockslide, Langfjorden. *NTNU, Department of Geology and Mineral Resources Engineering***,** 123.

SHEOREY, P. R. 1994. A theory for in-situ stresses in isotropic and transversely isotropic rock. *International Journal of Rock Mechanics and Mining Sciences & Geomechanics Abstracts 31 (1), 23,* 31 (1)**,** 23-34.

SKREDNETT. 2012. *Skreddata på nett* [Online]. http://geo.ngu.no/kart/skrednett/.

SOCIETY, C. G. 1992. Canadian Foundation Engineering Manual. *BiTech Publichers, Ltd, Vancouver, Canada*.

SØRBEL, L. 2011. Skred.

TERRANUM. 2011. *Coltop3D* [Online]. www.terranum.ch: IGAR. [Accessed 2012 2011].

TERZAGHI, K. & PECK, R. B. 1967. *Soil mechanics in engineering practice,* New York, Wiley.

TEZA, G., GALGARO, A., ZALTRON, N. & GENEVOIS, R. 2007. Terrestrial laser scanner to detect landslide displacement fields: a new approach. *International Journal of Remote Sensing,* 28(16)**,** 3425-3446.

THORNHILL, M. 1999. *Atomic spectroscopy,* [Trondheim], [M. Thornhill].

TVETEN, E., LUTRO, O. & THORSNES, T. 1998. Geologisk berggrunnskart Ålesund Målestokk 1:250.000.

USGS 2006. Landslide types and processes.

VOIGHT, B. 1978. Rockslides and Avalanches. *1.Natural Phenomena*.

WOOLLEY, E. A. 1996. *The problems of classification* [Online]. http://www.geol.lsu.edu/henry/Geology3041/lectures/02IgneousClassify/IUGS-IgneousClassFlowChart.htm#PyroClass: The IUGS Subcommission on the Systematics of Igneous Rocks.

WYLLIE, D. C. & MAH, C. W. 2004. *Rock slope engineering: civil and mining,* London, Spon Press.

YR. 2012. *Været som var* [Online]. http://www.yr.no/sted/Norge/M%C3%B8re_og_Romsdal/Sunndal/Gj%C3%B8ra/statistikk.html.

ØIESVOLD, M., B, G. 2007. OVERGANGEN FRA EKLOGITT TIL AMFIBOLITT – ET DETALJSTUDIUM.

Appendix

1. XRD analyses

NTNU
Fakultet for ingeniørvitenskap og teknologi
Institutt for geologi og bergteknikk

Vår dato 24.04.2012 | Vår referanse KD / 12-065
Deres dato | Deres referanse

Gudrun Majala Dreiås

XRD-analysar av 5 prøve av bergartsmateriale.

Analysane er utført på ein Bruker D8 ADVANCE. DIFFRAC^{plus} SEARCH programvare i kombinasjon med databasen PDF-2, føreslår følgjande mineralfasar for prøvane.

Prøve		5	7	11	12	13
Journalnummer		120139	120140	120141	120142	120143
Mineralgruppe	Mineral					
Kvarts	Kvarts	34	52	62	36	14
Glimmer	Muskovitt	47	7			22
	Biotitt			8	17	
	Flogopitt					15
Kloritt	Klinoklor	< 1		1	< 1	
Feltspat	Plagioklas	7	28	11	25	27
	Kalifeltspat	11	13	18	21	22
Amfibol	Aktinolitt					
Pyritt	Pyritt	< 1	< 1	< 1		
Graphite	Graphite					1
Total		99	100	100	99	100

Semikvantifiseringa av prøve 13 er unøyaktig grunna høgt glimmerinnhald og kornigheitseffekt. Vedlagt ligg diffraktogram for køyringane.

Med helsing

Kristian Drivenes
Stipendiat

Torill Sørløkk
Avdelingsingeniør

Postadresse 7491 Trondheim
Org.nr. 974 767 880
E-post: igb-info@ivt.ntnu.no
http://www.ivt.ntnu.no/igb/
Besøksadresse Sem Sælands veg 1 Gløshaugen
Telefon +47 73 59 48 10
Telefaks +47 73 59 48 14
Kristian Drivenes Tlf: +47 73 59 48 09 Mobil: +47 40 22 34 26

NTNU

Fakultet for ingeniørvitenskap og teknologi
Institutt for geologi og bergteknikk

Vår dato 24.04.2012 | Vår referanse KD / 12-065
Deres dato | Deres referanse

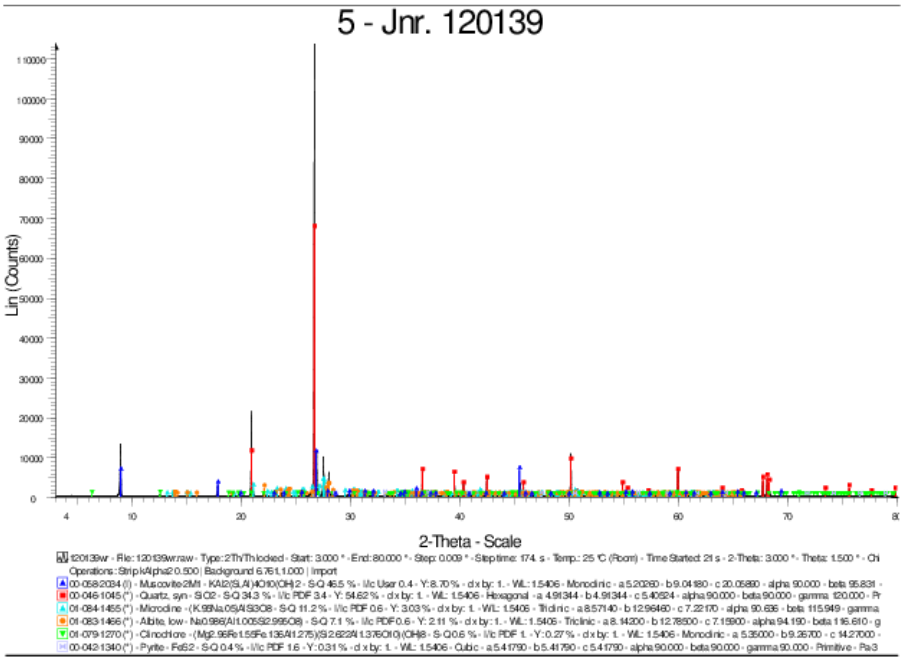

Norges teknisk-naturvitenskapelige universitet

Vår dato 24.04.2012 | Vår referanse KD / 12-065

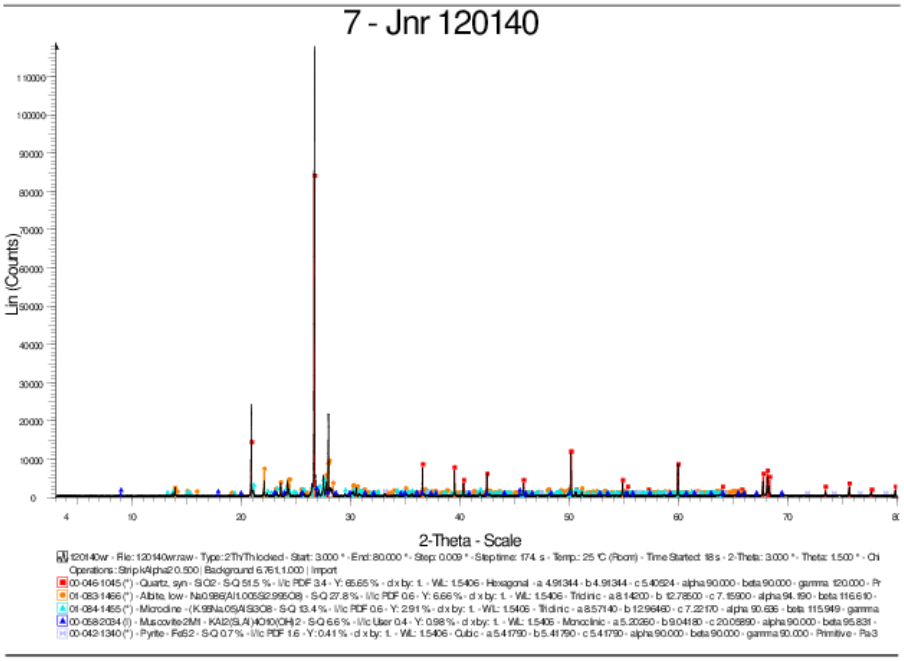

Norges teknisk-naturvitenskapelige universitet

Vår dato 24.04.2012

Vår referanse KD / 12-065

11 - Jnr 120141

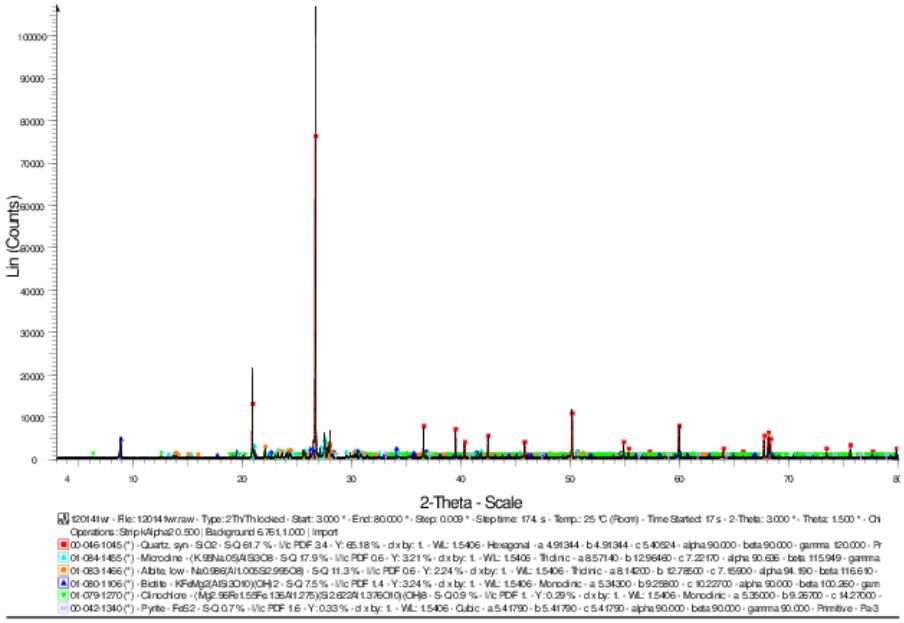

Norges teknisk-naturvitenskapelige universitet

Vår dato 24.04.2012

Vår referanse KD / 12-065

12 - Jnr 120142

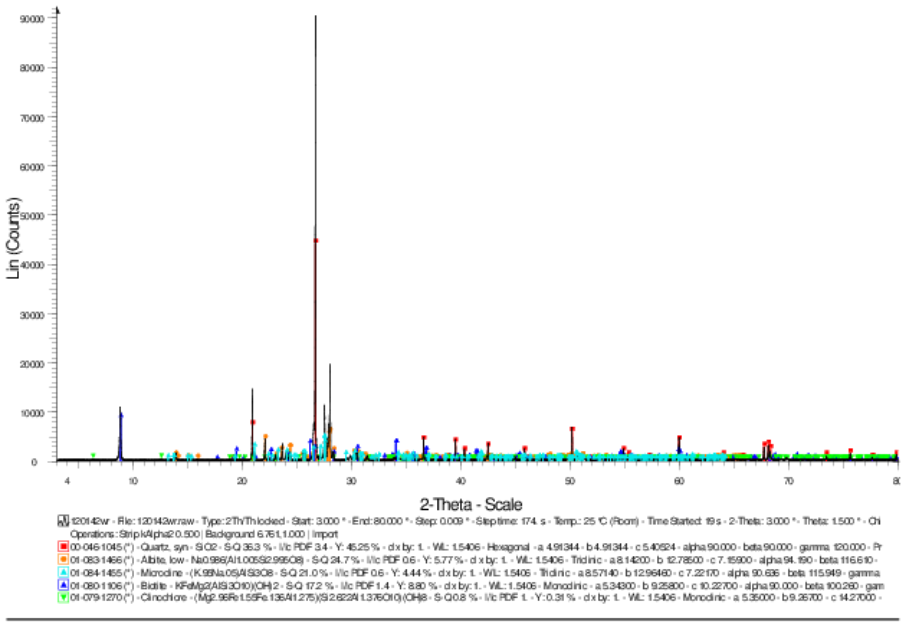

Norges teknisk-naturvitenskapelige universitet

Vår dato 24.04.2012

Vår referanse KD / 12-065

13 - Jnr 120143

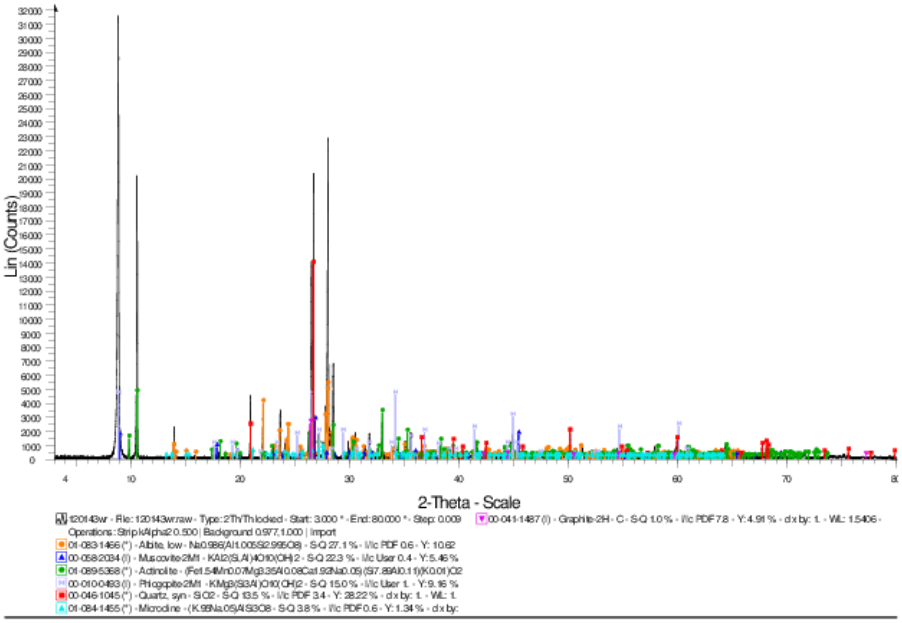

2. Estimated volumes for the historical rockslide and the unstable rock slope at Ivasnasen.

Volume calculations for reconstructed topography for the historical rockslide at Ivasnasen are shown in table 27. Scenario 1 represent the whole area and scenario 2 the upper part of the rockslide.

Table 27 Historical rockslide

	Count	Area	Min	Max	Range	Mean	STD	SUM	Volume
Scen 2	7745	193625	0,0	50,3	50,3	27,0	13,4	209491	5237265,8
Scen 1	2504	62600	0,0	47,1	47,1	19,5	12,6	48933,1	1223329,2

Volume calculations for each scenario for the unstable part at Ivasnasen are shown in table 28. All three scenarios are represented, and all three shows a minimum, mean and maximum scenario. Scenario 1 is "the worst case scenario", the entire unstable part. Scenario 2 is the middle part, and scenario 3 is the smallest part that is located lowest in the path.

Table 28 Unstable rock slope

	Scenario 1, c0	Scenario 1, mean	Scenario 1, max	Scenario 2,c0	Scenario 2,mean	Scenario 2, max	Scenario 3, c0	Scenario 3, mean	Scenario 3, max
Volume	2088675	3981250	5395325	1104200	1867800	2784850	113875	319075	633925
Median	17,0	33	46	17	28	44	3	12	23
Minority	63,0	97	133	43	68	92	16	26	45
Majority	0,0	0	0	0	0	0	0	0	35
Variety	64,0	98	134	43	69	93	17	27	45
SUM	83547	159250	215813	44168	74712	111394	4555	12763	25357
STD	16,5	30	39	12	20	27	4	7	12
Mean	20,9	40	54	17	29	44	4	11	22
Range	63,0	97	133	43	68	92	16	26	45
Max	63,0	97	133	43	68	92	16	26	45
Min	0	0	0	0	0	0	0	0	0
Area	99800	100150	100150	63375	63375	63375	29000	29000	29000
Count	3992	4006	4006	2535	2535	2535	1160	1160	1160

3. Residuals values of peak calculations

High water table, 0, 5, 10% residual values of peak			
	φ_{res} (^{0})	c_{res} (MPa)	σ_t (MPa)
Material, 0 %	42	0.24	0.094
S1, 0 %	53	0.24	0.094
J3, 0 %	77	0.24	0.094
Material, 5%	39.9	0.228	0.0893
S1, 5 %	50.35	0.228	0.0893
J3, 5 %	73.15	0.228	0.0893
Material, 10%	37.8	0.216	0.0846
S1, 10 %	47.7	0.216	0.0846
J3, 10 %	69.3	0.216	0.0846

Medium water table, 15, 20% residual values of peak			
	φ_{res} (^{0})	c_{res} (MPa)	σ_t (MPa)
Material, 15 %	35.7	0.204	0.0799
S1, 15 %	45.05	0.204	0.0799
J3, 15 %	65.45	0.204	0.0799
Material, 20%	33.6	0.192	0.0752
S1, 20 %	42.4	0.192	0.0752
J3, 20 %	61.6	0.192	0.0752

Low water table, 30 & 35% residual values of peak			
	φ_{res} (^{0})	c_{res} (MPa)	σ_t (MPa)
Material, 30 %	29.4	0.168	0.0658
S1, 30 %	37.1	0.168	0.0658
J3, 30 %	53.9	0.168	0.0658
Material, 35%	27.3	0.156	0.0611
S1, 35 %	34.45	0.156	0.0611
J3, 35 %	50.05	0.156	0.611

4. Weather report 2011-2012

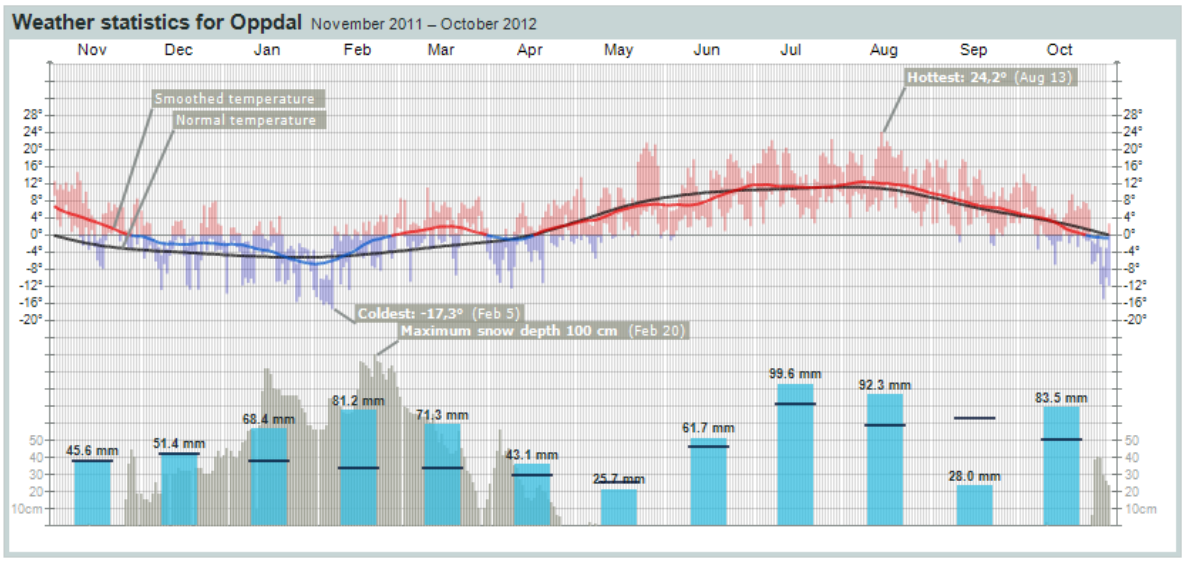

Hide explanation

The black line shows mean value (both precipitation and temperature). Some stations does not have mean values, and hence no black line.

The red/blue line shows average temperature during the day (24h) (equalized for 30 days). The line is red by pluss degrees, and blue by minus degrees.

The red/blue areas shows the temperature variations throughout the day (24h) with max- and min. temperature as endpoints. The area is red by pluss degrees, and blue by minus degrees.

The lightblue bars shows total precipitation this month. The black lines crossing is the normal (mean) value for precipitation.

The dark grey bars behind the precipitation bars shows snowdepth measured day by day.

Some stations only measures precipitation, while others only measures temperature. If an area or bar is missing the station does not measure this data.

NB! Precipitation is measured at 07 hours Norwegian time. The value (in mm) shows last 24 hours until 07 hours (08 hours summertime). Download other weather statistics from eklima.met.no.

Tabular view for temperature and precipitation per month

Months	Temperature				Precipitation			Wind	
	Average	Normal	Warmest	Coldest	Total	Normal	Highest daily value	Average	Strongest wind
Oct 2012	1.5°C	2.5°C	14.4°C Oct 1	-15.0°C Oct 29	84 mm	60 mm	48 mm Oct 26	2.4 m/s	9.4 m/s Oct 3
Sep 2012	7.2°C	6.5°C	17.8°C Sep 10	-2.5°C Sep 21	28 mm	75 mm	7 mm Sep 9	2.4 m/s	10.0 m/s Sep 4
Aug 2012	11.7°C	10.5°C	24.2°C Aug 13	2.1°C Aug 27	92 mm	70 mm	12 mm Aug 6	2.0 m/s	7.8 m/s Aug 30
Jul 2012	11.8°C	11.0°C	22.5°C Jul 27	2.7°C Jul 3	100 mm	85 mm	18 mm Jul 9	2.3 m/s	7.6 m/s Jul 2
Jun 2012	8.4°C	10.0°C	19.0°C Jun 22	-1.2°C Jun 1	62 mm	55 mm	17 mm Jun 19	2.8 m/s	8.3 m/s Jun 16
May 2012	5.8°C	6.5°C	21.7°C May 24	-5.5°C May 6	26 mm	30 mm	12 mm May 12	3.1 m/s	9.4 m/s May 14
Apr 2012	0.1°C	0.5°C	10.8°C Apr 30	-12.5°C Apr 7	43 mm	35 mm	14 mm Apr 2	2.8 m/s	10.2 m/s Apr 26
Mar 2012	1.7°C	-2.5°C	11.2°C Mar 9	-10.9°C Mar 3	71 mm	40 mm	13 mm Mar 20	4.1 m/s	13.6 m/s Mar 9
Feb 2012	-3.1°C	-4.5°C	8.7°C Feb 29	-17.3°C Feb 5	81 mm	40 mm	20 mm Feb 15	3.0 m/s	13.0 m/s Feb 14
Jan 2012	-4.2°C	-5.0°C	4.5°C Jan 18	-15.6°C Jan 24	68 mm	45 mm	20 mm Jan 13	2.7 m/s	13.1 m/s Jan 26
Dec 2011	-2.0°C	-4.0°C	8.0°C Dec 27	-13.6°C Dec 31	51 mm	50 mm	10 mm Dec 27	3.4 m/s	17.2 m/s Dec 9
Nov 2011	3.7°C	-2.0°C	14.8°C Nov 9	-7.9°C Nov 18	46 mm	45 mm	17 mm Nov 27	2.5 m/s	10.2 m/s Nov 25